INVESTIGATION OF THE FLOW DYNAMICS OF A VERTICAL BIOREACTOR USING THE RESIDENCE TIME DISTRIBUTION

by

Mark Edney

BEng Ryerson University 2011

A thesis presented by Ryerson University

In partial fulfillment of the

requirements for the degree of

Master of Applied Science

in the program of

Chemical Engineering

Ryerson University

Toronto, Ontario, Canada, 2020

September 17, 2020

Author's Declaration

AUTHOR'S DECLARATION FOR ELECTRONIC SUBMISSION OF A THESIS

I hereby declare that I am the sole author of this thesis. This is a true copy of the thesis, including any required final revisions, as accepted by my examiners.

I authorize Ryerson University to lend this thesis to other institutions or individuals for the purpose of scholarly research.

I further authorize Ryerson University to reproduce this thesis by photocopying or by other means, in total or in part, at the request of other institutions or individuals for the purpose of scholarly research.

I understand that my thesis may be made electronically available to the public.

Investigation of the flow dynamics of a Vertical Bioreactor using the Residence Time Distribution

Mark Edney, Master of Applied Science, Chemical Engineering

Abstract

In the wastewater industry, conventional activated sludge processes are still the dominant technology. This process relies on large concrete tanks with poor mixing profiles, due to their rectangular cross-section.

Hitherto, Water Engineering has failed to see the relevance of vertical bioreactors. The STAR (Simultaneous Treatment of Ammonia and Phosphorous Removal) is a vertical bioreactor with three stages for the elimination of biological nutrient removal in wastewater. The STAR vertical bioreactor is capable of delivering high quality effluent within a significantly reduced footprint.

In this study, the mixing and fluid flow through the reactor is investigated using residence time distribution tests. A single pulse of conductive tracer is introduced into the first stage of the reactor. Conductivity sensors were used to measure tracer concentration at the exit of each stage. This conductive tracer represents a non-reactive component introduced into the process flow. Data generated from this experiment found evidence of a bypass rate of 7.5% of the feed rate. The data were compared with two theoretical models: The ideal Continuous Stirred Tank Reactor and the Generalized Nth CSTR in series model and found to approximate the residence time distribution.

Acknowledgments

I give my sincerest appreciations to my advisor Dr. Manual Alvarez Cuenca for both providing me the opportunity and the challenge to grow as a researcher. I would like to thank Dr. Cuenca for his expertise, leadership and financial support. If I see further, it is because I stand on his shoulders.

I would like to thank my co-advisors Dr. Maryam Reza and Dr. Samant Upreti for their expert knowledge, which has been instrumental for this research.

All of my work would be impossible without the generosity and the facilities of the Chemical Engineering Department at Ryerson University. I thank Daniel Boothe and Ali Hemmati for their tireless efforts assisting in the construction of this experiment. I thank Tondar Tajrobehkar for his assistance with the installation of the newly acquired sensors.

Table of Contents

List of Tables

List of Symbols

Symbol	Description	Dimensions
E (t)	Probability Density Function	
F (t)	Distribution Function	
T	Unit of Time	
M	Unit of Mass	
L	Unit of Length	
μ	Specific Growth Rate of Microorganism	(T^{-1})
μ_{max}	Maximum Specific Growth Rate	(T^{-1})
S	Concentration of Substrate	(ML^{-3})
K_S	Half Velocity Constant	(ML^{-3})
r_a	Reaction Rate	(MT^{-1})
k	Rate Constant of First Order Reaction	(T^{-1})
C_a	Concentration of Component A	(ML^{-3})
X_{seg}	Conversion Rate for a Segregated Fluid	
X_{mm}	Conversion Rate for a Maximum Mixedness Fluid	
τ	Mean Residence Time	(T)
V	Volume	(L^3)
v	Flow Rate	(L^3T^{-1})
v_O	Overall Flow Rate	(L^3T^{-1})
v_E	Entering Flow Rate	(L^3T^{-1})
v_B	Flow Rate of By-pass	(L^3T^{-1})
τ_{obs}	Observed Residence Time	(T)
V_D	Dead Space Volume	(L^3)
V_A	Active Volume	(L^3)
H	Hold-back	
S	Quantity of Segregation	
t	Time	(T)
θ	Dimensionless Time	

Symbol	Description	Dimensions
N_i	Molar Amount of Component I	(mol)
$R_{gen,\ ij}$	Sum of All Reaction Rates	($molT^{-1}$)
δ	Dirac Delta Function	
$\overline{t}$	Sample Mean Time	(T)
σ	Standard Deviation	
$\overline{f}$	Mean Function Value	
σ_{PFR}	Standard Deviation of Ideal CSTR	
σ_{PFR}	Standard Deviation of Ideal PFR	
$\left(\frac{D}{uL}\right)$	Dimensionless Dispersion Coefficient	
π	Pi	
Γ	Gamma function	
u	Velocity Vector	(LT^{-1})
P	Pressure	($ML^{-1}T^{-2}$)
ρ	Density	(ML^{-3})
μ	Dynamic Viscosity	($ML^{-1}T^{-1}$)

List of Figures

List of Appendices

Chapter 1 : Introduction

The function of wastewater treatment has evolved over the years from the original purpose of managing human organic waste. Wastewater treatment has developed to include the management of environmental damaging nutrients. The problems of releasing nitrogen compounds into the environment are well documented; causing anoxia, causing harm to aquatic life, eutrophication and decreasing the efficiency of chlorine disinfection. The potential cost of eutrophication alone in the USA is estimated to be $2.2 billion USD [1]. The role of wastewater treatment has expanded to meet developing concerns of modern life.

In the early 70's, the consequences of phosphorous release were originally identified [2]. As the population of Canada nears 36 million, there will be an estimated 43,000 tons of phosphorous released annually into municipal wastewater [3]. It wasn't until the 80s that the first advanced wastewater treatment plant, based on the principles of Biological Nutrient Removal (BNR), was built in Kelowna, British Columbia [4]. It was the first BNR plant in North America.

1.1 The Canadian Perspective

The regulation of wastewater treatment in Canada has sorely lagged behind the rest of the developed world. Regulation requiring secondary treatment has only taken place since 2012 in Canada, which is compared to regulation in the EU from 1991 and the United States from 1972 [4]. Secondary treatment entails processes to reduce the concentration of carbon-compounds in wastewater. This slow response has created an underdeveloped industry in Canada. Only 62% of Canada's wastewater treatment goes to the extent of secondary treatment, either through Waste Stabilization Ponds (WSP) or through mechanical treatment. Surprisingly, 18% consist of only primary treatment while 3% entails virtually no treatment at all. Primary treatment refers to the separation of large solids. Only 17% include

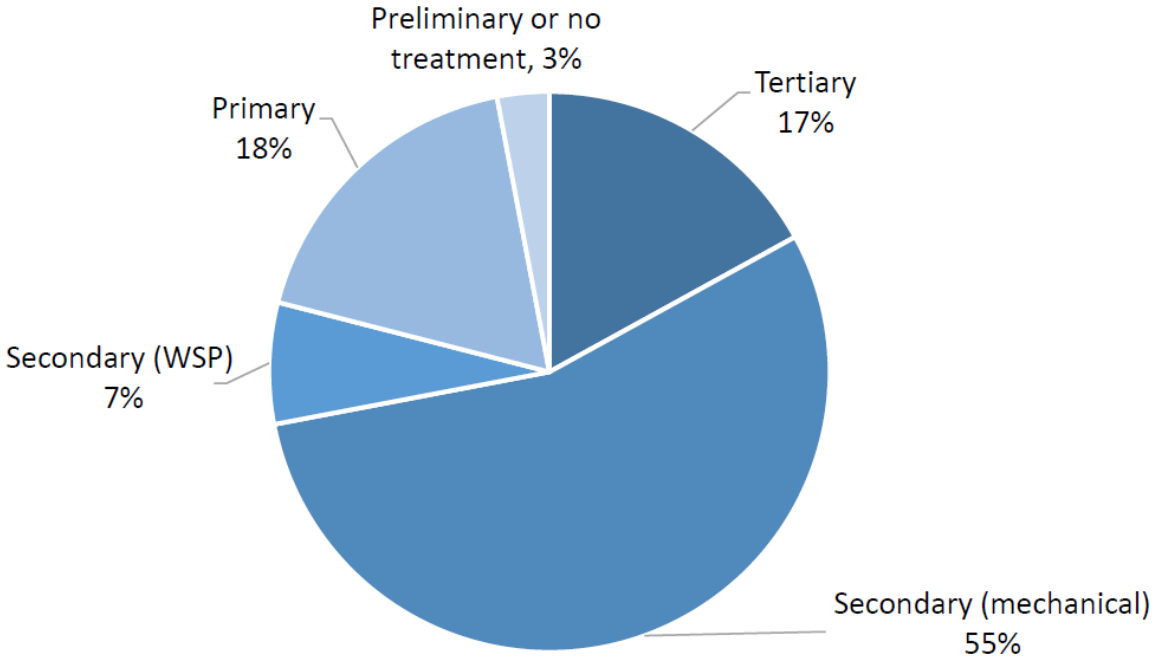

FIGURE 1.1: LEVELS OF WASTEWATER TREATMENT ACROSS CANADA [4]

an amount of tertiary treatment (Figure 1.1) [4]. Tertiary or advanced treatments include disinfection and biological nutrient removal.

Although the first BNR plant in North America was constructed in Canada and the environmental concerns of untreated nutrient rich water was well understood, this did not stimulate the development of new wastewater treatment technologies in Canada. The municipal water sector in Canada tends to be risk-adverse and slow to adopt new technologies. This has created a verging market for the upgrading of Wastewater Treatment Plant (WWTP) rather than the construction on new ones. It is estimated that 1 in 4 wastewater treatment facilities in Canada will require substantial upgrades. The total cost of these upgrades is estimated to be $5.5 billion [4].

Technological retrofits represent an attractive opportunity to meet the demands of future regulations. The two main restrictions with retrofits are cost and size. The city of London, Ontario retrofitted its Oxford Pollution Control Plant (previously a conventional activated sludge process) with Membrane Bioreactors. This has enabled the plant to double its capacity with minimal footprint expansion [5]. Despite their improvements over the

years, Membrane Bioreactors remain an energy intensive and expensive technology, as membrane cartridges require replacement every 8 years [3]. Future solutions will require module and scalable designs, decentralized facilities and flexibility.

In recent years, there has been a shift in attitudes in water engineering from one of waste treatment to one of resource recovery. This shift is due to the increase in the price of phosphorous as it has been identified as a non-renewable resource. Phosphorous can be recovered in wasted activated sludge or from digested sludge. A study of 11 wastewater treatment facilities in North American that practiced phosphorous recovery, shown a return on investment between 7 to 14 years [3]. While nutrient concise practices in municipal wastewater are important, they only account for 5% to 20% of the total nutrients in the watershed. Agricultural conservation practices can play a much bigger role, costing 7 to 10 times less [6]. The recovery of nitrogen is not cost-effective when comparing the cost of ammonia recovery versus nitrogen-compound removing processes such as the Anammox process.

1.2 Bioreactors in Water Engineering

Conventional biological nutrient removal bioreactors represent improvements to conventional activated sludge processes (CAS), but are still beholden to some of the same limitations. It is a technology still reliant on the same large concrete reactors with rectangular cross-sections. These reactors have un-uniform flow patterns, which have the potential for stagnancies. These stagnancies can produce anaerobic conditions due to a lack of oxygen transfer. This can introduce new species of microbes that disrupt normal microbial activities. The new species can also produce undesirable toxic products. Figure 1.2 demonstrates the kinetic energy field in a reactor with a rectangular cross-section using a Computerized Fluid Dynamics (CFD) model [7]. The darker regions represent low kinetic energy.

The opportunity created by the need to retrofit old facilities has sparked research into different technologies including Biofilms, Membrane Bioreactors (MBR) and Algae-

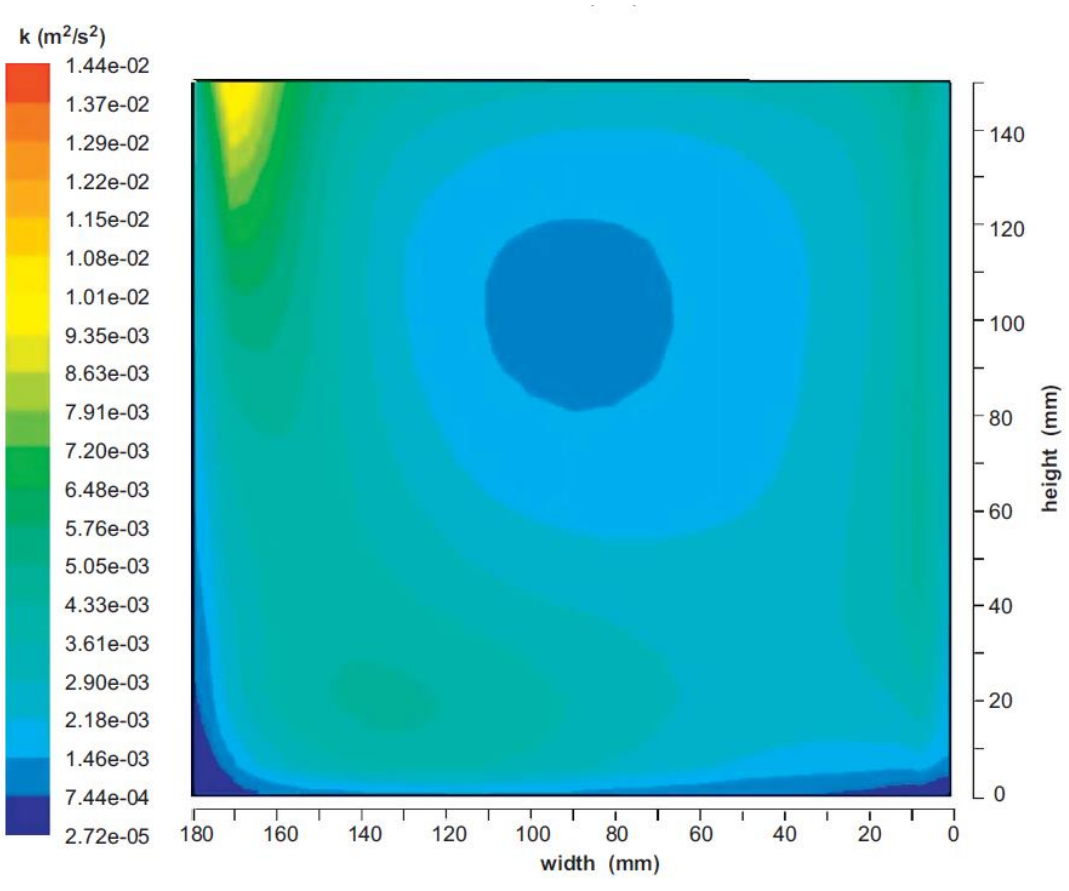

FIGURE 1.2: CFD OF A RECTANGULAR REACTOR [7]

based technologies. Biofilm processes introduce a material, such as media, that develops a biological film. These films develop higher concentrations of bacteria than suspended-growth populations. These biofilms can also assist in the development of slow-growth bacteria, which may play an important role in nitrification. MBR utilize a membrane to separate the sludge from the effluent, replacing the clarifier unit in the CAS process. Retrofitting CAS facilities with membranes is very common and has a proven record of accomplishment. Algae-based technologies depend on different algae cultures, being suspended or fixed, rather than microbial cultures. Algae-based technologies produce algae biomass, which can be used for methane production, composting, production of liquid fuels or as animal feed.

Vertical bioreactors present a fundamental change in water engineering, utilizing a circular cross section rather than a rectangular. As their name indicates, vertical bioreactors have a vertical orientation, which reduces their footprint while retaining the same reactor volume. Reza collected the following information in Table 1 [8] about the footprints of

different BNR facilities. Reza has also shown vertical bioreactors to be effective Biological Nutrient Removal (BNR) bioreactors with high removal efficiencies of phosphorus (90%) and nitrogen-compounds (95%) [9].

Treatment Method	Design Flowrate/area (m^3 / m^2/d)
Multi-stage vertical bioreactor	180
SBR BNR	5.43
3-Stage Bardenpho	0.031
5-Stage Bardenpho	2.15
Modified Bardenpho	12.42
Modified UCT	5.74
Biolac Extended Aeration	1.0

TABLE 1: DESIGN FLOW RATES AND FOOTPRINTS OF DIFFERENT BNR REACTORS [8]

1.3 Thesis Overview

The objective of this study is to analyze the flow dynamics of a multi-stage vertical bioreactor through the Residence Time Distribution (RTD) technique. This technique is a diagnostic tool that identifies regions of stagnation and by-passing within a reactor. A tracer, representative of the flowing fluid, is injected in the feed stream of the bioreactor and monitored as it exits each stage. The three stages of the reactor are outlined in the 3D model of Figure 1.3. Statistical analysis of the observed concentration change creates a series of curves that represent the true mixing profile of the vertical bioreactor. Through the study of these curves, different qualitative characteristics of the reactor can be found such as, the rate of by-passing or the fraction of dead space. After the mixing profile of the reactor is produced, it will be compared to different reactor models to determine a fit.

Due to the cylindrical geometry of the vertical bioreactor, it is proposed to exhibit a high level of mixing. With this high level of mixing, there should be no significant indication of by-passing or dead space. The ideal continuous stirred tank reactor will approximate the observed mixing profile.

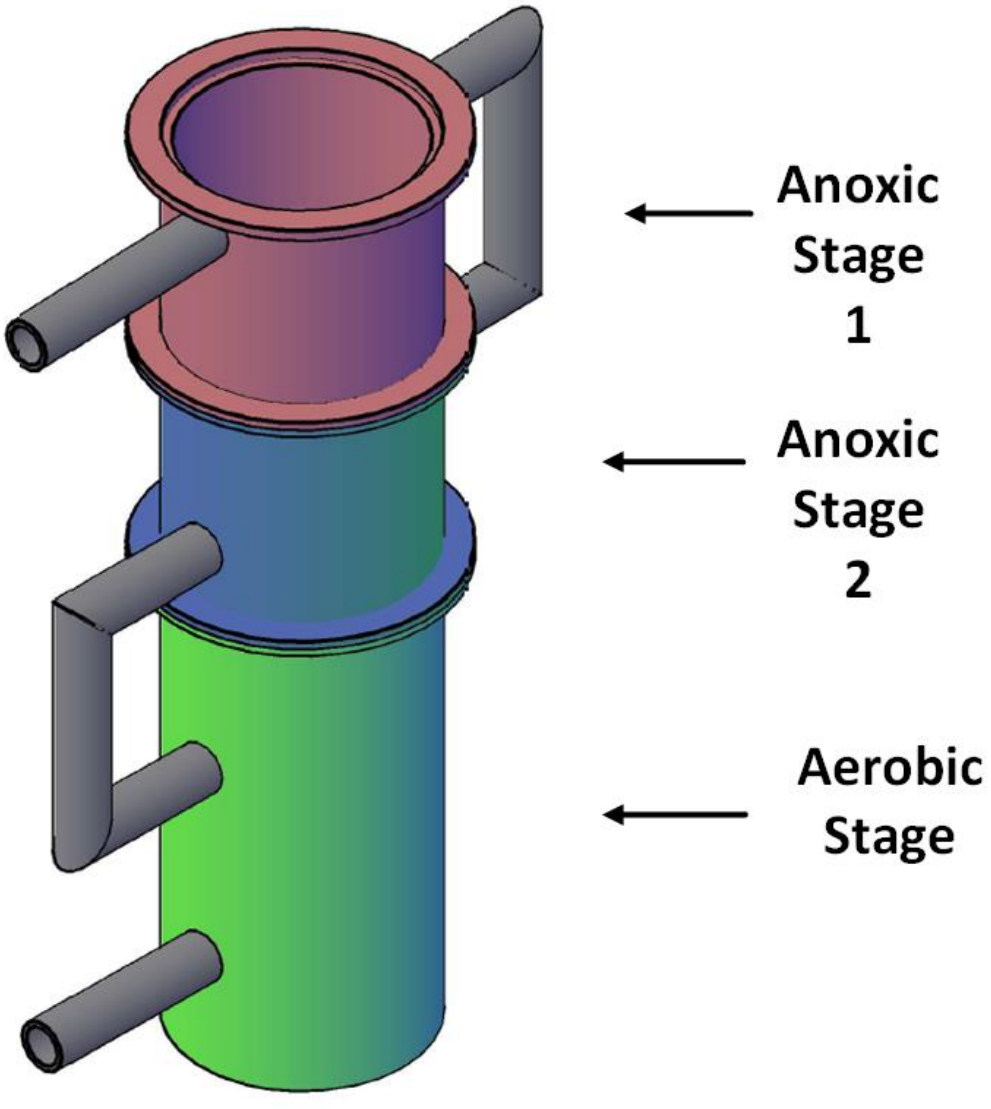

FIGURE 1.3: 3D MODEL OF STAR REACTOR

Adoption of advanced technologies for the removal of nutrients will take place in Canada. Due to the high capital and excavation costs, retrofitting current facilities is an attractive alternative to the construction of new facilities. The retrofitting of current facilities poses a unique challenge where footprint, costs and effective removal rate are of great concern. The vertical bioreactor seeks to address these concerns.

Chapter 2 : Literature Review

2.1 Wastewater Bioreactors

In water engineering, no technology fits every situation. There will always be a trade-off between nutrient removal efficiencies, system complexity and costs. As a result, there are many investigations into different avenues of treatment. The most promising technologies includes Sequencing Batch Biofilm Reactors, Moving Bed Biofilm Reactors, Membrane Bioreactors and Algae-based technologies. The criteria for examining a bioreactor include simplicity, expense, scale, and nutrient removal efficiencies.

2.1.1 Moving Bed Biofilm Reactors

A Moving Bed Biofilm Reactor (MBBR) functions and operates very similarly to a [10]Conventional Activated Sludge (CAS) reactor. MBBR include a biofilm that grows on a small-suspended carrier (Figure 2.1) that is in constant motion throughout the reactor volume. The media retain microbial populations which aides in the growth of slower

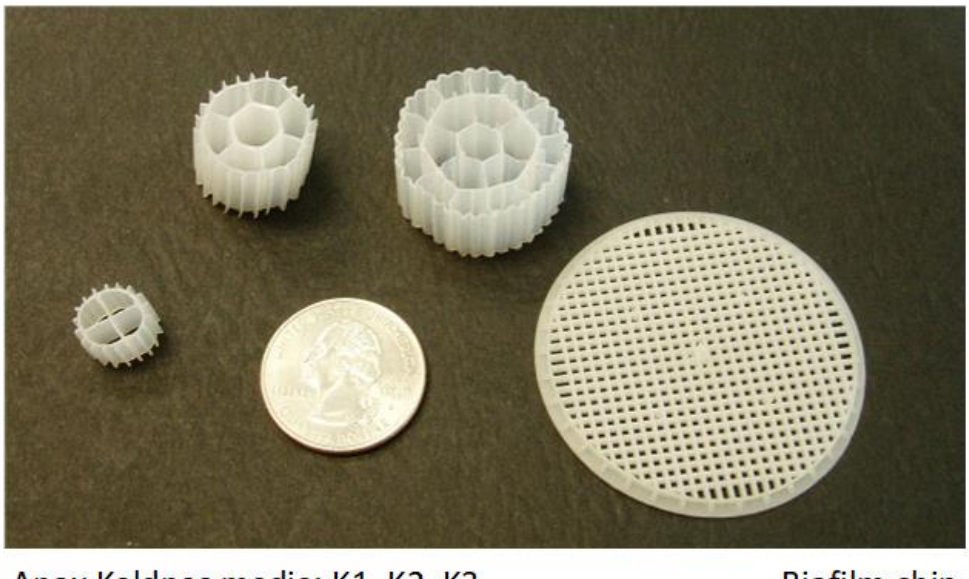

FIGURE 2.1: SAMPLE MEDIA [10]

developing organisms such as nitrifying bacteria. It is a cost effective and easy way to upgrade CAS reactors. MBBR have been shown to have an effect removal of 75-97% BOD and 40-85% total nitrogen [11].

In a MBBR, there is a constant collision of media within the tank. This shearing prevents the development of biofilm on the media's outer surface area making the internal surface area of the media an important design factor [11]. Younge has researched the effect of different carrier types and found many noteworthy discoveries [12].

- The highest surface area to volume carriers exhibit the highest level of clogging
- Cellular activity rates of Ammonia Oxidizing Bacteria (AOB) were not affected by carrier type
- Reactor performance is best described by the viable AOB cell coverage of the carriers

The prominent media material is plastic, but they provide a low denitrification capacity in MBBR. Research shows that sponge is a suitable alternative where it has increased nitrogen removal from 72-86% and phosphorous removal from 70-85% [13]. Also from that study, the sponge material showed less pore blocking and cake layer resistances.

One of the disadvantages of a MBBR is the lack of research in the mechanism of biofilm detachment. It is a complicated function of hydrodynamics, flow velocity, biofilm morphology and support characteristics [11]. An additional liquid-solid separation unit is required to recover media and return them to the reactor entrance.

2.1.2 Sequencing Batch Biofilm Reactors

A Sequencing Batch Biofilm Reactor (SBBR) is a modification of the traditional Sequencing Batch Reactors (SBR) in which a tank cycles through stages of filling, aeration, settling, drawing and idling as outlined in Figure 2.2. The distinction for a SBBR from the SBR is the inclusion of a media material as with a Moving Bed Biofilm Reactor. This technology seeks to combine the advantages of an activated sludge process with a biofilm process. SBBR has

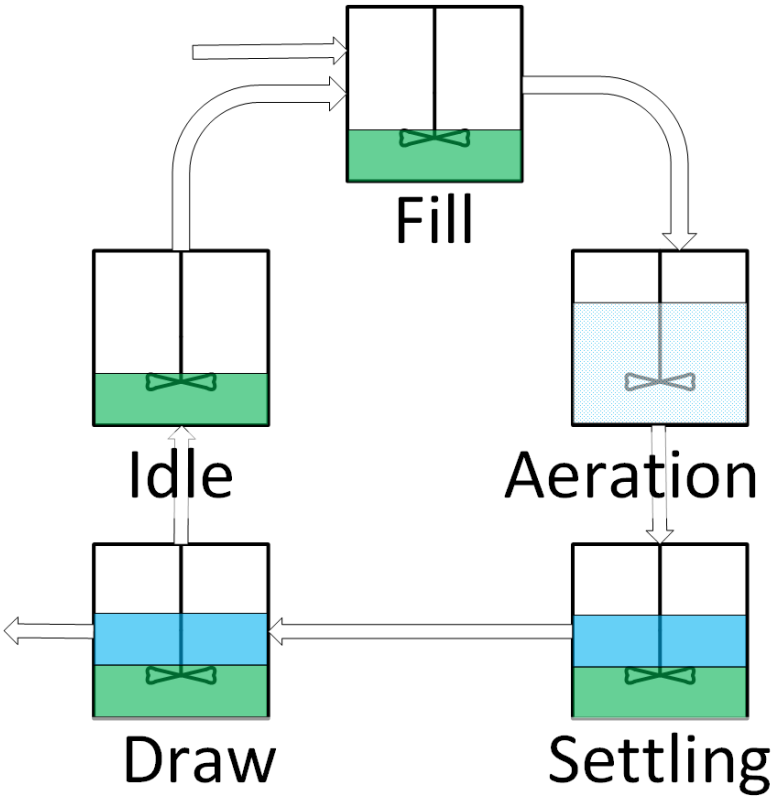

FIGURE 2.2: SEQUENCING BATCH REACTOR SCHEMATIC

been shown to be more efficient than the activated sludge SBR, but at the cost of an increase in the process knowledge requirement [14].

The activated sludge and the attached growth cultures in a SBBR are identical, but at different proportions [15]. Anaerobic Ammonium Oxidation (ANAMMOX) bacteria, bacteria that reduce ammonium directly to nitrogen gas, are found in higher concentrations in the attached growth [15]. SBBR can achieve high levels of total nitrogen and total phosphorous removal (94% and 97%) as they can provide a better environment for Phosphate Accumulating Organisms (PAO), denitrifying phosphate accumulating organisms (DPAO), nitrifying and denitrifying bacteria without carbon source competition [16].

There are several drawbacks of SBBR as they are prone to clogging [17]. There is also the potential of floating or settled sludge in the effluent as there is no clarifier unit in the design [18].

2.1.3 Membrane Bioreactors

Membrane bioreactors (MBR) are likely the most popular bioreactors and have attracted a large amount of research. MBRs are recognized as the replacement of the secondary clarifier of the conventional activated sludge process with membrane filtration [19]. MBRs are an attractive option for retrofitting conventional plants due to its small footprint and high quality effluent [20].

One of the main advantages of the MBR over the Conventional Activated Sludge (CAS) process is a higher concentration of slowly growing microbes [21]. This is significant as nitrifying bacteria exhibit this behaviour.

The best phosphorous removal performance comes from incorporating MBR in hybrid configurations. Membranes that utilize well established Biological Nutrient Removal processes, such as the University of Cape Town, have been shown to have phosphorous removal rates of 88% [22] and 87% [23]. Without this additional consideration, the phosphorous removal for MBR can be quite low at 53% [24]. Bracklow performed a series of four different recirculation schemes with different arrangements of three stage reactors (anaerobic\anoxic\aerobic) and found that there were insignificant differences in nutrient removal rates between schemes. The average removal rates were 97% COD, 88% nitrogen and 99% phosphorous [25].

Membrane aerated biofilm reactors (MABR) are more complicated technology than MBR. Pressurized air flows on one side of the membrane while water flows co-current on the other side (Figure 2.3). Consequently, the membrane itself becomes the site of biological growth rather than acting as a separation unit. A biofilm then develops on the surface of the membrane. There are significant increases in aeration rates with a MABR when compared to bubble aeration all in a smaller tank size [26]. Through careful control of the dissolved oxygen levels, both nitrifying and denitrifying kinetics can take place in a single stage [27]. MABR have shown to have a significant power reduction of up to 86% when compared to CAS mainly due to the efficiencies for aeration [28].

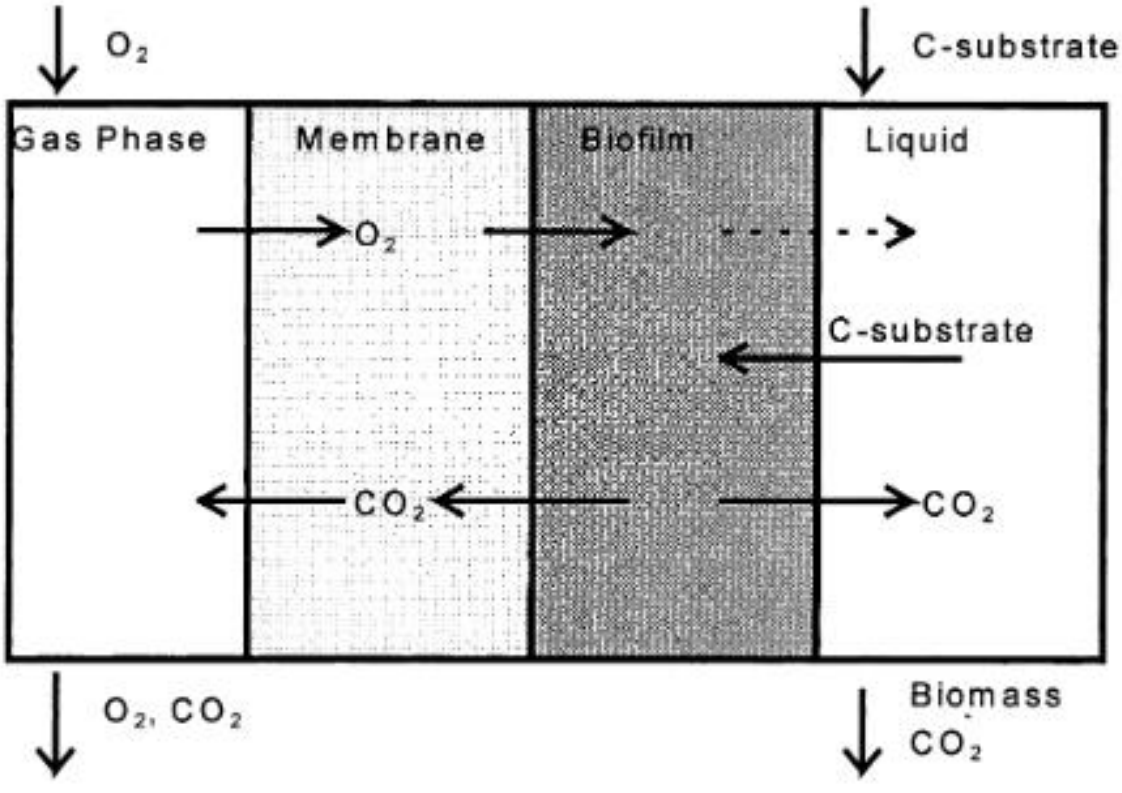

FIGURE 2.3: MEMBRANE AERATED BIOFILM REACTOR [28]

The main difficulty with membranes are their high costs. Their expense comes from two sources, a high initial cost of the modules ($50 US/m^2 as of 2005 [29]) and high maintenance costs. The membrane cartridges require replacement every 8 years [3]. The high maintenance cost comes from the energy demand to deal with membrane fouling. Even after a decade of research and extensive reviews([30]–[32]), there is no consensus on membrane fouling. A lack of standardized fouling characterization method has led to results that sometimes conflict.

2.1.4 Algae-based Technologies

The application of algae cultures for wastewater treatment has become a developed technology ([33], [34]), but it has not been applied at the pilot and full-scale. The mechanism of phosphorous removal by algae is illustrated in Figure 2.4. Algae cells reach a saturated stage of phosphorous uptake at about 3% phosphorous by dry weight with a critical minimal level of 1% [35]. Algal treatment can take place in a variety of techniques, as

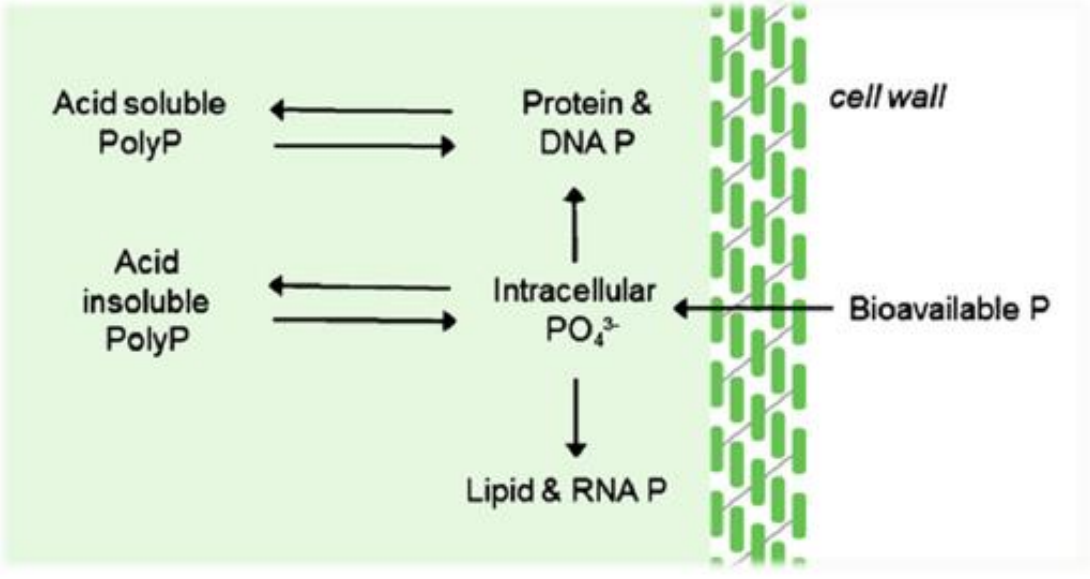

FIGURE 2.4: MECHANISM OF ALGAL PHOSPHOROUS REMOVAL [32]

a suspended solution or as a biofilm. A system using a microporous tissue for cell immobilization has been shown to remove 90% of phosphorous and 69-78% nitrogen [34]. Algal growth can even be incorporated in Membrane Bioreactors (MBR) for increased effluent efficiencies (92% nitrogen and 91% phosphorous removal) [36].

Wastewater represents a cheap feed for algae biomass production. This biomass can have multiple applications including methane production, composting, production of liquid fuels, and as animal feed [37]. There are some disadvantages to this technology. Algae growth is highly dependent on temperature and exposure to light. This creates a large challenge for locations with conditions of lower seasonal temperatures and sun exposure present at higher latitudes. Algae-based systems is still a technology in its infancy, there lacks research on long term studies and at different flow regimes [38]. The technology has still attracted research despite these deficiencies.

2.2 Biological Nutrient Removal

Biological Nutrient Removal (BNR) is an increasingly important field of research. Regulations regarding the concentrations of nutrients in the wastewater industry have become more stringent with chemical or biological treatments available. Biological treatments are an inexpensive and effective solution to chemical treatments [39].

The two nutrients in wastewater are nitrogen and phosphorous compounds. Poor nutrient treatment can lead to environmental catastrophes including eutrophication. Eutrophication is caused by the over stimulation of algae growth due to the higher concentrations of nutrients. This higher concentration of algae eventually decomposes, creating layers of decaying material on the bottom of the body of water. High Algae concentration have now changed the body of water to a dark green colour. The increased decomposition has released hydrogen sulfide compounds producing an unpleasant odour. This darkening of the water, decreases the mass transfer of oxygen into the water. The initial wildlife response can be deceptive with increased fish populations from the increased food source. The increase in microbial activity and the decrease in mass transfer reduces the concentration of dissolved oxygen. Fish can no longer obtain the oxygen they require for respiration, increasing the amount of decaying material.

Phosphorous and nitrogen play two different roles in microbiological life and as such require two distinct sets of reaction kinetics.

2.2.1 Biological Nitrogen Removal

Conventional nitrogen-compound removal has been treated as a three-stage process: Hydrolysis and Ammonification, Nitrification and Denitrification (Figure 2.5). The first two processes take place under aerobic conditions (presence of dissolved oxygen) while the Denitrification step takes place under anoxic conditions (no dissolved oxygen but the presence of other dissolved oxygen compounds). Hydrolysis and Ammonification is the process for the conversion of particulate organic nitrogen-compounds into soluble

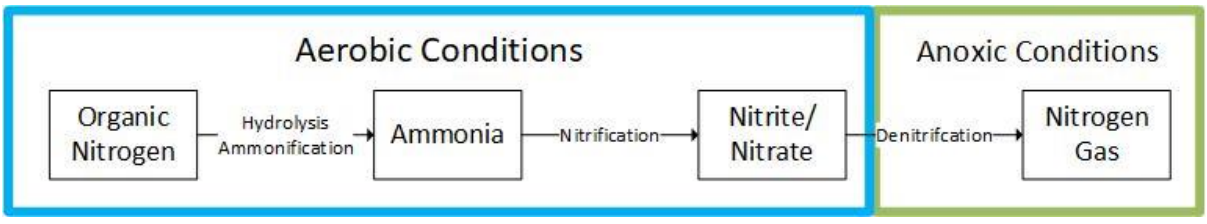

FIGURE 2.5: BIOLOGICAL NITROGEN REMOVAL FLOW CHART

ammonia. Ammonia is then oxidized by nitrosomonas and nitrobacter bacteria into nitrites and nitrates. Heterotrophic bacteria can than reduce nitrates into nitrogen gas [40].

Nitrogen removal processes had been the same for many years but they were drastically changed with the introduction of anaerobic ammonium oxidation (Anammox) processes. In the absence of dissolved oxygen, certain Planctomycete bacteria are cable of consuming ammonia instead. These processes are highly exergonic which means they go from a high-energy state to a low-energy state. These types of reactions are referred to as spontaneous and will proceed forward without any additional intervention [41].

In the denitrifying stage, Anammox bacteria utilize nitrite as an electron acceptor to yield nitrogen gas as described in the following chemical reaction:

$$NH_4^+ + NO_2^- \rightarrow N_2 + 2H_2O$$

The second important reaction by Anammox bacteria is that they can utilized carbon dioxide (CO_2) as a carbon source. This frees up the other carbon sources to be used for other reactions such as being converted to volatile fatty acids to be consumed by Phosphate Accumulating Organism (PAOs) for phosphorous removal. The reaction is described as the following:

$$CO_2 + 2NO_2^- + H_2O \rightarrow CH_2O + 2NO_3^-$$

A few technologies that utilizes these processes include: the single reactor system for high-rate ammonium removal over nitrite (SHARON), the completely autotrophic nitrogen removal over nitrite (CANON) and the nitrifier denitrification in the presence of NO_x (NO_x). What these technologies have in common is the utilization of the Anammox

bacteria and the conditioning of partial nitrification. They require partial nitrification as the Anammox bacteria consumes nitrites and not nitrates. The overall stoichiometry of an Anammox reaction has been found after 336 and 531 days in a batch reactor as [42]:

$$NH_4^+ + 1.32NO_2^- + 0.066HCO_3^- + 0.13H^+ \rightarrow 0.0066CH_2O_{0.5}N_{0.15}S_{0.05} + 1.02N_2 + 0.26NO_3^- + 2.03H_2O$$

Anammox-based processes may reduce energy cost for nitrogen removal by 35% and carbon requirements by 90% [3].

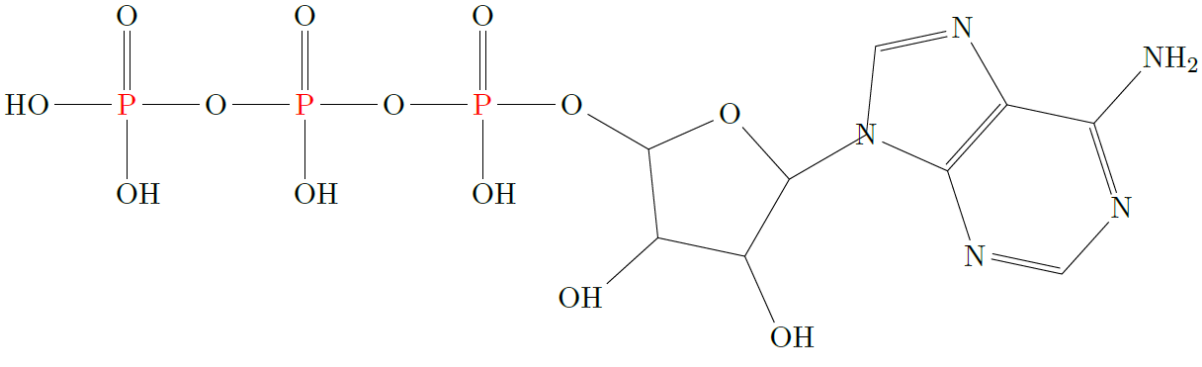

FIGURE 2.6: SKELETAL STRUCTURE OF ATP

2.2.2 Biological Phosphorous Removal

The main biological role of phosphorous is facilitating the storage of energy. Cells including microbes use a compound called Adenosine Triphosphate (ATP). The skeletal structure can be found in Figure 2.6. There are three phosphorous bonds available in ATP. These bonds require a large amount of energy to form and likewise releases a lot of energy when broken. When ATP under goes hydrolysis into Adenosine Diphosphate (ADP), the reaction releases 7.4kcal/mole [43]. ADP still has two more phosphorous bonds, which can further hydrolyze to release more energy.

All heterotrophic bacteria in the activated sludge utilize phosphorous but at relatively low concentrations (0.02 mgP/mgVSS) with a removal rate about 15-25%. Additional phosphorous removal requires selecting for Phosphorous Accumulating Organisms (PAOs). PAOs have a higher utilization rate of phosphorous (0.38mgP/mgVSS) [44]. The growth of PAOs need special considerations for the selectivity.

In the anaerobic stage (Figure 2.7), PAOs uptake volatile fatty acids (VFA) to create long carbon chains called polyhyrdoyalkanoates (PHA). The cells use their internal energy by breaking phosphorous bonds which releases phosphorous in the wastewater. Thus the PAOs absorb VFA which other heterotrophic bacteria cannot [44].

In the aerobic stage (Figure 2.7), PAOs digest the newly formed PHA with the dissolved oxygen playing the role of an electron acceptor. This digestion releases energy for the cell, which it can use for cell growth. The excess energy is stored in the form of poly-phosphates (such as ADP and ATP) which facilitates phosphorous transfer from the wastewater into the cell. Phosphorous is than fully removed from the BNR reactor as it is trapped in wasted sludge [44].

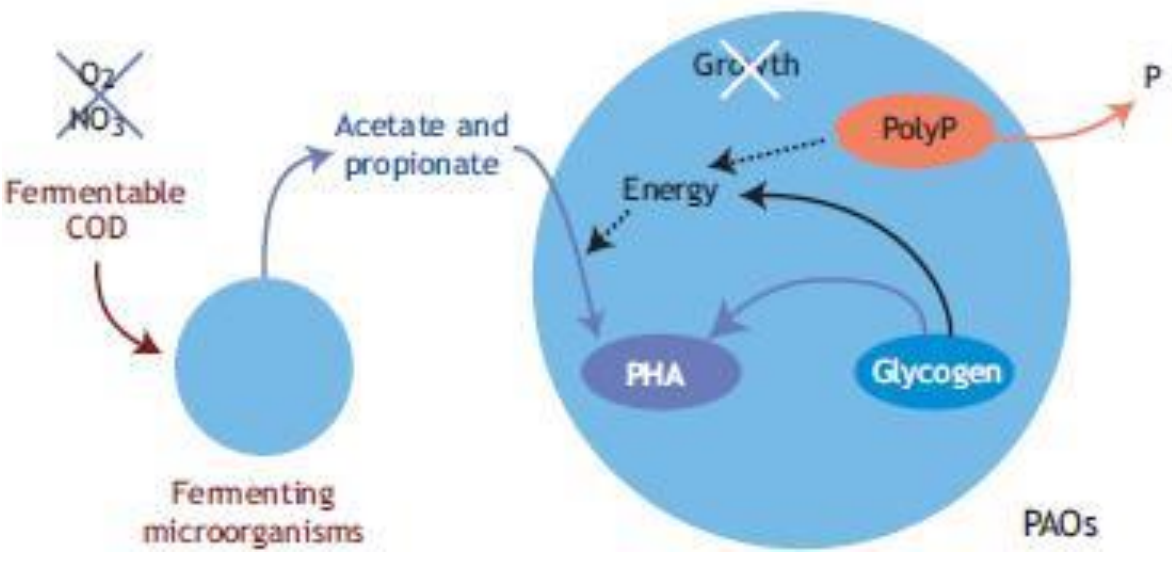

FIGURE 2.7 BIOCHEMICAL MODEL FOR PAOS UNDER ANAEROBIC CONDITIONS [39]

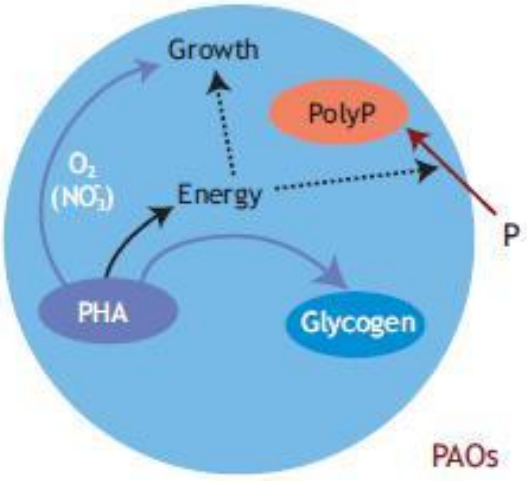

FIGURE 2.8: BIOCHEMICAL MODEL FOR PAOS UNDER AEROBIC CONDITIONS [39]

Organisms in the Acinetobacter group have been widely considered as the ideal PAO population [45]; however, Nguyen has found that Tetrasphaera bacteria in many different Enhanced Biological Phosphorous Removal (EBPR) plants. This is of interest as Tetrasphaera exhibit a more flexible substrate uptake [46]. Through a gene study, it was confirmed that Tetrasphaera is capable of denitrification [47]. These are important developments as they can change the model of EBPR and affect the design of Biological Nutrient Removal (BNR) treatment plants in the future.

2.2.3 Activated Sludge Models

The microbial kinetics of wastewater treatment processes have been a field of study for many years and the most influential model is the Activated Sludge Model (ASM). The initial ASM model was limited as it only pertained to the removal of carbon components. It did however introduce the matrix model, which simplifies the expression of the series of different microbial reactions taking place. A sample of the matrix can be found in Table 2. A mass balance, for each component j, can be constructed by following a column. Each column will contain coefficients that need to be multiplied by the process rate ρ_j ($ML^{-3}T^{-1}$) at the end of the row. The mass balance is than the summation of the product of the coefficients and process rates. This is a significant development as it organizes the reactions where each column represents the mass balance for a component and each row represents

a specific reaction rate. Organization is required as more development into the field increases the number of reactions and substrates, which become difficult to follow.

The different reactions are based on the Monod equation, which is defined as:

$$\mu = \mu_{max} \frac{S}{K_S + S} \tag{2.1}$$

where μ is the growth rate (t^{-1}), μ_{max} is the max growth rate (t^{-1}), S is the substrate concentration (M/L^{-3}) and K_S is the half-velocity constant (M/L^{-3}).

The development in activated sludge models required the addition of nitrogen and phosphorus removal kinetics which were included in the ASM2D model [48]. An increased level of complexity accompanies additional reaction kinetics. As an example, the Activated Sludge Model for Nitrogen (ASMN) models 3 different groups of microbes, 18 biological processes, 20 components and contains 54 parameters in total [49]. The ASMN includes significant advances such as the activities of ammonia-oxidizing bacteria (AOB). This creates a model that is more robust, allowing increased accuracy in the modelling of Biological Nutrient Removal processes. As with any model, an increase in the number of parameters produces a more complicated model.

An Activated Sludge Model can be convenient tool as the reaction kinetics in wastewater treatment reactors can be complicated; however, as with any model, the number of parameters dictates their practicality. These models can easily become cumbersome and difficult to work with.

Component →j	**1**	**2**	**3**	**Process Rate,**
	X_B	**S_S**	**S_O**	**ρj ($ML^{-3}T^{-1}$)**
Process ↓i				
Growth	1	$\frac{1}{Y}$	$-\frac{1-Y}{Y}$	$\frac{\mu S_S}{K_S + S_S} X_B$
Decay	-1		-1	bXB
Observed Conversion Rates ($ML^{-3}T^{-1}$)	$r_i = \sum_j r_{ij} = \sum_j v_{ij}\rho_j$			
Stoichiometric Parameters: **True growth yield: Y**	Biomass (ML^{-3})	Substrate (ML^{-3})	Oxygen (ML^{-3})	Kinetic Parameters: Maximum Specific growth rate: μ (T^{-1}) Half-velocity constant: KS (ML^{-3}) Specific decay rate: b (T^{-1})

TABLE 2: ACTIVATED SLUDGE MODEL (ASM) TABLE [50]

2.3 The Residence Time Distribution

2.3.1 Definition

Continuous flow systems are categorized into two simplified models, the Plug Flow Reactor (PFR) and the Continuous Stirred Tank Reactor (CSTR). The CSTR model requires the assumption of perfect mixing throughout the reactor, while the PFR model requires the assumption that elements of fluid flow into the reactor travels in parallel paths and they leave at the same moment. In reality, most reactors do not well represent either of these cases very well. The assumptions are made however to significantly reduce the complexity of a model. Danckwerts [51] and Zweitering [52] developed a technique to better understand the behavior of flow with the Residence Time Distribution (RTD). This is an incredible development as it represents a diagnostic tool that accurately describes the true mixing profile.

The technique requires the introduction of a traceable element into the continuous flow reactor. The traceable element is then measured as it exits with a sensor that is specific to the parameter that the element is traceable by. For more information on the process of tracer selection, please refer to Section 3.1.1 Tracer Selection. A C-diagram can be created by plotting the concentration of the tracer at the exit versus time. The first RTD function, the Probability Density Function (E (t)), can then be obtained from dividing the concentration of the tracer by the area under the C-diagram (equation 2.2). The area under the C-diagram (or the integral) represents the mass of the tracer injected [53]. The E (t) function represents the probability of the tracer exiting the system at time (t) when excited by a single pulse.

$$E(t) = \frac{C(t)}{\int_0^\infty C(t)dt} \tag{2.2}$$

The second RTD function is the Distribution Function (F (t)). The F (t) function represents the fraction of tracer that has exited the reactor at any time. It represents the cumulative sum of the E (t) and thus can be represented by the following equation. It also

represents the system response to a step change. A pulse is a quick (as close to instantaneous as possible) injection of a set volume of tracer while a step change is the continuous injection of a tracer for the duration of the experiment

$$F(t) = \int_0^t E(t)dt \tag{2.3}$$

2.3.2 Application of RTD Measurements

The main applications for RTD measurements, as outlined by Missen, are the following [54]:

1. As a diagnostic tool for the detecting and characterizing flow behavior
2. The estimation of values of parameters for non-ideal flow models
3. The assessment of performance of a vessel as a reactor

The graphs that represent the RTD functions for a reactor are important tools in identifying issues with the mixing. One such example was when Goswami found the RTD for a constructed wetland described a dead space in the reactor to be between 0% and 41% of the entire volume [55]. The theoretical residence time, measured by the volume of the reactor divided by the fluid volumetric flow rate, was found to be larger than the experimentally observed mean residence time. This suggests that the tracer did not travel throughout the entire volume. The volume of which the tracer did not travel through is referred as the dead space because no reaction would take place there.

The simplest application is comparing the reactors RTD to that of the ideal graphs. It can provide a quick and simple visualization of the discrepancy from the ideal conditions.

The true value of the RTD experiment comes from the creation of the parameters for the non-ideal flow models. Non-ideal flow models seek to represent the flow of real reactors. These models rely on the fact that every flow model has a unique RTD but not every RTD has a unique flow model. "Real reactor" models are generated and their RTD are calculated. These models are then compared to the experimentally collected results. If the RTD that describes the non-ideal model also fits the experimental data, then the non-ideal model also fits flow dynamics of the reactor.

The final application of the RTD is the assessment of the reactors performance. This assessment relies on three factors:

- Whether the fluid behaves as a segregated or a maximum mixedness fluid
- When mixing occurs
- The overall reaction order

A first order reaction is expressed as the following:

$$r_a = kC_a$$

where r_a (M/s) represents the reaction rate, k (1/s) the rate constant and C_a (M/l) the concentration of component A. In this instance, only the RTD effects the conversion as the reaction takes place with a single molecule and does not require any collision. For reactions of any other order, the RTD data are not enough [52].

A segregated fluid enters as globules with perfect mixing within each globule but no mixing between globules. This is also referred to as a macro-fluid. A micro-fluid, or a maximum mixedness fluid, has the opposite behaviour where each element is free to mix fully throughout the system (Figure 2.9).

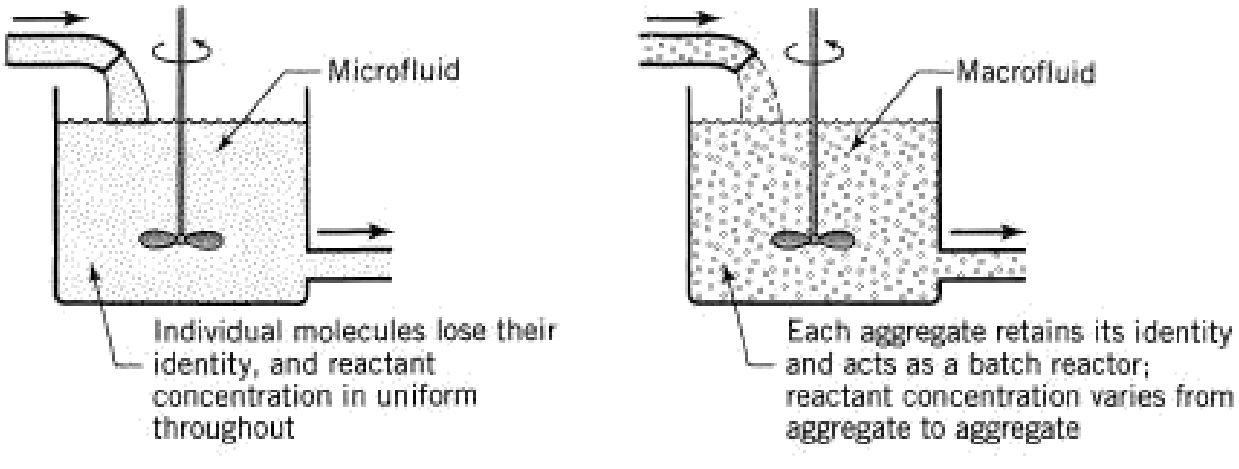

FIGURE 2.9: MICRO VS MACRO MIXING [54]

Reaction Order	Conversion
n < 0	$X_{seg} > X_{mm}$
0 < n < 1	$X_{seg} < X_{mm}$
n = 1	$X_{seg} = X_{mm}$
n > 1	$X_{seg} > X_{mm}$

TABLE 3: MICRO-MIXING EFFECT ON CONVERSION BY REACTION ORDER [56]

The conversion rates for a reaction of order n can vary depending on whether the fluid behaves as a micro-fluid or as a macro-fluid as described in Table 3 [57]. The proof for these relationships is quite complicated as they require modeling both systems and integrating them for a reaction of nth order. The derived model equations can be found in literature [56]. It is also important to note that wastewater treatment reactions are often of mixed order, between first and zero [58]. There is no effect on the conversion in a PFR due to the degree of segregation as a PFR can be considered as a flow of batch reactors with the same residence time.

The effect of mixing timing was first explored by Zwietering [52]. The simplest way to explain it is illustrating a CSTR and a PFR in series (Figure 2.10). No matter the order of the reactors, the overall RTD will be the same. Both systems will have the same overall mixing profile. The second case, where the CSTR precedes the PFR, mixes much sooner than the alternative. If the reaction rate depends on the mixing than the earliness or lateness of mixing will affect the overall conversion.

In reactors with a single reaction, the effects of segregation and earliness of mixing can usually be ignored. For reactors with multiple reactions, such as the vertical bioreactor for the treatment of wastewater, these effects can become more prominent.

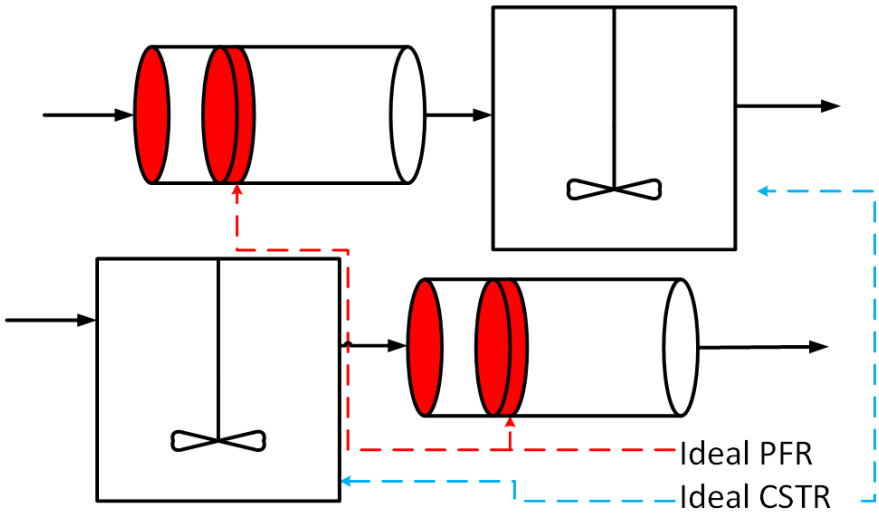

FIGURE 2.10: DEMONSTRATION OF EARLY VS LATE MIXING

2.3.3 Dead Space and By-passing

Dead space and By-passing are two undesirable conditions in a reactor as they represent deviations in the Mean Residence Time (MRT). Dead space is an area stagnation with undesirable reactions. By-passing refers to the formation of channels through the reactor were reagents do not mix and are not utilized for the reaction. Both represent inefficiencies in the mixing profile.

These conditions are understood by modeling them[57]. For the definition of the Mean Residence Time, where MRT is represented by τ (T), volume as V (L^3) and flow rate as v (L^3T^{-1}):

$$\tau = V/v$$

For a reactor exhibiting the condition of by-pass, the portion that is by-passed can be modelled as split stream from the main fluid flow that does not enter the reactor. The overall flow rate (v_0) (L^3T^{-1}) is the summation of the flow that enters (v_E) (L^3T^{-1}) and the flow that by-passes (v_B) (L^3T^{-1}) :

$$v_0 = v_E + v_B$$

where the observed residence time, τ_{obs} (T), is:

$$\tau_{obs} = {}^{V}/_{v_E}$$

$$\tau_{obs} = \frac{V}{v_0 - v_B}$$

followed by the ratio of the two MRTs:

$$\frac{\tau_{obs}}{\tau} = \frac{V/(v_0 - v_B)}{V/(v_0)}$$

$$\frac{\tau_{obs}}{\tau} = \frac{v_0}{v_0 - v_B}$$

$$\tau_{obs} = \tau \times (\frac{v_0}{v_0 - v_B})$$

From the last line, it is apparent that a model with by-passing will have an observed MRT higher than average.

For a system with dead space, part of the volume does not take part in the reaction. The overall volume (V) (L^3) is the summation of the dead space (V_D) (L^3) and the active volume (V_A) (L^3).

$$V = V_D + V_A$$

where the new observed MRT is:

$$\tau_{obs} = \frac{V - V_D}{v}$$

and then comparing the ratio of the two MRTs:

$$\frac{\tau_{obs}}{\tau} = \frac{(V - V_D)/v}{V/(v)}$$

$$\frac{\tau_{obs}}{\tau} = 1 - \frac{V_D}{V}$$

$$\tau_{obs} = \tau \times (1 - \frac{V_D}{V})$$

The last line shows that for a reactor with dead space, the observed MRT will be smaller. As a summary, the following has been shown:

$$\tau_{Dead\ Space} < \tau < \tau_{By-pass}$$

2.3.4 Hold-back and Segregation

Danckwerts had described two additional quantities of interest to describe the RTD: The Hold-back (H) and the Segregation (S) [51]. These quantities are related and both are observed from the Distribution Function (F (t)).

The Hold-back represents the fraction of fluid that spends more time in a reactor than average. It is defined by the following equation where θ is the dimensionless time found by dividing time t (T) by the mean residence time τ (T):

$$H = \int_{\theta=0}^{\theta=1} F(\theta) d\theta \tag{2.3}$$

This quantity is represented as the area under the curve (Figure 2.11) of the dimensionless F (t) between θ = 0 and θ = 1. The two values of the shaded areas are the same due to the symmetry (both labeled as A). The value of H will vary from 0 for plug-flow conditions to 1 for total dead space. The value for H will be e^{-1} (≈ 0.3679) for the ideal CSTR.

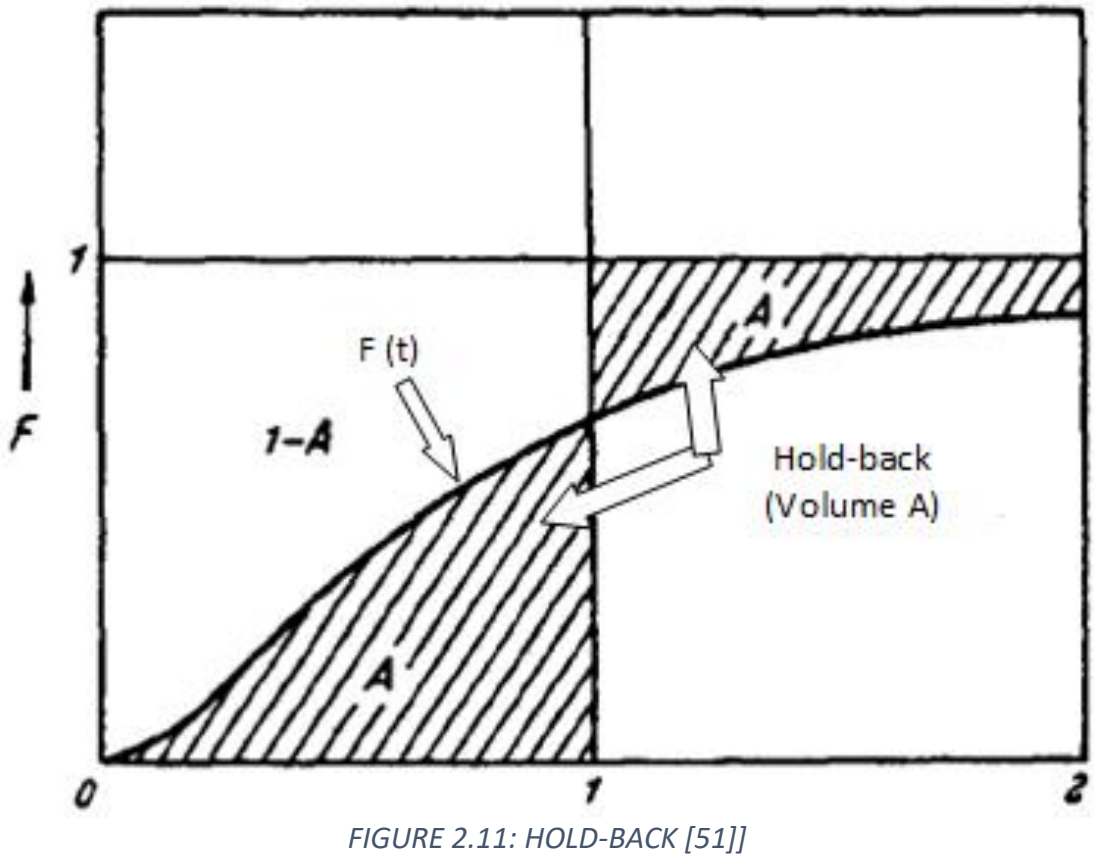

FIGURE 2.11: HOLD-BACK [51]]

The quantity of segregation (S) on the other hand, represents the deviation from perfect mixing from a CSTR. The value is found from superimposing the plot of F (θ) with that of the ideal CSTR which is $F(\theta) = 1 - e^{-\theta}$ (Figure 2.12). There is a second case which represents a reactor with dead space where the reactor F (t) precedes the ideal CSTR F (t) (Figure 2.13). This provides another test for the presence of dead space. The two shaded areas again represent the same value due to the symmetry (labeled A1 in both Figure 2.12 and Figure 2.13). To show that this represents a deviation from the ideal conditions; the value is taken to be as negative. The quantity varies from e^{-1} for plug-flow to -1 for entirely dead space.

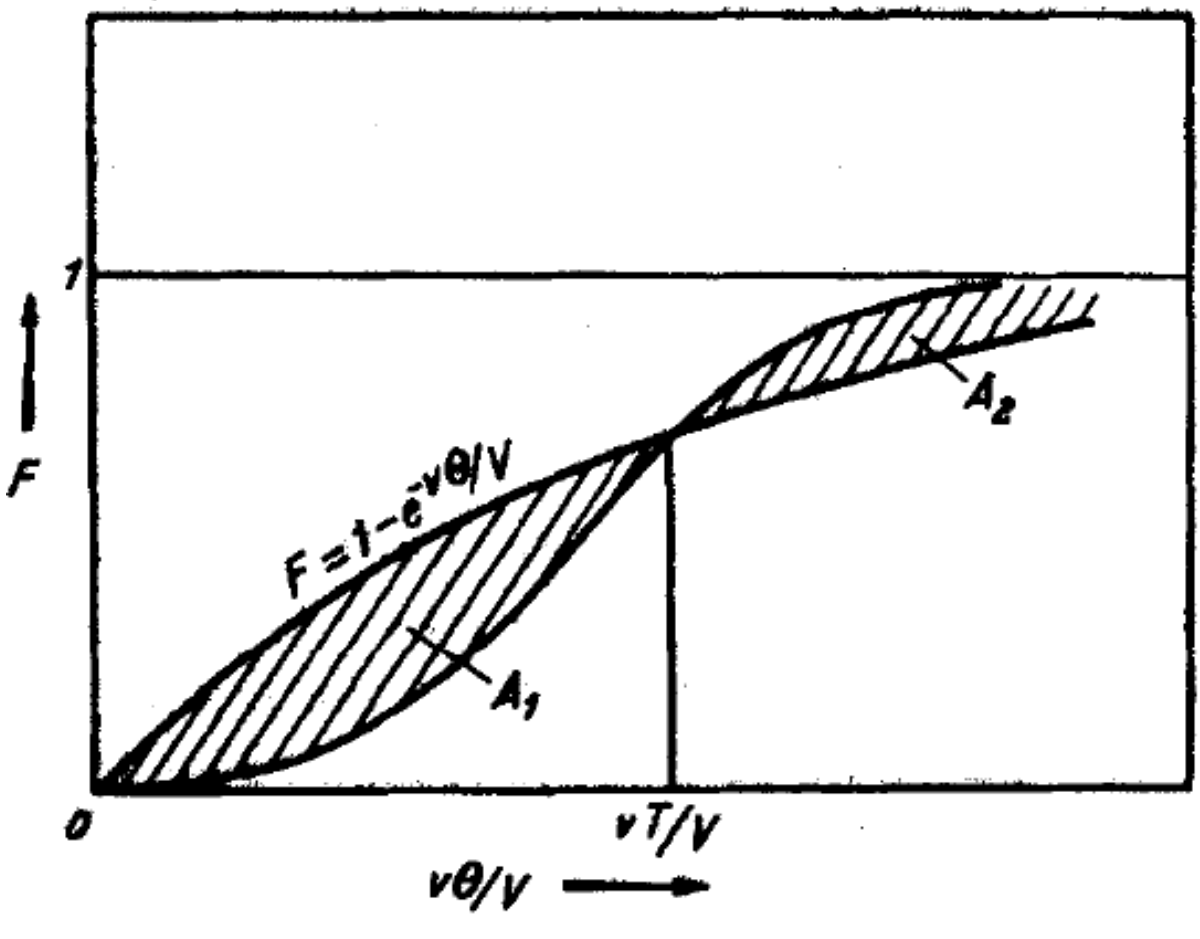

FIGURE 2.12: SEGREGATION QUANTITY (S) [51]

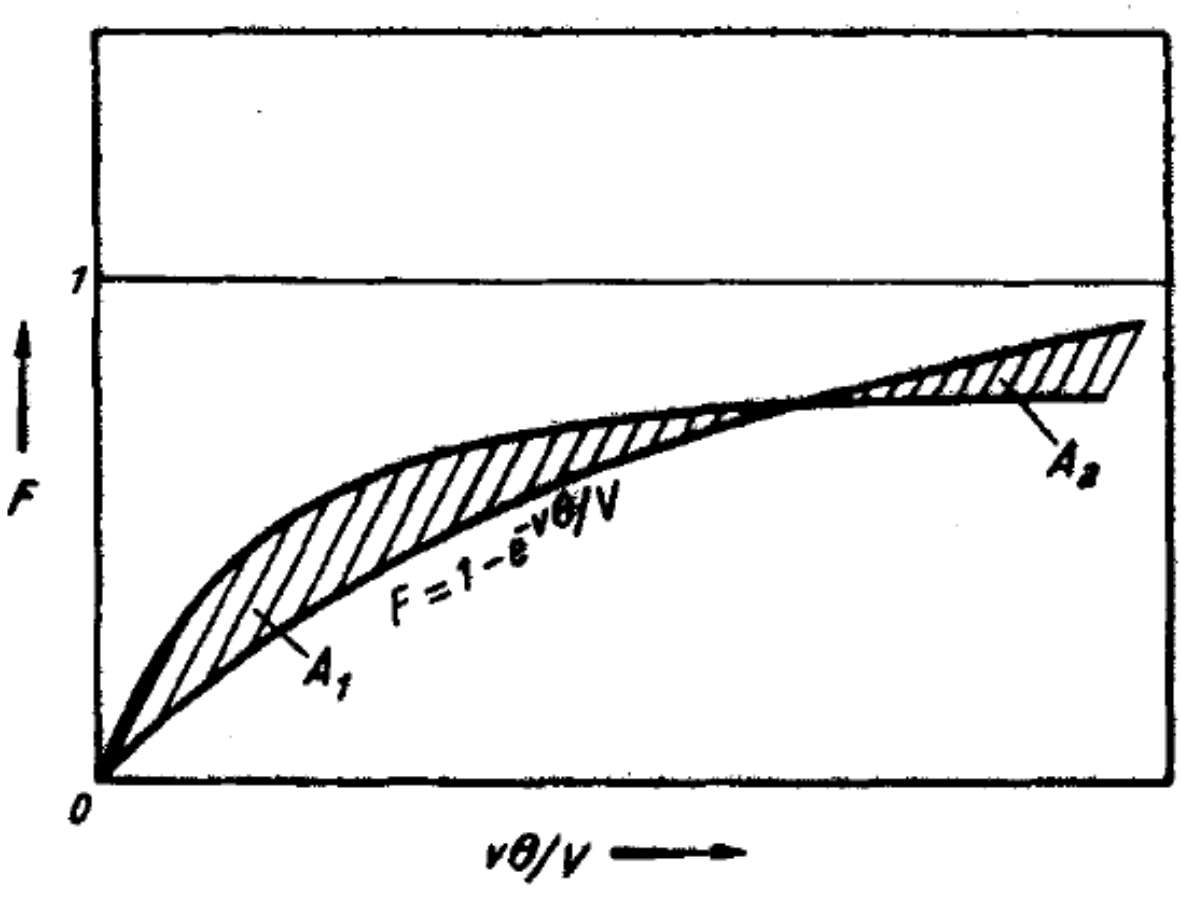

FIGURE 2.13: SEGREGATION QUANTITY (S) WITH DEAD SPACE [51]

2.4 Ideal Models

The first step to modeling the behavior of idealized flow is utilizing the first principles of chemical engineering and performing a mass balance across the reactor. This procedure was outlined by Salmi [53]. Performing the Macroscopic Molar balance for the system obtains:

[accumulation] = [flow in] [flow out] + [generation] (2.4)

alternatively, it can be represented mathematically as:

$$\frac{dN_i}{dt} = -\Delta[\dot{N}_i] + V\sum_{j=1}^{N_R} R_{gen,ij} \quad (2.5)$$

Where$\frac{dN_i}{dt}$ (molT^{-1}) represents the accumulation/consumption of component i in the reactor $-\Delta[\dot{N_\iota}]$ ((mol)) represents the net change in the molar flow rate of component i entering and exiting the reactor, V (L^{-3}) represents the volume of the reactor and $\sum_{j=1}^{N_R} R_{gen,ij}$ (molL^{-3}T^{-1}) represents the sum of all reactions. The molar amount can be represented as concentration by the definition of molar concentration.

$$C_i = \frac{N_i}{V} \tag{2.6}$$

$$N_i = C_i V \tag{2.7}$$

Substituting equation (2.7) into equation (2.5) to obtain:

$$\frac{d(C_i V)}{dt} = -\Delta\left[\dot{C_\iota V}\right] + V\sum_{j=1}^{N_R} R_{gen,ij} \tag{2.8}$$

equation (2.8) can be simplified with the assumption of a constant reactor volume, V (L^3), and constant flow rate, v (L^{3}T^{-1}), to become:

$$V\frac{dC_i}{dt} = -v\Delta[C_i] + V\sum_{j=1}^{N_R} R_{gen,ij} \tag{2.9}$$

dividing both sides by the flow rate v (L^{3}T^{-1}):

$$\frac{V}{v}\frac{dC_i}{dt} = -\Delta[C_i] + \frac{V}{v}\sum_{j=1}^{N_R} R_{gen,ij} \tag{2.10}$$

utilizing the following definition of the mean residence time (τ) (T):

$$\tau = V/v \tag{2.11}$$

in addition, substituting it back into equation (2.9):

$$\tau\frac{dC_i}{dt} = -\Delta[C_i] + \tau\sum_{j=1}^{N_R} R_{gen,ij} \tag{2.12}$$

2.4.1 Continuous Stirred Tank Reactor

To find the response of a CSTR to a tracer injection, we can first simplify the mass balance in equation (2.10) by recognizing that for a tracer there is no reaction term. The equation can be further simplified due to no initial concentration of the tracer in the reactor at time t = 0.

$$\tau \frac{dC_i}{dt} = -\mathrm{C} \qquad \mathrm{C} = \mathrm{C}_0, t = 0 \tag{2.13}$$

The model is described by a first order differential equation. Rearranging the equation integrating for the initial boundary condition becomes:

$$\int_{C_0}^{C} \frac{dC}{C} = -\frac{t}{\tau} = \ln \frac{C}{C_0} \tag{2.14}$$

where the concentration at any time can then be represented by the following:

$$C(t) = C_0 e^{-t/\tau} \tag{2.15}$$

now that the C (t) function for a CSTR has been found, equation (2.2) can be utilized to find the E (t) function.

$$E(t)_{cstr} = \frac{C(t)}{\int_0^\infty C(t)dt} = \frac{C_0 e^{-t/\tau}}{\int_0^\infty C_0 e^{-t/\tau}\, dt} \tag{2.16}$$

Solving the integral in denominator and evaluating it at the points t=∞ to t=0.

$$\int_0^\infty C(t)dt = \int_0^\infty C_0 e^{-t/\tau} dt = C_0 \left[-\tau e^{\frac{\infty}{\tau}} - \left(-\tau e^{\frac{0}{\tau}}\right)\right] = C_0 \tau \tag{2.17}$$

Substituting the integral back into equation (2.16):

$$E(t)_{cstr} = \frac{1}{\tau} e^{-t/\tau} \tag{2.18}$$

this idealized behavior is represented in Figure (2.12). The sample mean ($\overline{t}$) (T) of the probability function E (t) can be expressed as:

$$\overline{t} = \int_0^\infty tE(t)dt \tag{2.19}$$

substituting the value for the probability function for the ideal CSTR as described in equation (2.18):

$$\overline{t}_{cstr} = \int_0^\infty \frac{1}{\tau} e^{-\frac{t}{\tau}} dt = \tau \tag{2.20}$$

This proves for the case of the ideal CSTR, the sample mean residence time is equal to the mean residence time. The general equation for the standard deviation (σ) of a function is expressed as:

$$\sigma^2 = \int_0^\infty \left[\overline{f} - f(t)\right]^2 E(t)dt \tag{2.21}$$

where $\overline{f}$ represents the mean or average of a function, f (t) represents the function value at time (t) and E (t) represents the distribution function or the probability function. For the special case of the ideal CSTR probability function:

$$\sigma^2_{cstr} = \int_0^\infty \left[\overline{t} - t\right]^2 \frac{1}{\tau} e^{-t/\tau}\, dt = \tau^2 \tag{2.22}$$

The distinction between $\overline{t}$, τ and t can easily become confusing. ($\overline{t}$) represents the average sampling time from a discreet series of samples. (τ) represents the mean residence time as part of a continuous function. (t) is the time scale of which samples or continuous functions are measured on.

This shows that the standard deviation for a CSTR is equal to the residence time. This implies that no distribution can be broader than the ideal CSTR.

The final step is the calculation of the Distribution Function (F (t)) which again can be calculated from the E (t) and equation (2.3).

$$F(t)_{cstr} = \int_0^t E(t)dt_{cstr} = \int_0^t \frac{1}{\tau} e^{-t/\tau} dt = \frac{1}{\tau}\left[-\tau e^{-\frac{t}{\tau}} - \left(-\tau e^{-\frac{0}{\tau}}\right)\right] = 1 - e^{-t/\tau} \qquad (2.23)$$

The plots for the E (t) and the F (t) functions for the ideal CSTR are displayed in Figure 2.14 and Figure 2.15 respectively. From the E(t) plot, it is apparent that the maximum value of tracer exiting an ideal CSTR is at time = zero with the value of 1/τ.

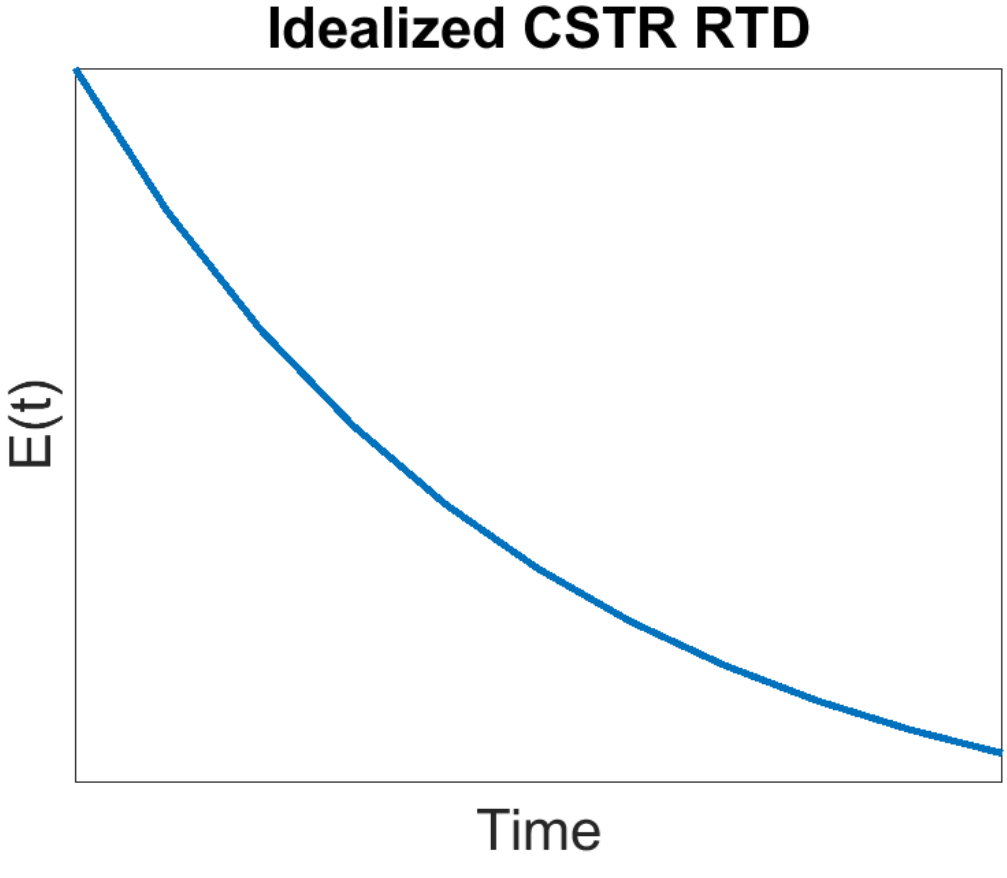

FIGURE 2.14: E-DIAGRAM OF IDEAL CSTR FLOW

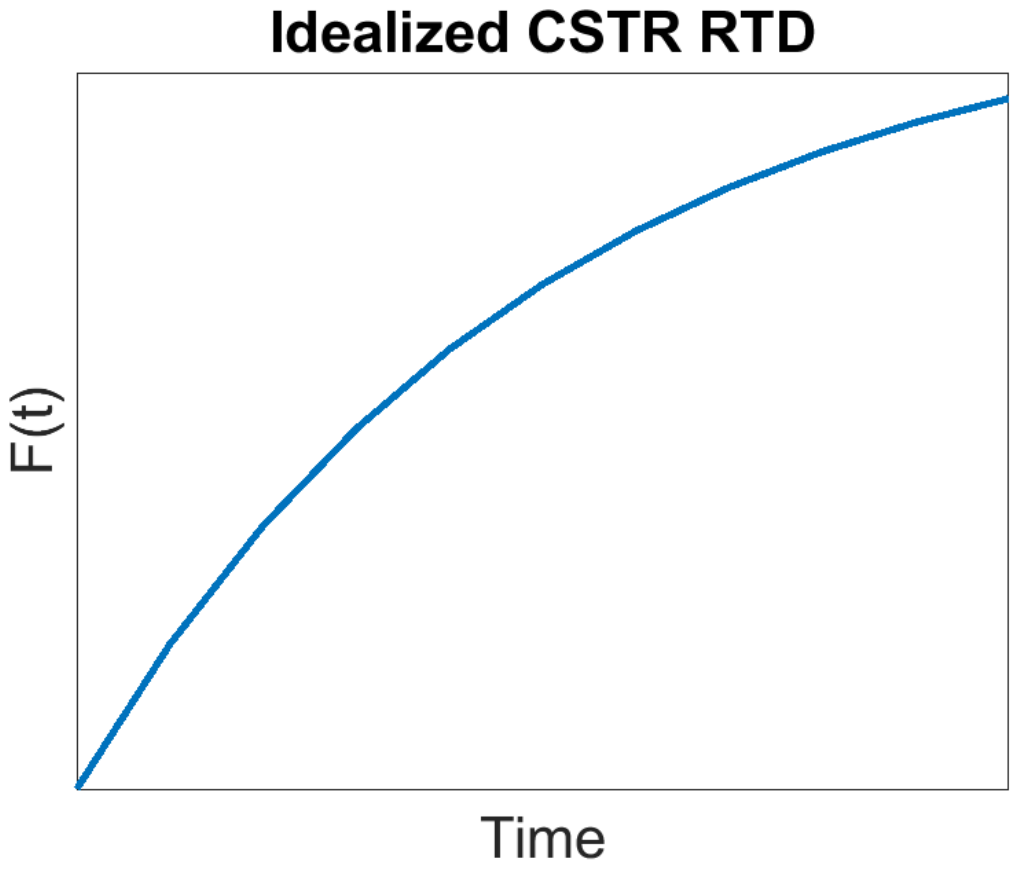

FIGURE 2.15: F-DIAGRAM OF IDEAL CSTR FLOW

2.4.2 Plug Flow

The RTD functions for a Plug Flow Reactor can be derived in a similar manor but due to the condition of no mixing, their values are simply the undisrupted signals travelling the length of the reactor [59]. The Dirac delta function (δ) represents a single value at time zero. At all other values of time, the Dirac delta function returns the value of zero. It is because of these properties that it is appropriate to represent an impulse injection. The impulse moves down the length of the reactor without broadening because of the assumption of perfect plug flow behavior in which no mixing takes place. The tracer then exits at the mean residence time, which can simply be expressed as the length of the reactor divided by the velocity of the fluid as explained in equation (2.11). Figure 2.16 shows an approximation of the E (t) diagram for the ideal PFR as the true function would not have any width.

$$E(t)_{PFR} = \delta(\tau) \tag{2.24}$$

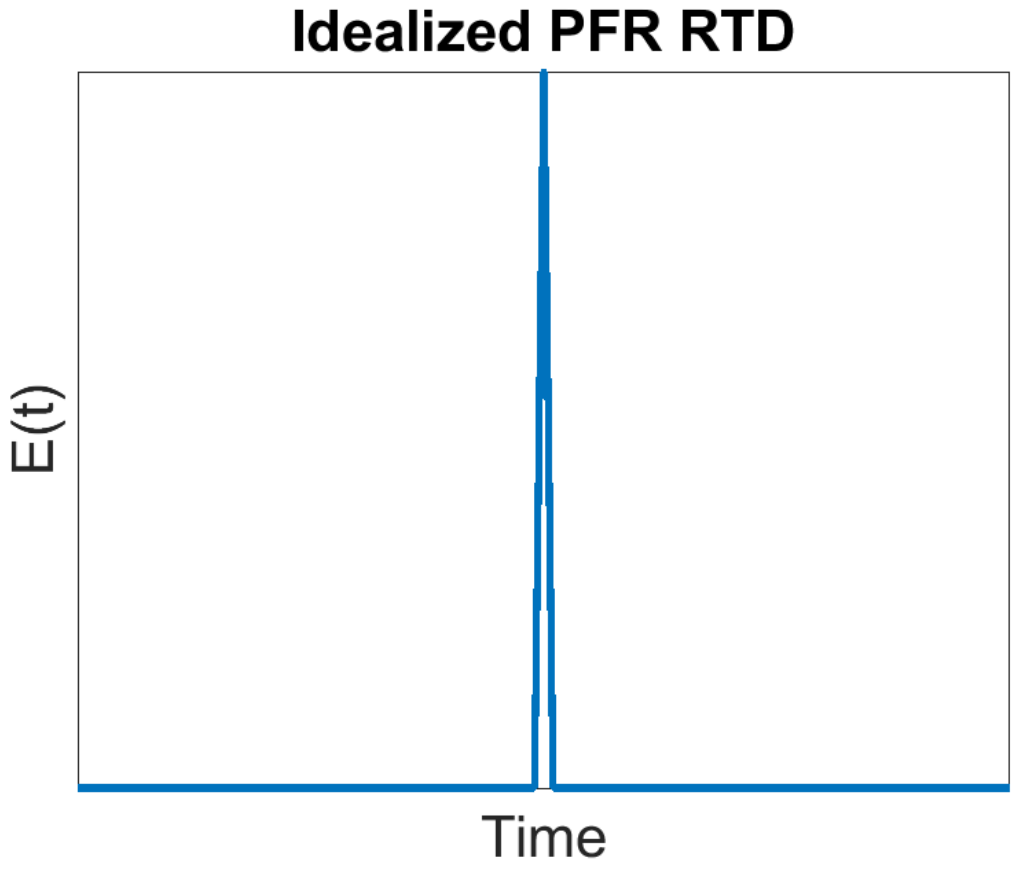

FIGURE 2.16: E-DIAGRAM OF IDEAL PFR FLOW

The F (t) for the PFR can be derived from equation (2.3) which represents the integral of the Dirac delta function (δ). The integral is the step function which is represented by the following equation:

$$H(\tau) = \begin{cases} 1 \; if \; \tau \geq 0 \\ 0 \; if \; \tau < 0 \end{cases} \tag{2.25}$$

For all values of t greater than or equal to time zero, the value is one. For all other values of time, the value is zero. The function can also step change for a tracer injection with continuous feed. Figure 2.17 represents the F (t) function for a PFR, as with the E (t) function the function is evaluated at Mean Residence Time.

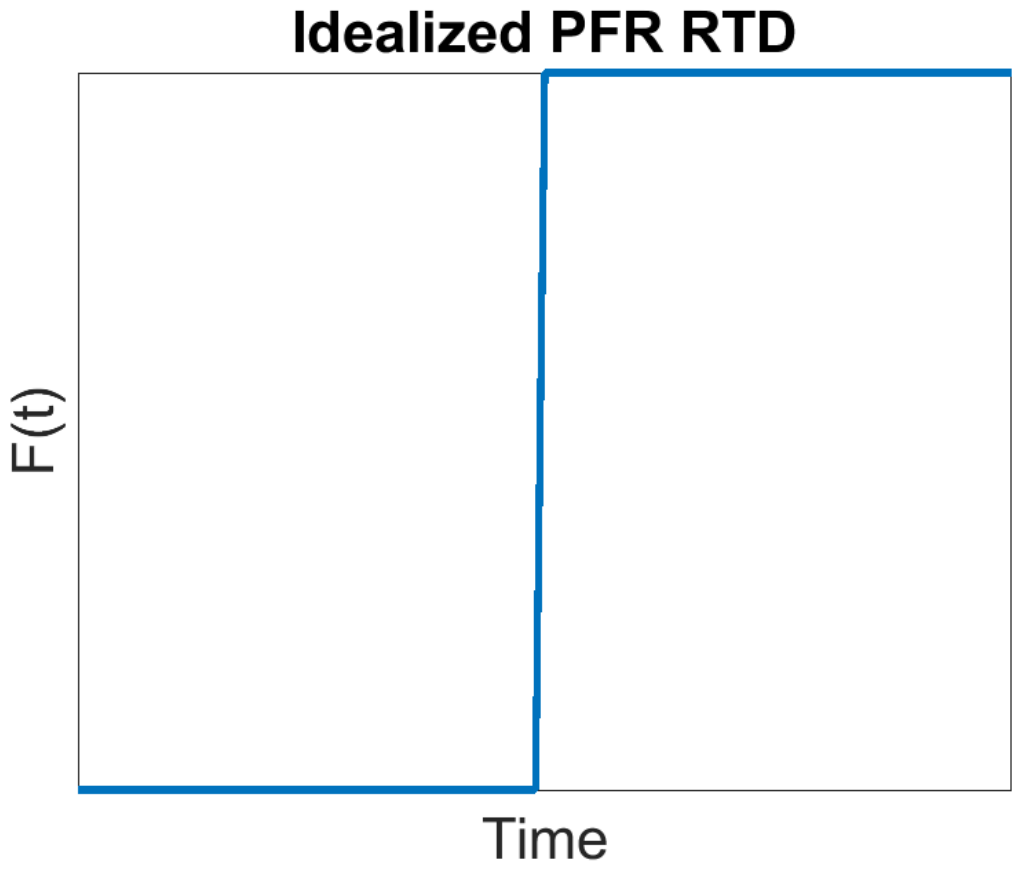

FIGURE 2.17: F-DIAGRAM OF IDEAL PFR FLOW

The standard deviation for a PFR can then be calculated from equation (2.21) however, recognizing that there is no axial mixing, the following is true:

$$\sigma_{PFR} = 0 \tag{2.26}$$

2.5 Real Reactor Models

Real Reactor Models are mathematically generated equations used to fit Residence Time Distribution curves. In this way, we can test different model parameters against the true behaviour of a reactor. The simplest of Real Reactor models are the single parameter models, which include the CSTR in series, and the axial-diffusion models (referred to as axial-dispersion models). More complicated models exist however their usefulness has diminishing returns as they become more complex with additional parameters.

2.5.1 CSTR in Series

The CSTR in series models the flow from one CSTR to another for a set number of CSTRs (Figure 2.18). These individual CSTRs are modeled by the ideal CSTR with identical reactor volumes. The modeling of multiple reactors in series starts with the molar balance of the nth CSTR as described in equation (2.9), taking the reaction term to be zero for the modeling of a non-reactive tracer.

$$V_{nth}\frac{dC_n}{dt} = -v_0\Delta[C]$$

where V_{nth} (L^3) is the volume of reactor one, v_0 (L^3T^{-1}) is the molar flow rate into a reactor one , $\frac{dC_n}{dt}$ ($molL^{-3}T^{-1}$) is the accumulation\consumption of in the nth reactor, $-v_0\Delta[C]$ ($molL^{-3}T^{-1}$) the net change flowing in and out of the reactor. The total volume for every reactor can be described by the following:

$$V_{Total} = nV_{nth}$$

where V_{Total} (L^3) is the total volume of all reactors and n is the number of reactors. This is true for reactors of equal size. The mean residence time τ (T) can be found for the entire volume or each individual volume:

$$\tau = \frac{V_{Total}}{v_0} = \frac{nV_{nth}}{v_0}$$

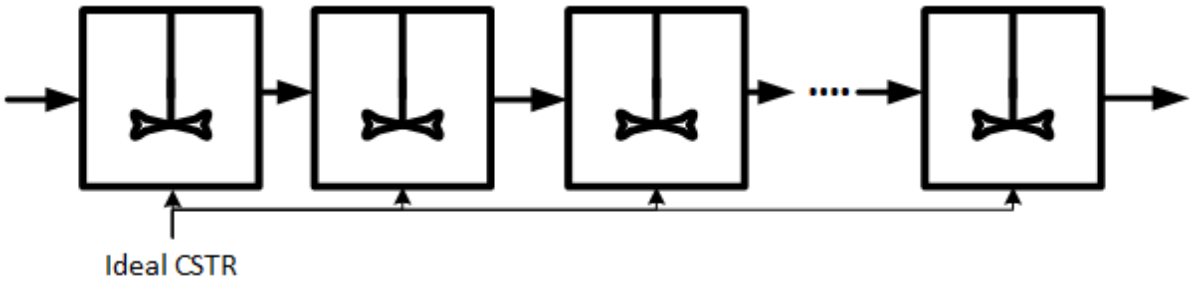

FIGURE 2.18: CSTR IN SERIES SCHEMATIC

This statement is true when the volumetric flow rate is constant from one reactor to the next. The molar balance expands as such:

$$V_{nth}\frac{dC_n}{dt} = -v_0\Delta[C] = -v_0[\mathrm{C_n} - C_{n-1}]$$

replacing the V_{nth} term:

$$\frac{v_0\tau}{n}\frac{dC_n}{dt} = -v_0[\mathrm{C_n} - C_{n-1}]$$

rearranging:

$$\frac{dC_n}{dt} + \frac{n}{\tau}(C_n - \mathrm{C_{n-1}}) = 0$$

using the following boundary conditions:

$$\mathrm{C_n} = 0\ for\ t = 0\ and\ n > 0$$

using the integrating factor ($\frac{nt}{\tau}$) to obtain (Refer to Appendix 2: Integrating Factor):

$$\mathrm{C_n} = e^{-nt/\tau}\int_0^t \frac{nC_{n-1}}{\tau}e^{nt/\tau}dt$$

for the case of n=1:

$$\mathrm{C_1} = e^{-t/\tau}\int_0^t \frac{C_0}{\tau}e^{t/\tau}dt = C_0e^{-\frac{t}{\tau}}\left(e^{\frac{t}{\tau}} - 1\right) = C_0(1 - e^{-\frac{t}{\tau}})$$

for the case of n=2 where $\tau_{reactor} = \tau_{Total}/n$ for the substitution of $\mathrm{C_1}$:

$$\mathrm{C_2} = e^{-2t/\tau}\int_0^t \frac{2C_1}{\tau}e^{2t/\tau}dt = e^{-\frac{2t}{\tau}}\int_0^t \frac{2C_0}{\tau}(1 - e^{\frac{2t}{\tau}})e^{2t/\tau}dt$$

rearranging as simplifying to become:

$$\frac{C_2}{C_0} = 1 - e^{-\frac{2t}{\tau}}(1 + \frac{2t}{\tau})$$

for the generalized expression to become:

$$\frac{C_n}{C_0} = 1 - e^{-\frac{nt}{\tau}}[1 + \frac{nt}{\tau} + \frac{1}{2!}\left(\frac{nt}{\tau}\right)^2 + \frac{1}{3!}\left(\frac{nt}{\tau}\right)^3 + \cdots \frac{1}{(n-1)!}\left(\frac{nt}{\tau}\right)^{n-1}]$$

using the definition of the E (t) in equation (2.2) and substituting the dimensionless time ($\theta = \frac{t}{\tau}$) to obtain the final expression:

$$E(\theta) = \frac{N(N\theta)^{N-1}}{(N-1)!} e^{-N\theta} \quad [60] \quad (2.27)$$

where N is the number of reactors.

Figure 2.19 shows the effect that changing the design parameter N, the number of CSTRs in a series, has on the RTD. With an increase in the number of CSTR in series from one to infinity, the flow behaviour deviates from the ideal CSTR to the ideal PFR. This variation in the flow dynamic profile provides a great flexibility to the system. A Matlab code was created that employs the algorithm along with a vector of different values or N (From 1 to 20). This model has been compared to different tracer experiments.

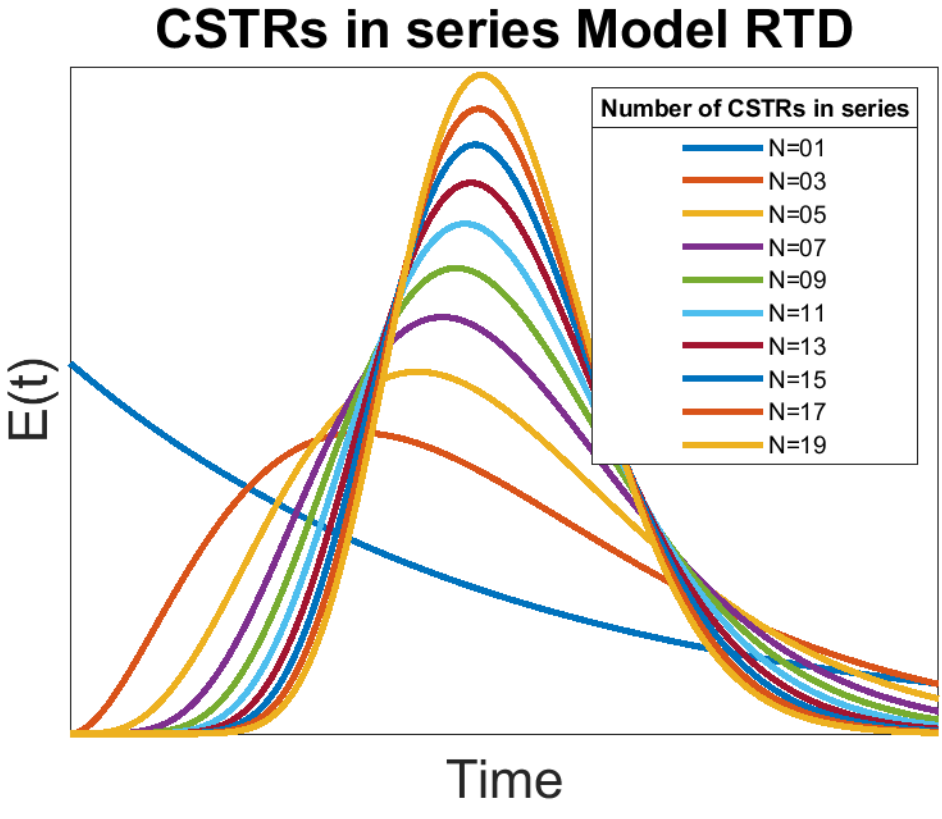

FIGURE 2.19: RTD FOR CSTRS IN SERIES FOR DIFFERENT NUMBER OF REACTORS

2.5.2 Axial Dispersion Model

The Axial Dispersion model starts with the foundation of the PFR and adds a degree of backmixing. The magnitude of the backmixing is independent of the position within the reactor. The concentration profile can be described by the following time dependent, second order partial differential:

$$\frac{\partial C}{\partial \theta} = \left(\frac{D}{uL}\right)\frac{\partial^2 C}{\partial z^2} - \frac{\partial C}{\partial z} \tag{2.28}$$

where θ represents the dimensionless time $\theta = \frac{t}{\tau}$, $\left(\frac{D}{uL}\right)$ represents the dimensionless dispersion coefficient, z (L) the direction of flow and C ($molL^{-3}$) as the tracer concentration.

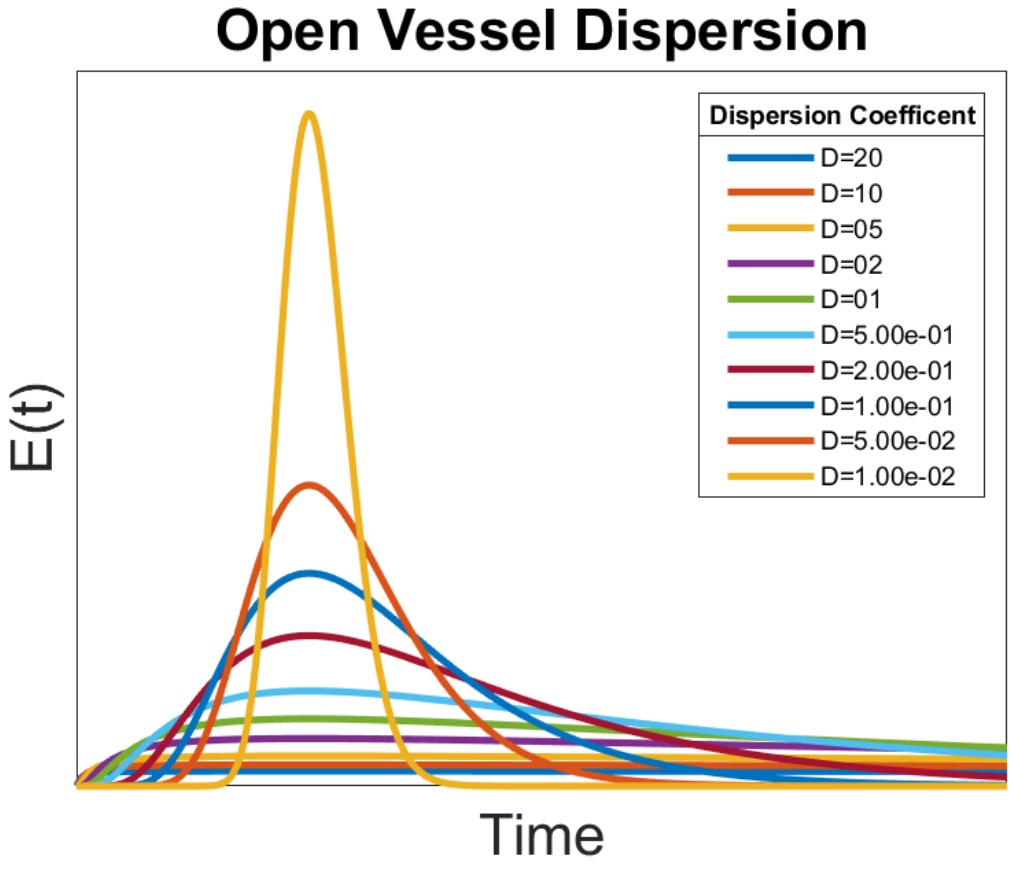

FIGURE 2.20: RTD FOR OPEN VESSEL DISPERSION

As the model has a second order partial differential equation, it requires two boundary conditions to solve and the initial time dependent condition. The boundaries are taken as the inlet and outlet of the reactor. Each boundary can either be considered open or closed (Figure 2.21). Open signifies undisturbed dispersion as it passes the boundary while closed signifies plug flow outside of the boundary. The two situations of greatest interest are the open vessel (open/open) and the closed vessel (closed/closed). The integration across all the boundary conditions are quite complex with the closed vessel condition only having a numerical solution and no analytical solution. The open vessel can be described by the following equation and Figure 2.20:

$$E(\theta_\infty) = \frac{1}{\sqrt{4\pi\left(\frac{D}{uL}\right)}} \exp\left[-\frac{(1-\theta)^2}{4\theta\left(\frac{D}{uL}\right)}\right] \tag{2.29}$$

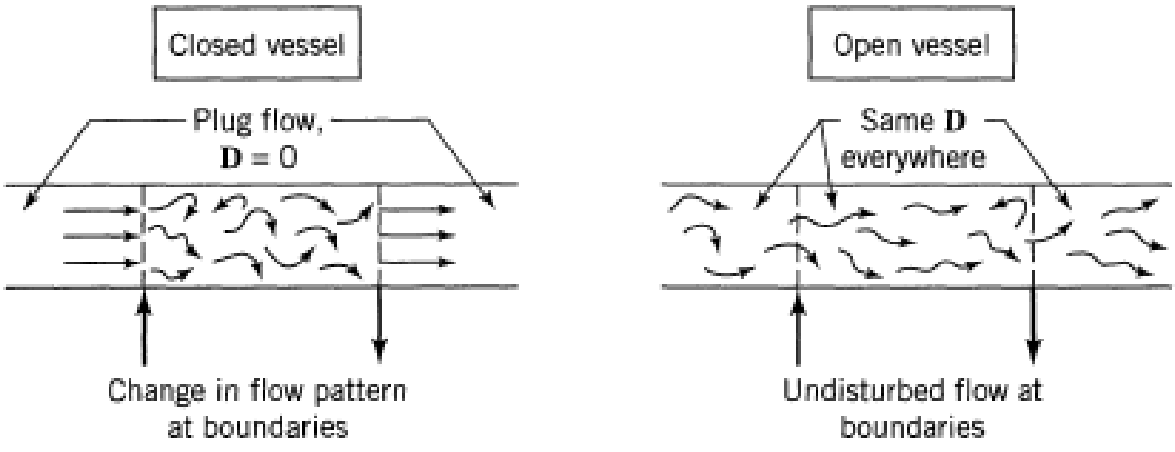

FIGURE 2.21: AXIAL DISPERSION BOUNDARY CONDITIONS [54]

The following equation describes the RTD for small levels of dispersion. This is a simplification and not a full solution to the differential. It should be noted that the equation that is within 5% accuracy when $(\frac{D}{uL})$ < 0:01 [56].

$$E(\theta) = \frac{1}{\sqrt{4\pi\left(\frac{D}{uL}\right)}} \exp[-\frac{(1-\theta)^2}{4\left(\frac{D}{uL}\right)}] \quad (2.27)$$

The difference observed from going from the low dispersion model to the open dispersion model is a shift to the left with a longer tail. The low dispersion model exhibits symmetry across the time axis. The solutions have been published for the boundary conditions open/closed and closed/open [61].

All of the axial dispersion models exhibit similar behaviour while changing the dispersion coefficient. A low coefficient behaves similar to the PFR while a higher coefficient approximates the CSTR. In this manner, the axial dispersion model acts as the opposite to the CSTR in series model.

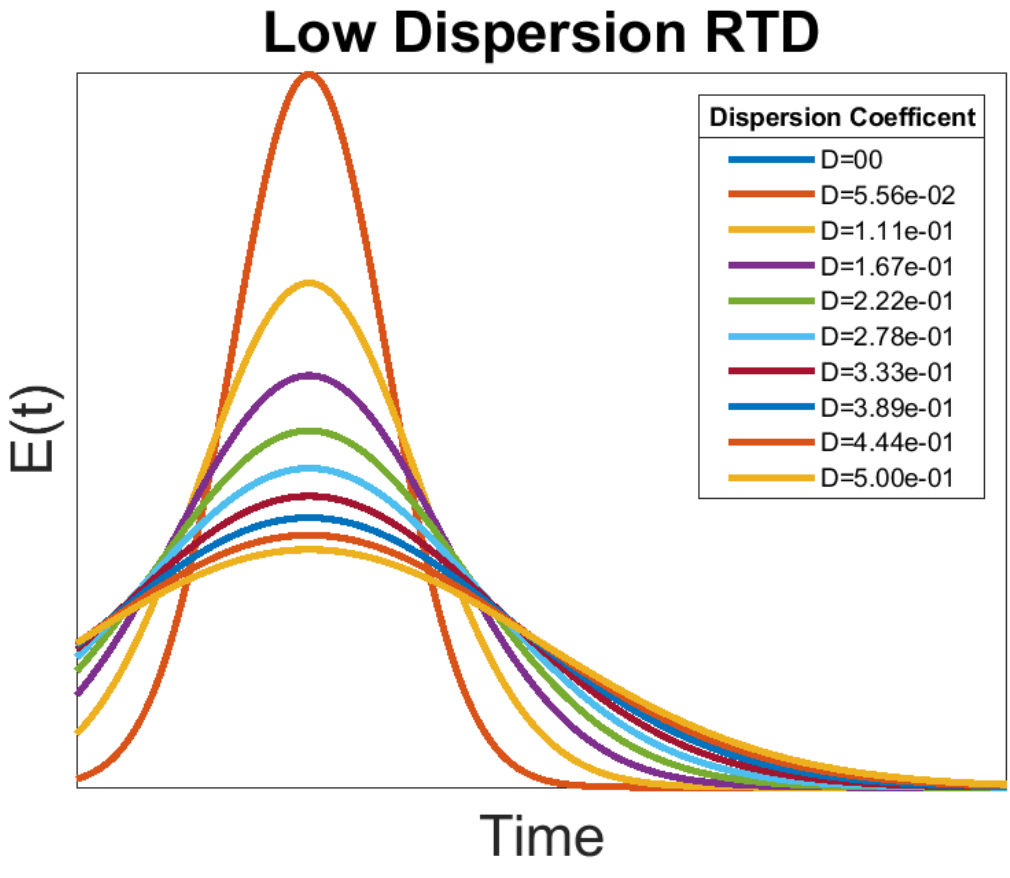

FIGURE 2.22: RTD FOR LOW DISPERSION

2.5.3 Enhanced CSTR in Series

The Enhanced CSTR in series model is based on the CSTR in series but it includes two additional parameters [62]. The model represents a series of CSTRs in series in which a portion (1-n) will bypass the specific CSTR (Figure 2.23). This variable ranges in value from 0-1 where n = 1 is 100% likely to enter the CSTR. The probability for bypass is equal for each CSTR in series. The second parameter M represents the opportunity for dead space within each CSTR. Just as in the previous parameter, the probability is the same at each CSTR and the range is from 0 to 1. These additional parameters significantly increase the complexity of the model. To solve this model a $N \times n \times M \times \theta$ grid needs to be created. The model is described by the following equation:

$$E(\theta) = \frac{Nn}{M}\sum_{i=1}^{N} \frac{N! e^{-\frac{nN\theta}{M}} \left(\frac{Nn\theta}{M}\right)^{i-1} n^{i}}{(N-i)!i!(i-1)!} + (1-n)\delta\left(\frac{Nn\theta}{M}\right) \qquad [62] \qquad (2.29)$$

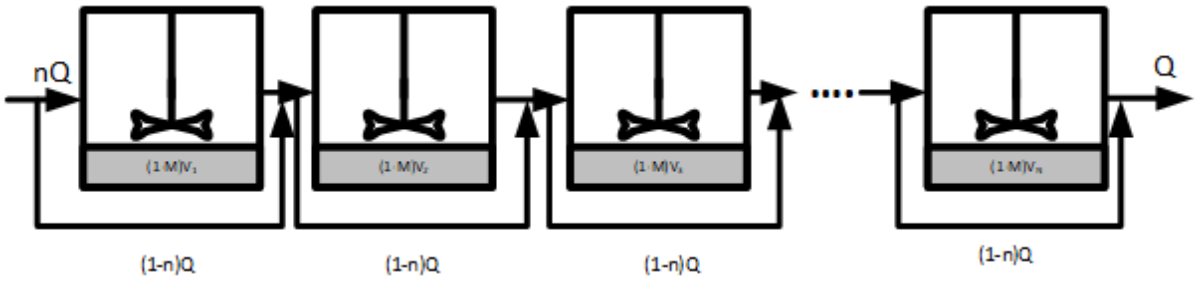

FIGURE 2.23: ECSTR SCHEMATIC

Where θ represents the dimensionless time $\theta = \frac{t}{\tau}$, N is the number of reactors, n is the probability that a tracer will enter a reactor (0-1), M is the percentage of the reactor volume that is active (0-1), δ is the Dirac delta function.

The behaviour change by varying the fraction of dead space (M) and the fraction of by-pass (N) for a set number of CSTRs in series (n=2) is observed in Figure 2.24 for dead space (M) and Figure 2.25 for by-pass (N). These variations are represented in 3D plots, as

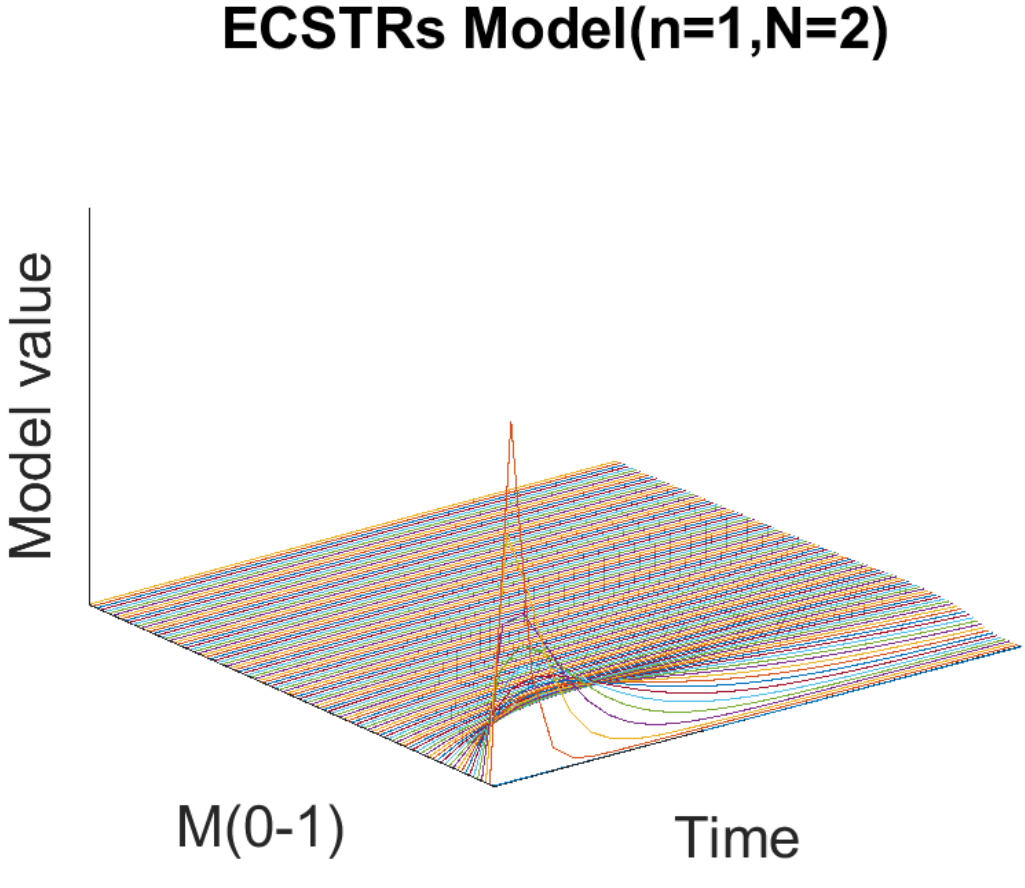

FIGURE 2.24: ENHANCED CSTR IN SERIES EFFECT OF M

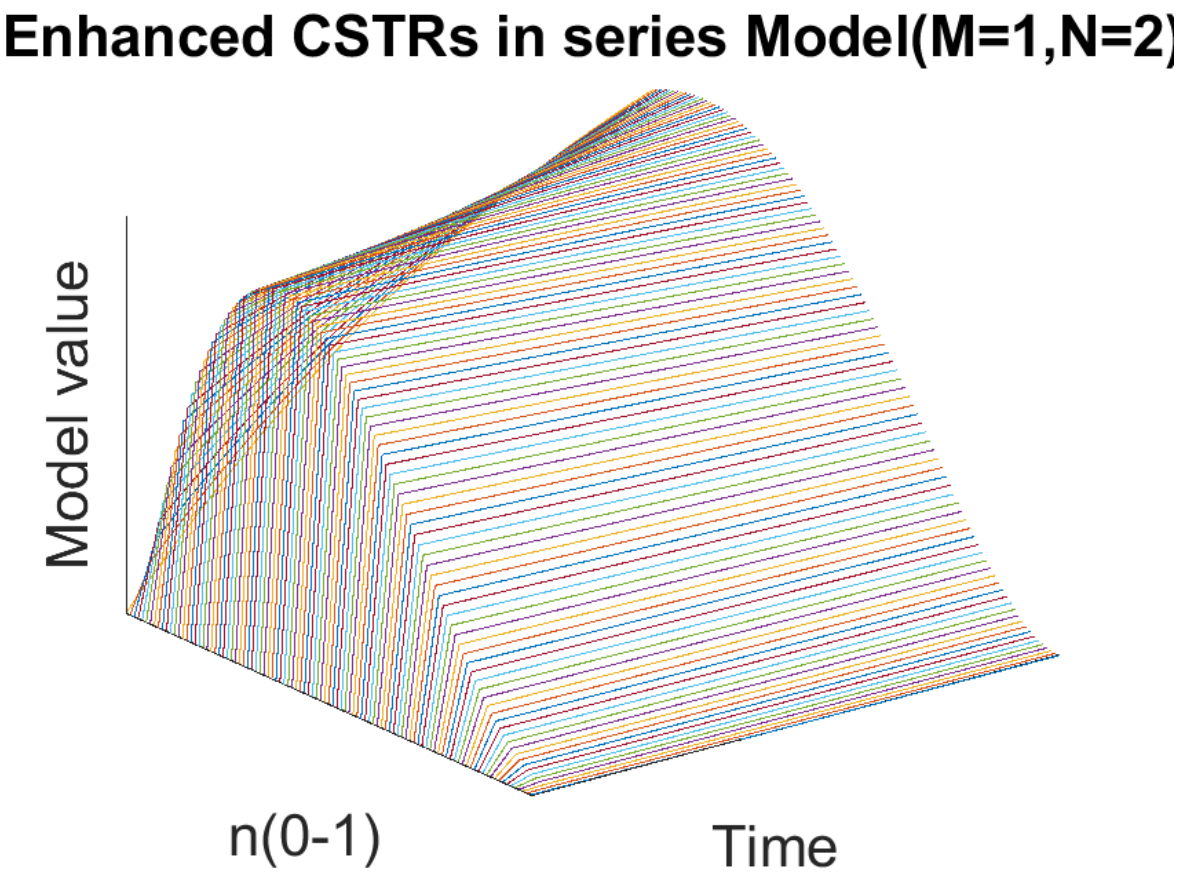

FIGURE 2.25: ENHANCED CSTR IN SERIES EFFECT OF N

there is one parameter change over a change in time. The magnitude of these plots represents the value E (θ).

The model equation is not very programming friendly. The summation term requires the use of a for loop in Matlab which prevents the function from becoming 100% vectorized. This will significantly increase the required computational time for simulation. The application of a four dimensional grid also requires a lot of system memory reducing the resolution for the parameters while also increasing the computational time.

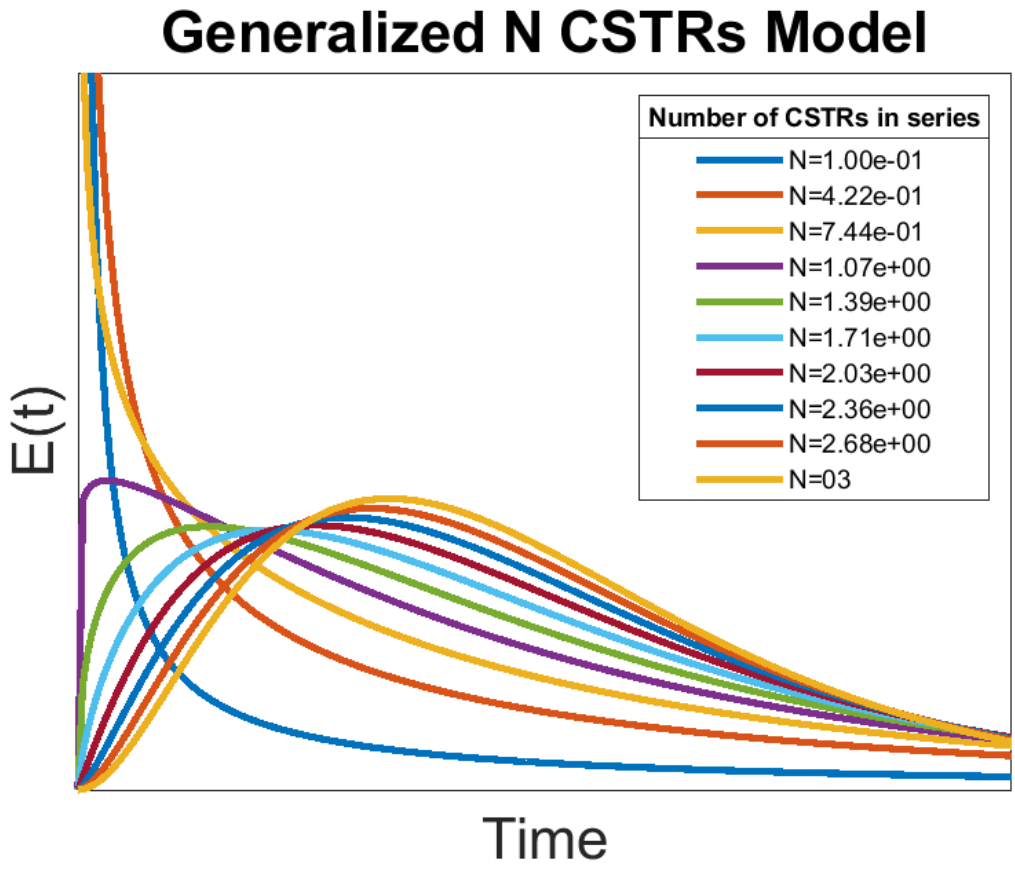

FIGURE 2.26: RTD FOR N-CSTR MODEL AT DIFFERENT NUMBER OF CSTRS

2.5.4 N-CSTR Model

One of the major limitations of the CSTR in series model is the reliance on the factorial of (n-1). This term limits the application of this model to natural numbers of n. Martin-Dominguez overcame this obstacle with the application of the Gamma function ($\Gamma(n)$) [63] [64]. Refer to Appendix 1: Gamma Function for more information.

There are two advantages to this modification: the representation of value between real numbers (such as values between 1 and 2 when neither of them quite fit well), and the representation of systems with by-passing were N < 1.

Figure 2.26 outlines the different Residence Time Distribution functions for different values of N using the n-CSTR Model. The n-CSTR Model approaches the PFR when the value of $N \to \infty$. Similarly, the model is equal to the ideal CSTR when N = 1. The unique behaviour of

this model allows the demonstration of the two extreme ideal models along with a model exhibiting bypassing when 0 < N < 1.

2.5.5 Error Analysis

In order to study the accuracy of an experiment, the experimental error was analyzed. The first step is to determine the mean value for measurement for each trial.

$$\overline{x} = \frac{x_1 + x_2 + \cdots + x_N}{N} \tag{2.30}$$

The mean deviation is utilized rather than the standardized deviation as the quantities of measurements is low (N<5).

$$Mean\ Deviation = \frac{|x_1 - \overline{x}| + |x_2 - \overline{x}| + \cdots + |x_N - \overline{x}|}{N} \tag{2.31}$$

The mean deviation gives a measure of accuracy in the experiment. In order to test models against collected data, some criteria for accuracy needs to be set. The criteria used in this experiment is the Root Square Mean Average (RSME) as described as:

$$\mathrm{RMSE} = \sqrt{\frac{1}{\mathrm{n}} \sum_{j=1}^{n} (y_i - \widehat{y_i})^2} \tag{2.32}$$

where y_i is the measured value, $\widehat{y_i}$ is the predicted value and n is the number of data points.

2.6 Computational Fluid Dynamics

There have been many interesting developments in the area of Computational Fluid Dynamics (CFD) over the last decade. CFD models have the potential to meet some of limitations of RTD. The RTD can provide insight on dead space and by-pass channeling, but it does not provide any indication of their locations [65]. The basis of CFDs is the simulation of

the Navier-Stokes equation extended over the three dimensions of the reactor. It is described by the following equation:

$$\frac{\partial u}{\partial t} + u \cdot \nabla u = -\frac{\nabla \mathrm{P}}{\rho} + \frac{\mu}{\rho}\nabla^2 u$$

Where u (LT^{-1}) is the fluid velocity vector, P ($ML^{-1}T^{-2}$) is the fluid pressure, ρ (ML^{-3}) is the fluid density and ∇ is the gradient differential operator.

Research has shown that a CFD can develop a series of steady moment transport equation to derive the moments of the RTD without the need for a tracer experiment [66]. CFDs are not a perfect solution, there are still parameters that need to be evaluated such as: approach, discretization scheme and turbulence model [67]. There are currently a wide selection of commercial CFD software including ANSYS, PowerFLow and Autodesk CFD to name a few.

Chapter 3 : Materials and Methods

3.1 Construction of the STAR Reactor

The original STAR reactor, developed by Reza and Alvarez Cuenca in 2016 [9], was deconstructed with some of the parts used for the study of an alternative reactor in another study. The components of the STAR reactor required reassembly following the process flow diagram outlined in Figure 3.1. The reactor is composed of three separate cylindrical sections staged vertically with piping connecting the following section. The first two stages have a volume of 10 liters and are maintained at anoxic conditions. The third stage is a larger 45 liters aerobic section with an air diffuser. The reactor includes an Anaerobic Lateral Unit (ALU) under anaerobic condition which supplies the first stage Volatile Fatty Acids (VFA) required for Enhanced Biological Phosphorous Removal (EBPR). The ALU is fed activated sludge from a clarifier unit connected to the aerobic stage.

3.1.1 Tracer Selection

It is important that the tracer selected acts as a good representation of a typical reagent in the reactor, thus the tracer selection process is paramount. It is important that the tracer exhibits the following characteristics [54]:

1. The tracer should be stable and conserved (non-volatile and won't precipitate)
2. The analysis for the tracer should be convenient, sensitive, and reproducible
3. The tracer should be inexpensive
4. The tracer should not be absorbed on or react with the surface of the vessel
5. The tracer should be chemically and physically similar to the fluid to replicate the behaviour of diffusion

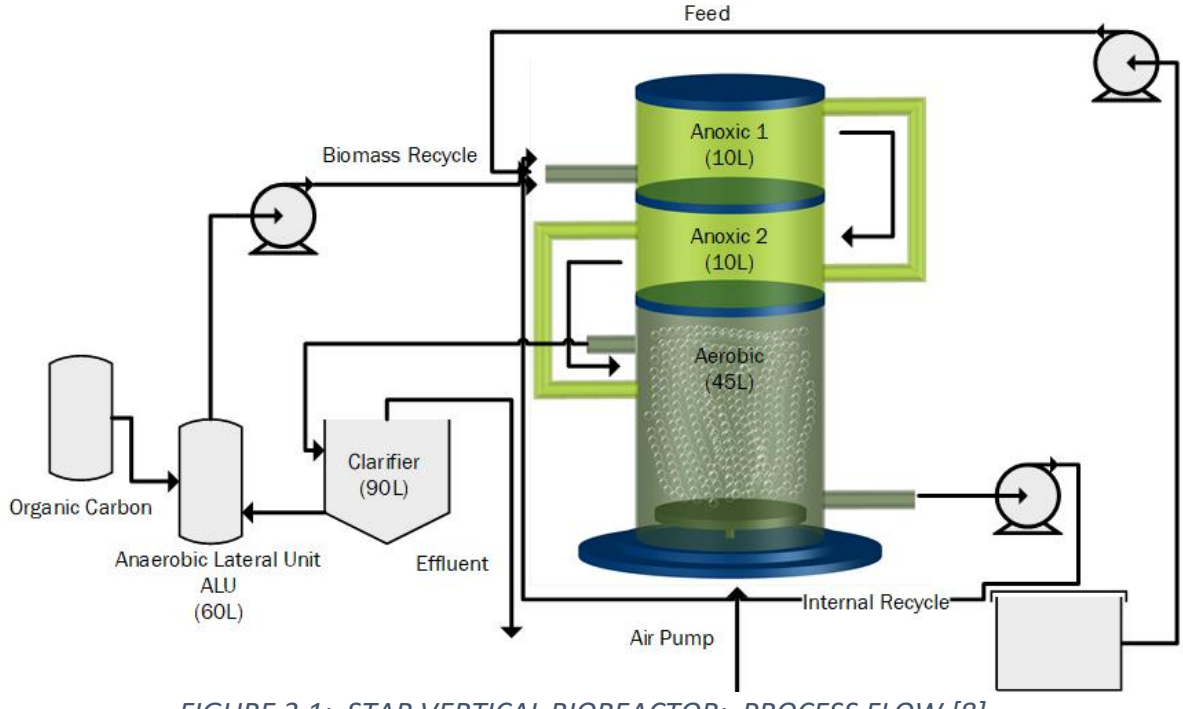

FIGURE 3.1: STAR VERTICAL BIOREACTOR: PROCESS FLOW [8]

Traditionally the tracer has been nonreactive but the reaction of a decaying tracer can be corrected [61]. There has been research in the use of reactive tracers for long term model monitoring; however, it doesn't allow for the determination of the RTD [58]. The benefit of a reactive tracer is that a process reagent can act as the tracer.

Missen suggests the following additional precautions when performing a tracer experiment [54].

- Inject properly: If the velocity profile at vessel inlet is at, introduce tracer uniformly across the cross section. If it is not at, introduce tracer proportional to the flow rate.
- Measure properly: Average over all flow rates. This is called the mixing cup measurement.

Through the field of water engineering, many different tracers are available. Some of the tracer technologies are summarized in Table 4. The tracer criteria are summarized in Table 5.

Method	Principle
Conductivity	Electrical Conductivity
Photometry	Light absorbance (visible or ultra-violent)
Mass Spectroscopy	Different mass numbers of components
Para-magnetic Analysis	Para-magnetic properties of compounds
Radioactivity	Radioactive radiation
Gas Chromatography	Adsorption of a compound on a carrier material
Liquid Chromatography	Adsorption of a compound on a carrier material

TABLE 4: COMMON ANALYTICAL METHODS FOR TRACER EXPERIMENTS [53]

The sensors for these different tracer technologies have to meet many criteria. This includes price, sensitivity, industrial application and the state of operation. The evaluation of these sensors are summarized in Table 5. The two most common sensors utilized in water engineering are conductivity and photometry sensors.

Technology	Criteria			
	Price	Sensitivity	Industrial Application	Operation
Conductivity	Cheap	Wide	Common [58], [62], [68]–[72]	Continuous
Photometry	Cheap	Wide	Common [70], [73]–[75]	Continuous
Mass Spectroscopy	Expensive	Wide	Common	Discontinuous
Para-magnetic	Cheap	Wide	Common	Continuous
Radioactive	Expensive	Wide	Uncommon [55]	Continuous
Chromatography	Expensive	Wide	Uncommon	Discontinuous

TABLE 5: TYPES OF SENSORS

After the type of tracer has been selected, it is important to select what type of signal one would like to simulate. The first and simplest signal is the Dirac Signal (δ), also known as a pulse signal. This signal requires the injection of a single volume of injectable material at time t = 0 with the concentration of C_0. It has the major advantage that it only requires a small amount of tracer. It also has a small impact on the process operation. Some trade-offs exist as it can be difficult to produce the perfect pulse. The full amount of the tracer needs to be injected at an instant. It can also make it difficult to perform a mass balance for the tracer. The pulse response is related to the Probability Density Function (E (t)) [54].

In some cases, a step input is preferred where a set constant flow rate of tracer is continuously added. This can be performed by a "step up" or a "step down" in tracer concentration. This creates a method that is easier and simpler to perform a mass balance. The opposite of the pulse function is also true. It requires larger amounts of tracer element and it is more likely to affect process operation. The step response is related to the Distribution Function (F (t)).Table 6 compares the application of a pulse to a step signal [54].

	Pulse Input	**Step Input**
Advtantages	• Small amount of tracer • Small impact on process	• Easier to achieve • Easier to achieve material balance • Can perform a step down after a step up to check consistency
Disadvantages	• Difficult to achieve perfect pulse • Difficult to achieve accurate material balance	• Larger amount of tracer • Large impact on process

TABLE 6: TRACER SIGNAL COMPARISON

A periodic signal or a random signal can also be used; however, these signals are much more complicated to generate than a step or a pulse. The random or periodic signals are also more difficult to interpret. The pulse method was selected due to the simplicity and minimal requirement for tracer.

There have been some interesting developments in the application of alternative tracers. Ahnert studied storm water events with cold water as a tracer signal for a Waste Water Treatment Plant (WWTP) [76]. This would be a very simple and cost-efficient method for performing tracer experiments. Reactive tracers are another potential possibility, such as the experiments performed by Braun [68]. The WWTP under study experiences fluctuations of ammonia and oxygen concentrations at night due to an unresolved issue in the process. Braun was able to use these fluctuations as a randomly generated tracer signal. The disadvantages of a reactive tracer include uncertainty of the measurement device and a lower detection limit [77].

Members of the Ryerson University Water Treatment Technologies Laboratory selected a solution of sodium chloride as a tracer. It is frequently used in industry as it behaves similarly to water. The tracer is also inexpensive and easy to obtain. The tracer however cannot be used for wastewater - it will be absorbed by microbes - but it is appropriate for clean water. Very little system modifications would be required to experiment with wastewater and a Lithium Chloride tracer. Lithium Chloride has the advantage of low absorption rates in the activated sludge. There are some concerns about the toxic effect of Lithium Chloride on aquatic life, including effects on algae and minnow larvae [78]. Table 7 summarizes the different characteristics of some commonly used tracer in water engineering.

Tracers	Cost	Flexibility	Pros	Cons
Sodium Chloride	$65.70/500g [79]	-Very flexible -Custom solutions	-Easy availability -Simple Analysis	-Reacts to wastewater
Lithium Chloride	$19.95USD/100g [80]	-Very flexible -Custom solutions	-Easy availability -Simple analysis -Does not react to wastewater	-May affect aquatic life[78]
Rhodamine WT (2.5%)	$29.95USD/pint [81]	-Moderately flexible -Custom solutions -May require adjustments due to photosensitivity	-Low detection limit 0.01µg/L[82]	-Requires transparent walls and fluid -Photosensitive
Radioactive Tracers (Ar, Kr, Br,Technetium-99)[82]	$1600-2800 USD/gram (Technetium-99) [83]	-Inflexible -Highly regulated	-High selectivity -Low detection limit	-Poor availability -High costs -Strict safety regulations

TABLE 7: COMMON TRACERS IN WATER ENGINEERING

3.1.2 Sensor Selection

The measurement of conductivity is not 100% standardized. There are a few different units, but one of the most common ones is the Micro Siemen per centimeter (µS/cm). Often the /cm is omitted for no apparent reason. It was determined that the maximum range required for saturated sodium chloride solution would be about 10,000 µS/cm [84]. A saturated solution of Lithium Chloride was found to be only slightly higher.

The CDCE-90-1 conductivity cell was chosen for this experiment as it was provided by a recommended supplier and it was capable of covering the required conductivity range (10-10000 µS/cm). Refer to Appendix 3: Sensor Specification for more information on the sensors. The range available for a cell is dependent on the cell constant. A higher cell constant has a higher range, but it will be less sensitive on the lower limit. The CDCE-90-1 was able to handle the highest conductivity reading of the saturated tracer solution and the lowest possible value as the conductivity of tap water, which is ≈ 300 µS/cm.

3.1.3 Sensor Placement

One of the tasks in assembling the tracer experiment was deciding how the sensors would fit into the reactor. The current sensors are submersed in the reactor, attached through the walls. This would not be acceptable for the conductivity sensors as this configuration assumes perfect mixing and constant parameters in each section. The entire purpose of the tracer experiment is to move from this simplified assumption into a model that better describes the true mixing dynamics.

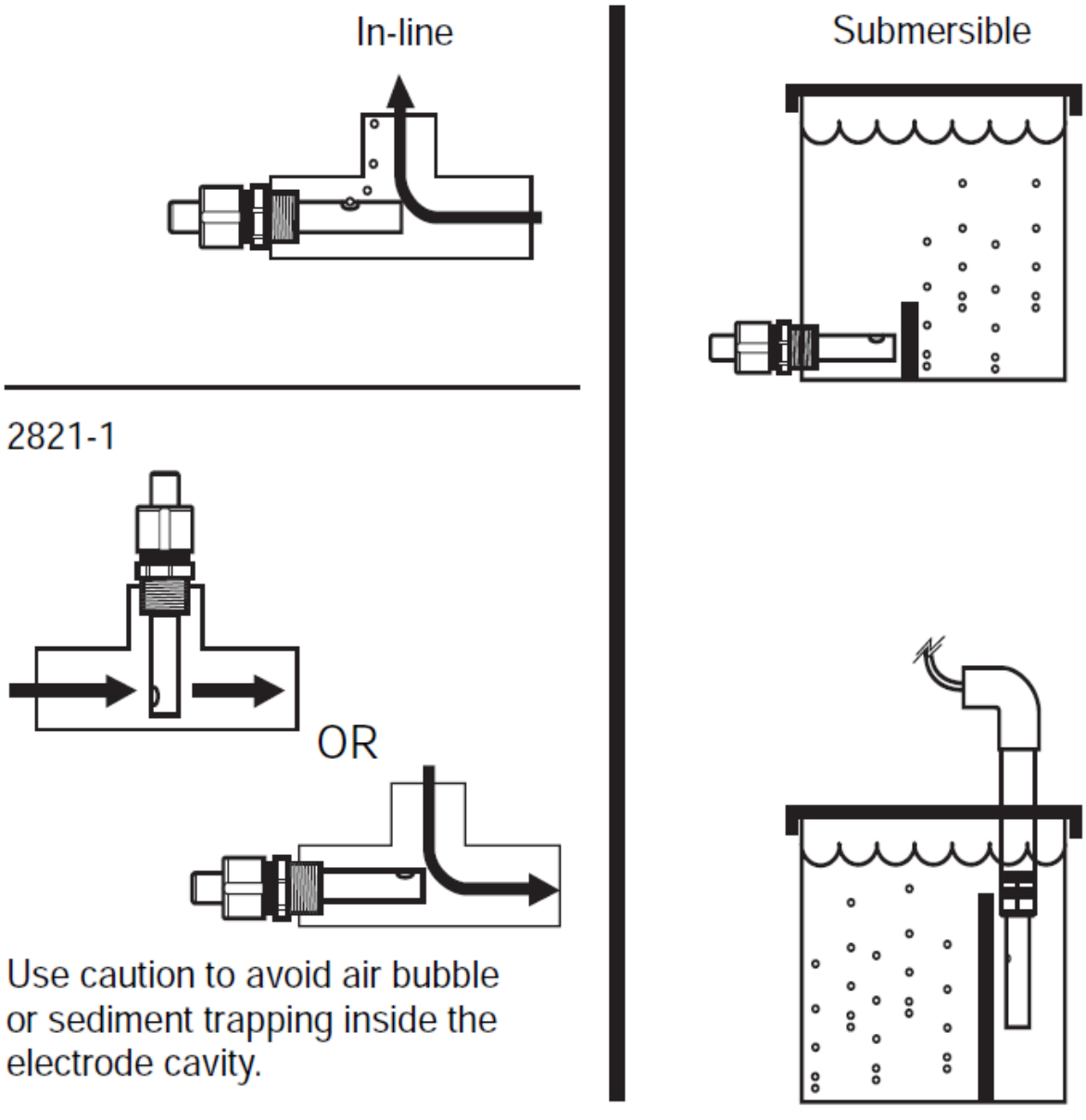

FIGURE 3.2: SENSOR ALIGNMENT, OMEGA MANUAL [83]

The sensors had to be attached in-line with the piping as per the suppliers' instructions (Figure 3.2). When the STAR reactor is in operation, the liquid level in the piping between the stages is quite low. This proved to be a challenge, as the sensors were required to remain submerged in the fluid. For some of the sensors this requires no modification as their location remained under the liquid level. The two sensors on the top of the reactor (measuring the recycle flow and the flow from stage 1 to 2) required the liquid to be held back in order to raise the liquid level. The first sensors used a cork, (Visible in Figure 3.3) while sensor two used a piece of rubber that was folded into the piping.

FIGURE 3.3: SENSOR #1

3.1.4 Instrumentation and Methodology

The original series of sensors were used to ensure the same operating conditions as in the previous study by Reza and Cuenca (Table 8) [85]. The system boundaries for this experiment cover the main body of the multistage reactor (refer to Figure 3.4). The locations of the sensors and the injector are indicated in blue. The conductivity sensors were strategically placed through the process to enhance the information collected while reducing costs by limiting the number of sensors. A sensor was placed at every entrance of each stage.

Stream	Flow Rate (L/hr)
Feed	10
Internal Recycle	20
Recycle Sludge	15

TABLE 8: VERTICAL REACTOR OPERATING CONDITIONS [9]

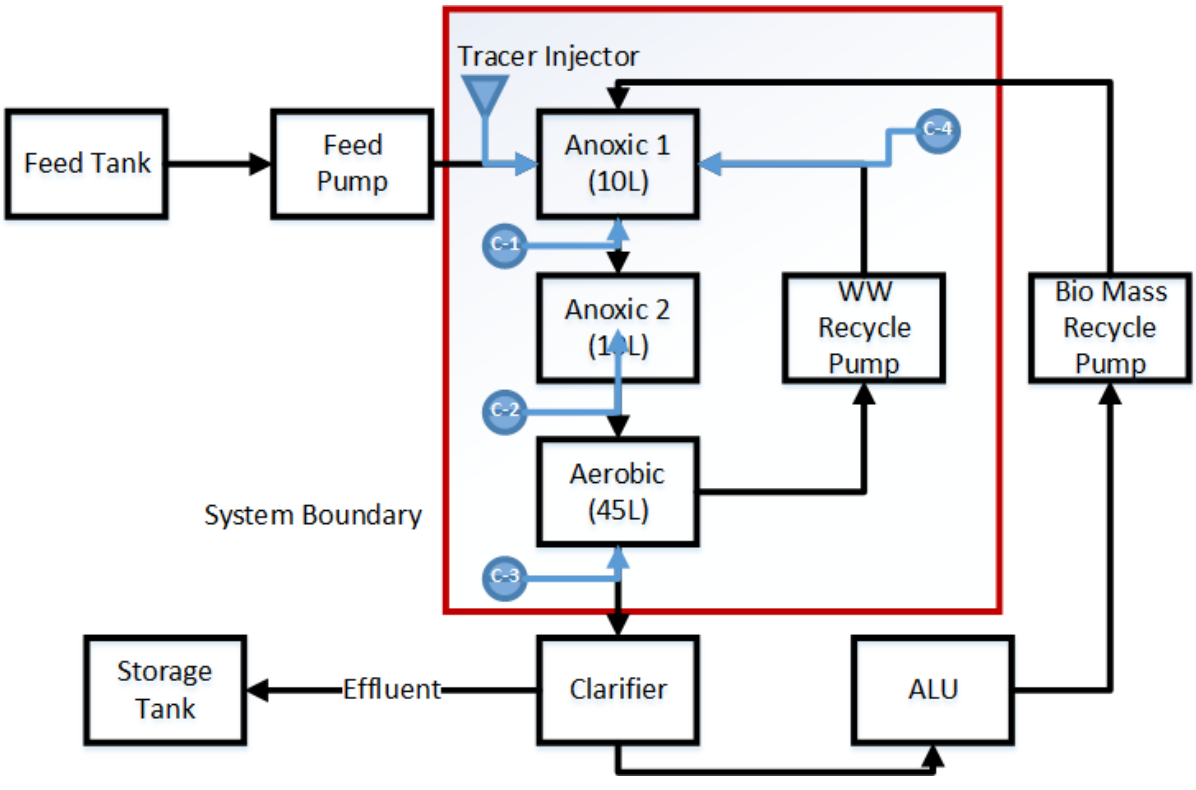

FIGURE 3.4: FLOW UNIT OF EXPERIMENTAL UNIT

The Data Acquisition System (DAS) was connected to a local computer that ran Lab-View to monitor the sensor data. Lab-view would record the sensor data for all the sensors and output excel spreadsheets that were used for analysis (refer to Appendix 4: Sample Data). The DAS recorded data on temperature, dissolved oxygen concentration, oxidation reduction potential and pH but the values have no importance in this experiment.

Figure 3.5 represents the process and instrumentation diagram for the STAR vertical bioreactor. In the diagram the new instrumentation, the conductivity sensors, are outlined in blue. Since the original sensors were still operational but not required for the experiment, they were still attached to the DAS.

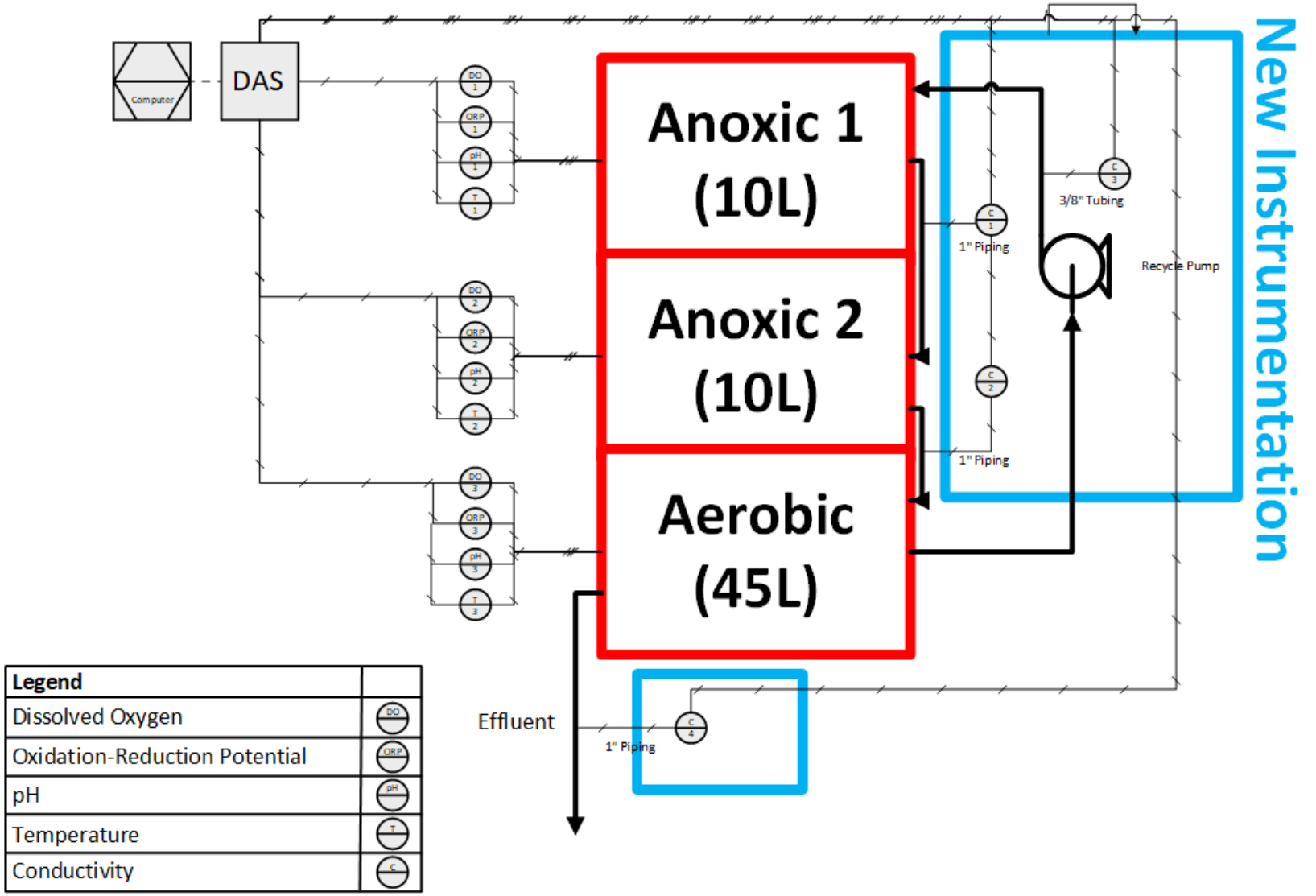

FIGURE 3.5: STAR REACTOR PROCESS AND INSTRUMENTATION DIAGRAM

3.1.5 Tracer Injector

The availability of injectors are limited. For example, the injector port used in medicine for different intravenous therapies (Figure 3.6). These injectors piggyback already attached intravenous lines, reducing the number of injections a patient receives. Researching such an injection port as well as obtaining one is difficult as it is highly regulated. The decision was made to design a custom solution.

There were two different tracer injector trials. The first trial utilized a t-connection, a rubber stopper, a syringe and a needle (Figure 3.7). The injector port design joined the t-connector and the rubber stopper. The tracer itself would be injected in a 10 mL syringe with a needle into the injection port. The T-connection was spliced into the feed line from

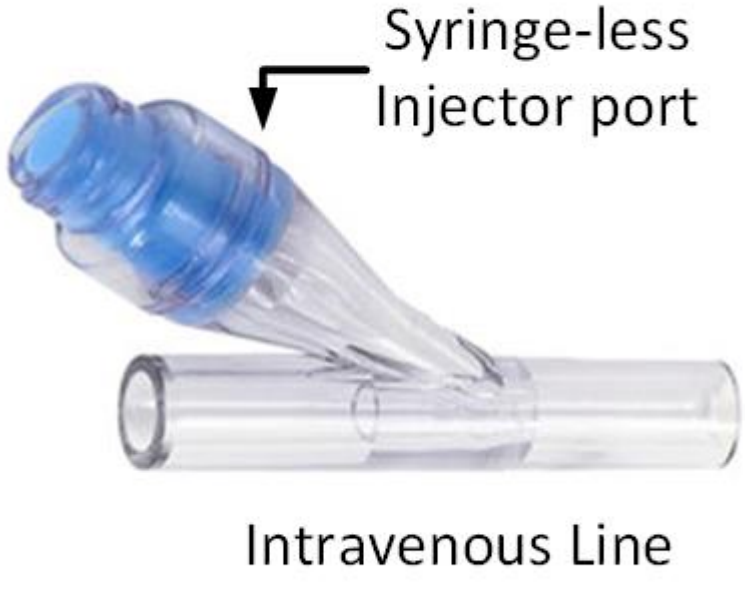

FIGURE 3.6: INTRAVENOUS INJECTOR PORT [84]

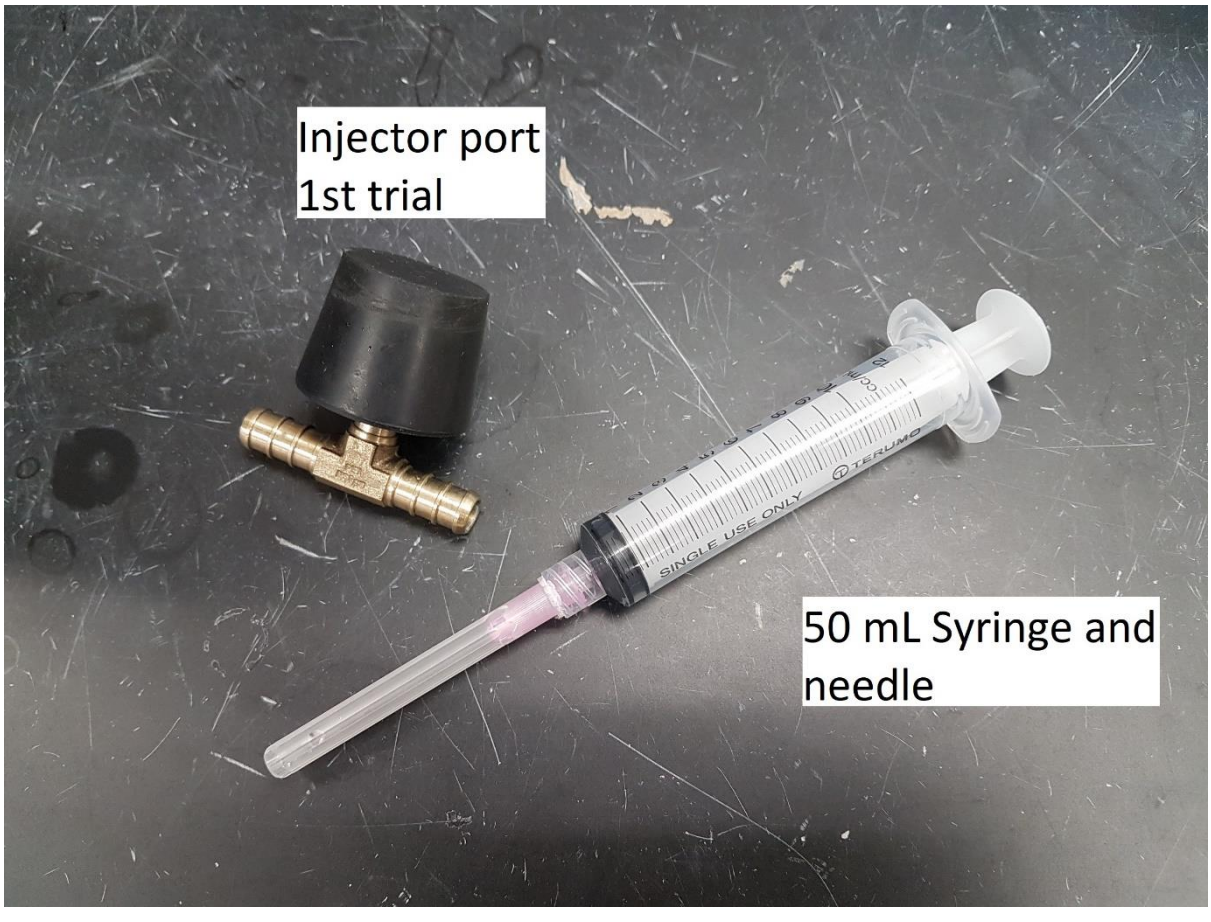

FIGURE 3.7: TRACER INJECTOR TRIAL 1

the feeding tank to the first anoxic stage. The connector was placed close to the reactor in order to reduce any amount of lag introduced by the injection process.

The T-connector was a 3/4 inch three-sided barbed connector that was purchased at a local Home Depot. The rubber stopper and the needle were supplied from the Chemistry department at Ryerson University. The syringe was provided by the Water Treatment Technology lab at Ryerson University.

There was a 3/4 inch hole bored partially into the stopper that allowed the stopper to fit onto the t-connector. The theory behind the stopper was that the thick rubber would withstand multiple injections without any leakage. This had been proven mostly successful; however, it was difficult to pierce the rubber with the needle. It was found that the 10 mL syringe did not deliver enough tracer solution to provide any measurable data at the end of the reactor. This had led to the development of the second injector design.

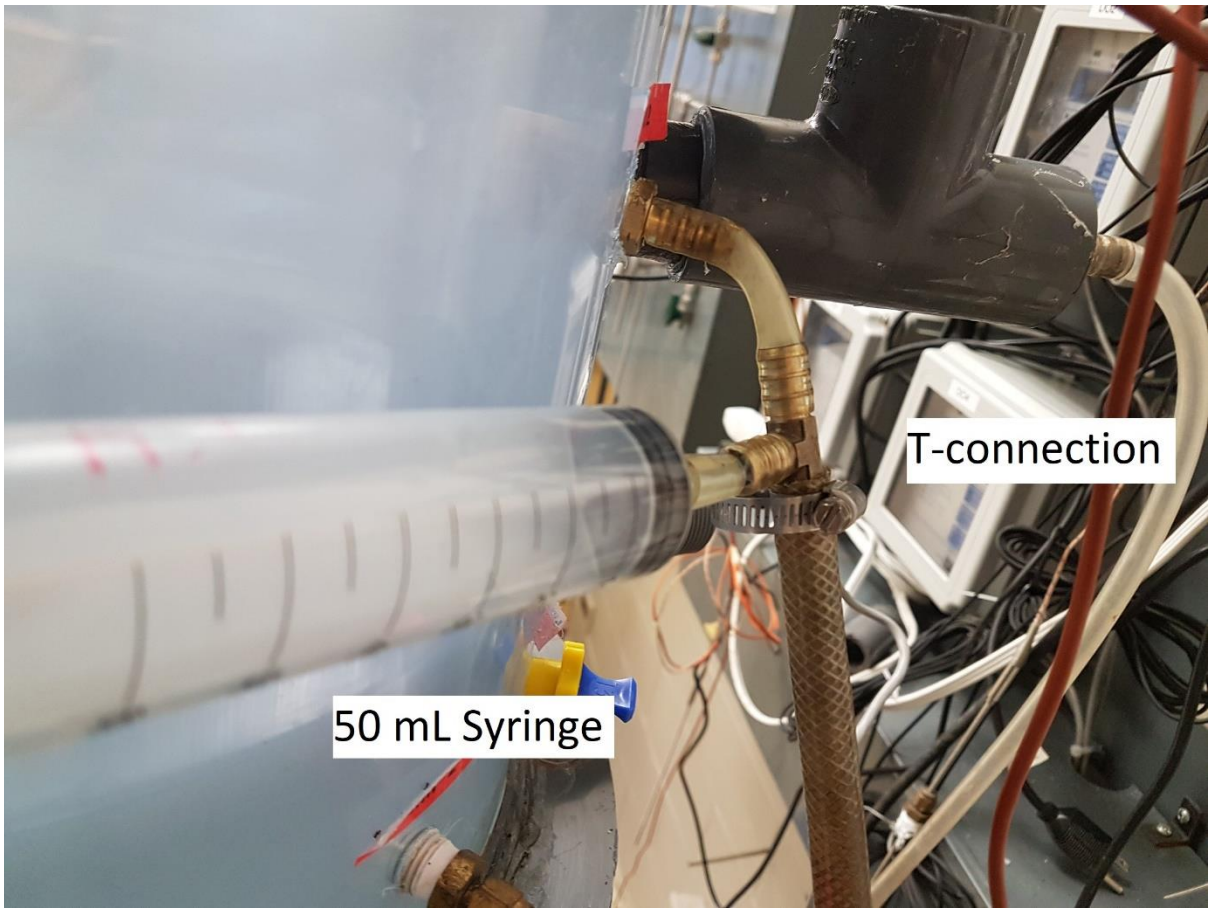

FIGURE 3.8: TRACER INJECTOR TRIAL 2

The second injector design was simpler; the injector port was removed all together (Figure 3.8). A larger 50 mL syringe was connected directly into the t-connection with a small length of tubing to the feed line in the first stage. The length of tubing was minimized in order to reduce any lag time and any dead space that would reduce that amount of tracer injected. Initially a rubber band was tied around the syringe to prevent back- flow into the injector, but the pressure in the line was found to be insufficient to cause this effect.

Different volumes of tracer were tested (between 10 and 50mL) and it was found that 50 mL produced the best response in the DAS. The operating conditions were maintained the same as literature values to ensure consistency (Table 8).

3.2 Data Analysis

3.2.1 Conductivity versus Concentration of Tracer Solution

Originally, the assumption was of a linear relationship between tracer concentration and conductivity. This assumption simplifies the creation of the RTD diagrams, as the conductivity measurements would require an additional conversion step to concentration.

Some of the conductivity sensors had shown strong evidence of deterioration with the formation of rust as evident in Figure 3.9 and Figure 3.10. Performing this assumption also had the additional benefit of eliminating the requirement of continuously re-calibrating the sensors. The sensor that exhibited deterioration still produced a reading, but it would be inconsistent with other sensors. When transforming the readings into the dimensionless E (t) charts, any deviation between sensors would be removed. The sensors required precision rather than accuracy.

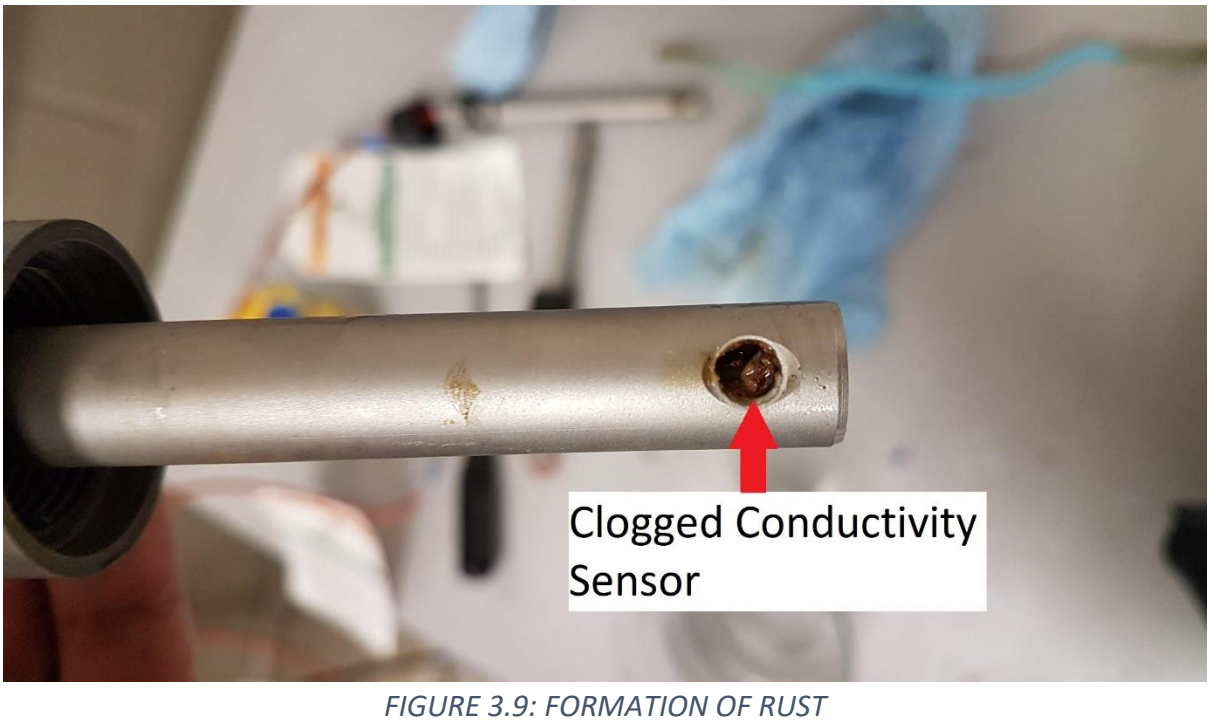

FIGURE 3.9: FORMATION OF RUST

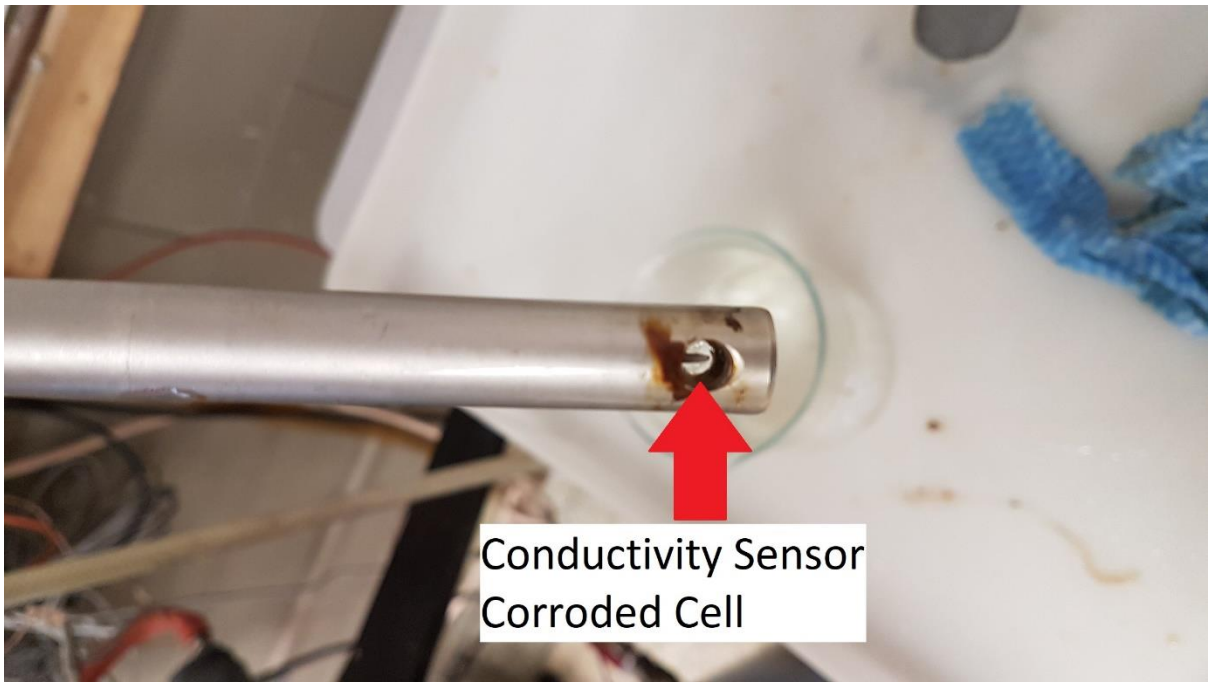

FIGURE 3.10: THE EFFECT OF RUST

Figure 3.11 shows, as expected, the linear relationship between concentration of sodium chloride in tap water and conductivity. Sodium chloride solutions act as the tracer in the experimental unit (vertical bioreactor). A beaker with tap water was placed on a hot plate with a magnetic stirrer. The heat was not turned on the hot plate, only the built in stirrer functionality was used. There was no requirement to use distilled or de-ionized water as the main feed in the reactor was tap water. The average conductivity would never be in the range of de-ionized water. With the use of a laboratory scale, small amounts of laboratory grade sodium chloride was added (about 0.5 grams) to the beaker of 500 mL of tap water. The experimental setup is outlined in Figure 3.12. It is important to note that the behavior of laboratory sodium chloride is different from regular table salt. Table salt includes an anti-caking agent that prevents clumping and enhances ease of pouring [86]. Without the anti-caking agent, laboratory sodium chloride is much more difficult in measuring equal weights. The actual sensors used to develop the RTD diagrams were used to ensure consistency. A laboratory conductivity meter would have provided more accurate results, but the main interest is the effect on the specific sensors that are used.

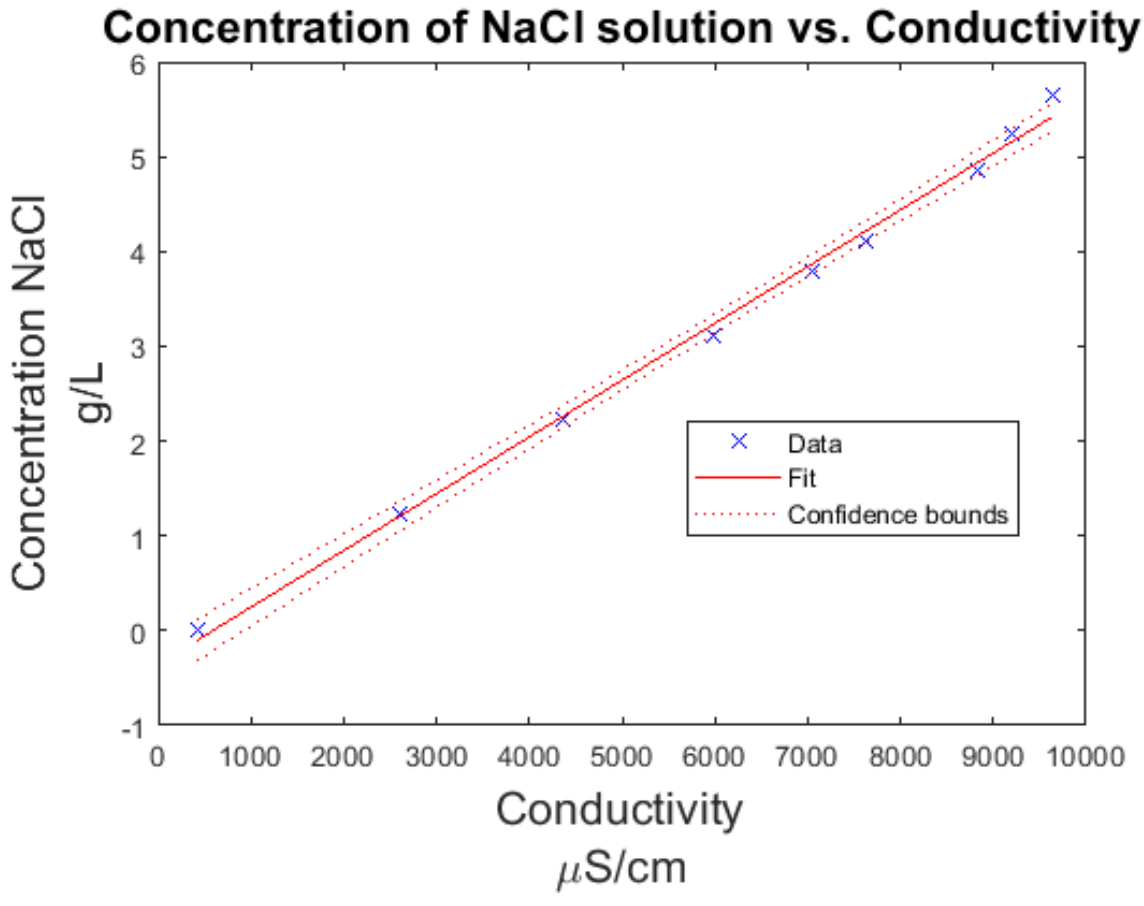

FIGURE 3.11: CONCENTRATION VS. CONDUCTIVITY

In total, eight different samples of sodium chloride salt were added to the solution for nine different conductivity measurements. The experiment continued to a conductivity reading of 10,000 µS/cm as that is the maximum reading for the sensor and very close to the upper limit for the solubility of sodium chloride in water. It is evident of a strong linear relationship as the R^2 value for the linear interpolation is 0.996.

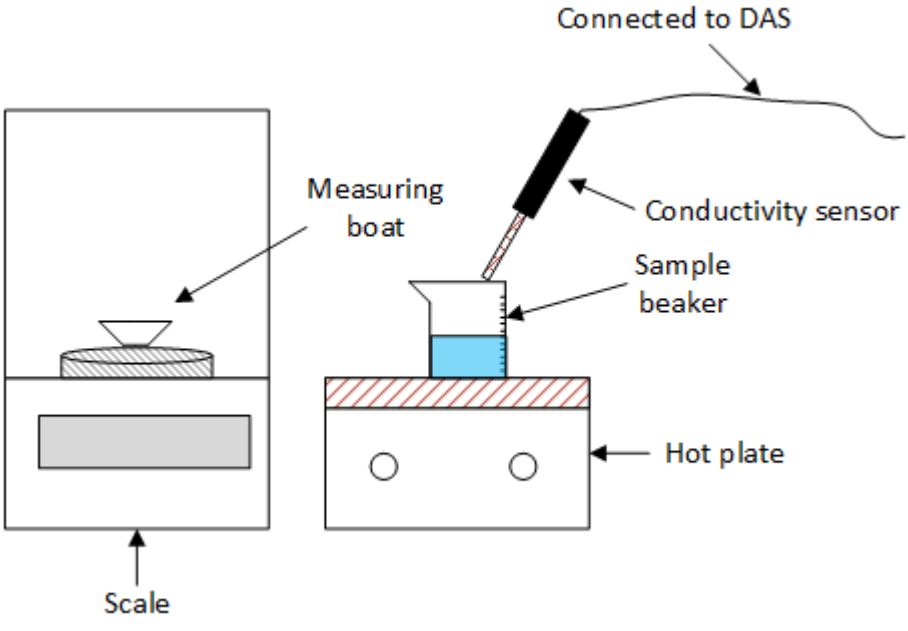

FIGURE 3.12: CONCENTRATION VS CONDUCTIVITY EXPERIMENT SETUP

3.2.2 Transformation to Probability Density Function

The tracer experiment produces results in a spreadsheet of the different conductivity measurements taken at a sample time of every three seconds (refer to Appendix 4: Sample Data for a sample of the results). These tables were then expressed in a graphical format.

A few issues need to be addressed to transform the sample results into the Probability Density Function (E (T)). The E (T) represents the probability of a tracer exiting the reactor as a function of time as described by the following equation:

$$E(t) = \frac{C(t)}{\int_0^\infty C(t)dt}$$

The conductivity of tap water is not uniform, variations in water treatment processes to different compounds leaching from piping cause this inconsistency. These variations need to be accounted for in order to transform the conductivity graphs into RTD graphs. This task was initially completed by simply subtracting the lowest value from every value. This did not provide satisfactory results as the initial and final conductivity values differed. The fouling of the sensors due to rust deposits likely causes this. A linear regression model was

implemented to solve this problem from the first ten and the last ten data points. This was achieved in Matlab utilizing the function “fitlm". Refer to Appendix 5: Sample Linear Regression Model for a sample of this regression model.

Additionally, there was a large amount of noise from the collected samples so a regression model was used to clean up the data. It was later decided that the Matlab function "filter" using a moving average was a better solution. The amount of points to be affected by the filter was chosen experimentally. The lowest value that significantly cleaned up the data, to the point where is looked like a smooth curve was selected.

The next step was to change the values from a function of the concentration to a probability. This is achieved with the following equation:

$$\mathrm{E(t)} = \frac{\mathrm{C(t)}}{\int_0^\infty C(t)dt}$$

where E (t) is the Probability Density Function and C (t) (M/L) is the concentration of tracer measured. This formula is based on the concentration of the tracer, but it is also true for any function of concentration such as the previously proven conductivity. There are a few numerical methods to find the integral from a set of data points, but the trapezoidal method was selected for its ease of use and because it is already built into Matlab as explained in Appendix 6: Numerical Integrations.

One advantage of using a concentration vs time graph is that the value of the integral across time is equal to the mass of tracer injected into the reactor. This provides an additional check to ensure that no tracer is absorbed by the reactor or lost. The value obtained from an arbitrary measurement, such as conductivity, provides no such benefit [56].

Now that the E (t) curve has been generated, the moments of the distribution can be evaluated. The first moment ($\bar{t}$)was describe in (2.19) as:

$$\bar{t} = \int_0^\infty tE(t)dt \tag{2.19}$$

and the second moment described as:

$$\sigma^2 = \int_0^\infty \left[\bar{f} - f(t)\right]^2 E(t)dt \tag{2.21}$$

For the ease of comparison between models and data, the dimensionless probability function E (θ) was found be normalizing the time as:

$$\theta = \frac{t}{\bar{t}} \tag{3.1}$$

where t (T) represents time and $\bar{t}$ (T) represents the sampling mean time. The dimensionless probability distribution is then defined by:

$$E(\theta) = E(t) \times \bar{t} \tag{3.2}$$

by changing to E (θ), the models can be evaluated with a mean residence time of 1, which simplifies the process. The models were evaluated by the root square mean average as described in 2.5.5 .

3.4 Recycle Experiment

The tracer experiment ran with the reactors internal recycle pump and recycled sludge turned off. This allowed the determination of the MRT through a single run of the reactor. This data was superimposed on a previously run experiment to observe the difference of the recycle streams. The optimization of the MRT by controlling the internal recycle rate can then be considered.

3.5 Characteristic Parameters

The data provided by the internal recycle testing allow for additional testing for dead space and by-passing (as described in section 2.3.3). The mean residence time can be calculated by the following equation:

$$\tau = \frac{V}{v}$$

where τ is the mean residence time (h), V is the total reactor volume (L) and v is the volumetric flow rate (L/h). The total volume is the sum of the volumes of each section: V = $V_{anoxic1}$ + $V_{anoxic2}$ + $V_{aerobic}$ = 10L + 10L + 45L = 65L. The volumetric flow rate was maintained at 10 L/hr resulting in a τ = 6.5hrs. The sampling mean time $\overline{t}$ (h) was defined as:

$$\overline{t} = \int_0^\infty tE(t)dt$$

as a summary of section 2.3.3, the following relationship is true:

$$\tau_{Dead-space} < \tau_{Theoretical} < \tau_{By-pass}$$

The quantities of Hold-back (H) and Segregation (S) were also found as described in section 2.3.4. The values were obtained after finding the Distribution Function (F (t)) from the Probability Density Function (E (t)). They are related from the following equation:

$$F(t) = \int_0^\infty E(t)dt$$

All of these values were obtained with the use of Matlab scripts.

Chapter 4 : Results

4.1 Error Analysis

Figure 4.1 represents the raw data collected from the tracer experiment on December, 19, 2019. A sample of 50mL of tracer solution (5 g/L) was injected a few seconds after the initial sampling. The sampling rate was set to three seconds for the conductivity sensors. There is a plot for the conductivity sensor for the recycle stream, the stream into stage 2 from stage 1, stage 2 to stage 3 and one for the reactor effluent. The graphs show the conductivity of the liquid flow trend of the tracer throughout the stages. Although some noise is observed in the raw data a general trend can be observed.

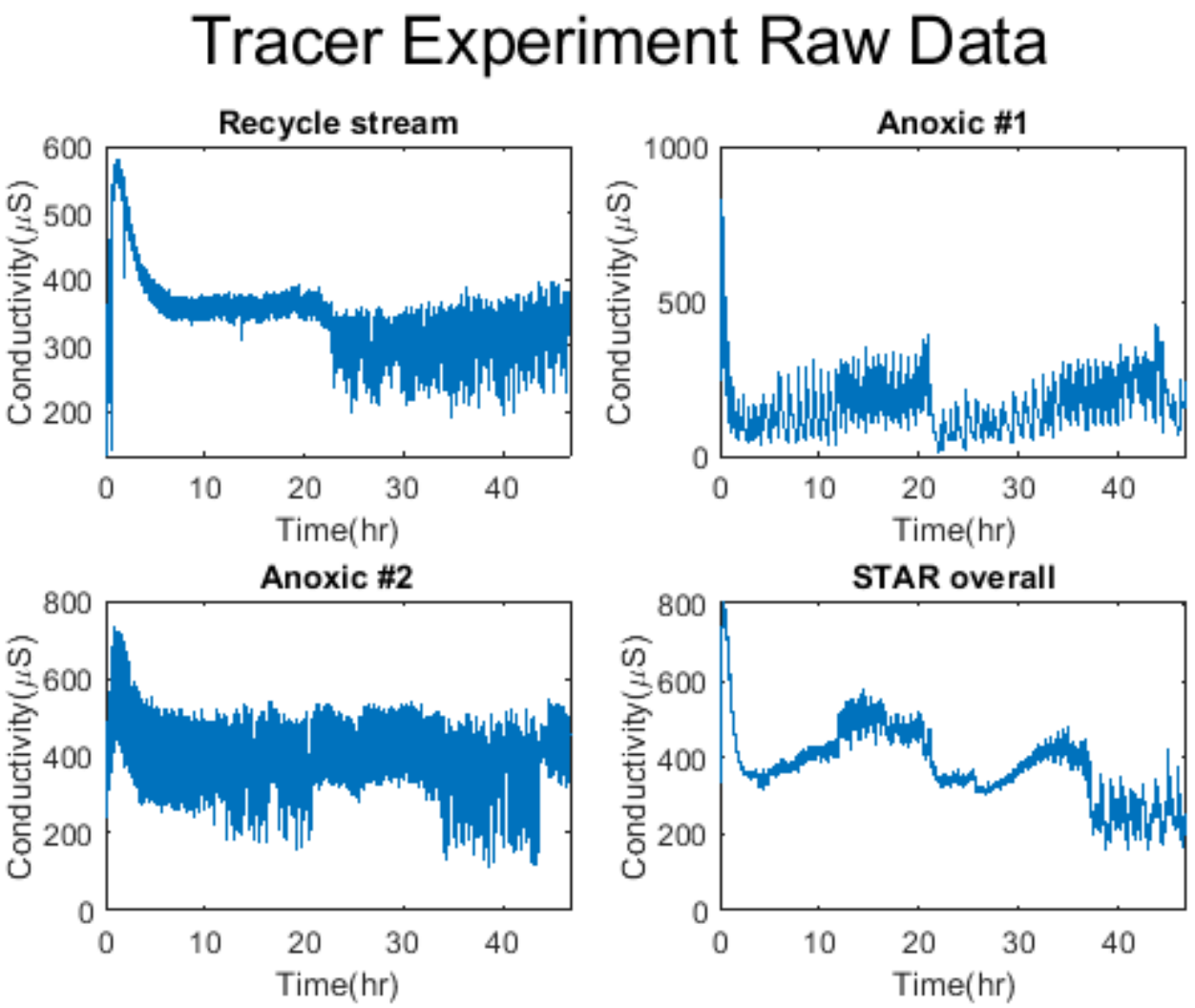

FIGURE 4.1: RAW DATA OF TRACER EXPERIMENT

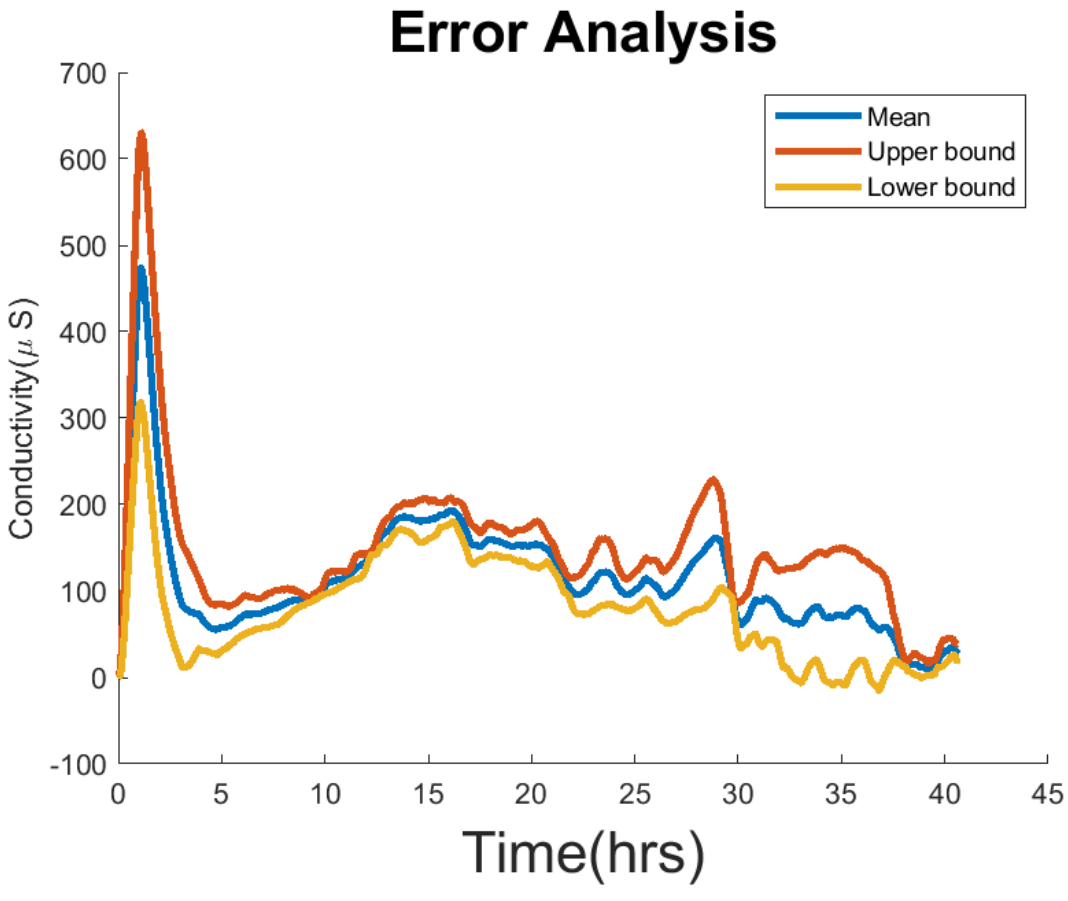

FIGURE 4.2: ERROR ANALYSIS

The experiment was performed over three trials. Although the curves comprises of a large quantity of points, each curve represents only one measurement. The mean was plotted with the upper and lower bounds in Figure 4.2. The bounds were found using the average deviation which is represented by a vector along the length of the curve. The average value of the deviation vector was found to be ± 34.6 µS.

The overall RTD for the different trials are examined on Figure 4.3. The trials exhibited different conditions (ex. tracer volumes), but their overall behaviour is consistent as shown in Table 9. Table 9 illustrates the error between each of the trials. This measurement of error will be used as a benchmark for the model testing. The first and second moments (Mean Residence Time and Variance) of the RTD for three different trials are summarized in Table 10.

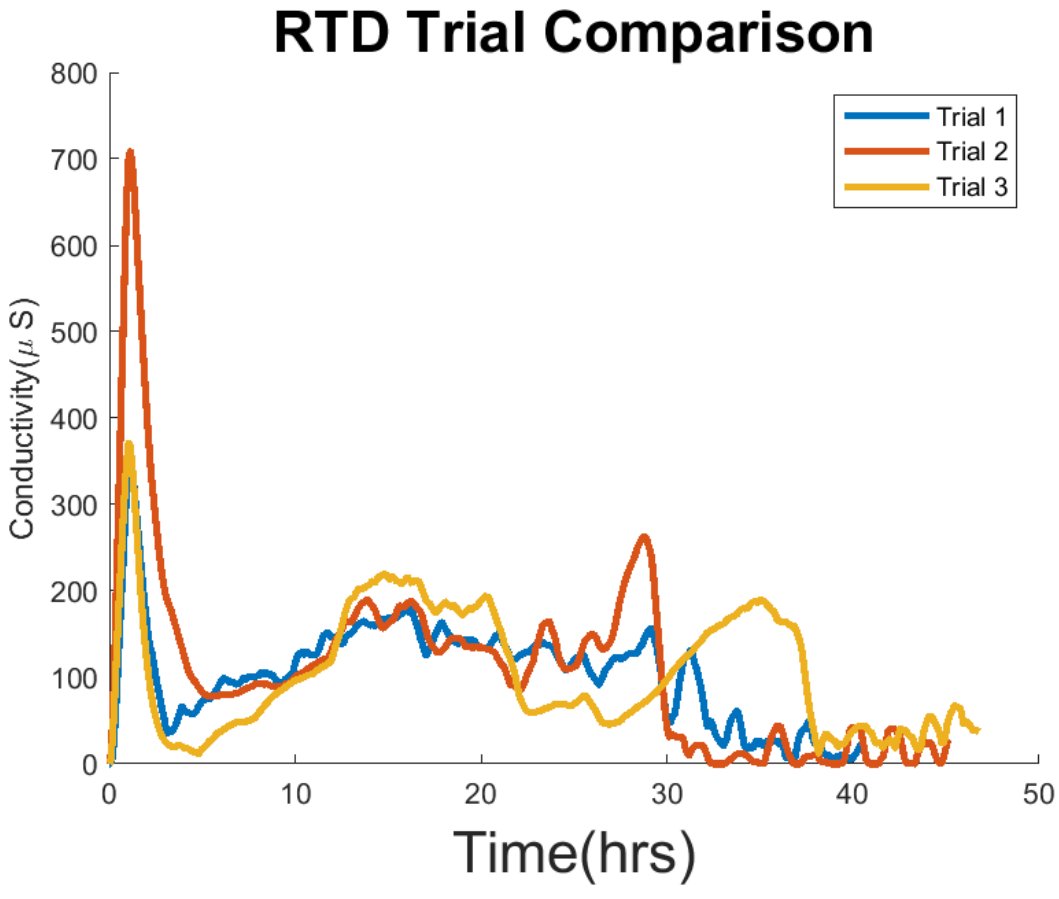

FIGURE 4.3: DIFFERENT RTD TRIALS FOR OVERALL REACTOR

Compared Trials	RSME
Trial 1 and 2	0.206
Trial 1 and 3	0.284
Trial 2 and 3	0.364
Average	0.285

TABLE 9: ERROR BETWEEN DIFFERENT TRIALS

	Mean Residence Time(hrs)	Variance
Trial 1	16.9	94.7
Trial 2	14.7	113.5
Trial 3	21.2	141.6
Average	17.6	116.6

TABLE 10: RTD CHARACTERISTICS OF DIFFERENT TRIALS

Figure 4.4 represents the dimensionless RTD function for the fourth sensor representing the effluent from the entire reactor. The plot exhibits a large thin peak followed by two wide, but shorter peaks. The distance between each peak is around 0.75 times the mean residence time. Figure 4.4 shows the dimensionless RTD for the raw data represented in Figure 4.1.

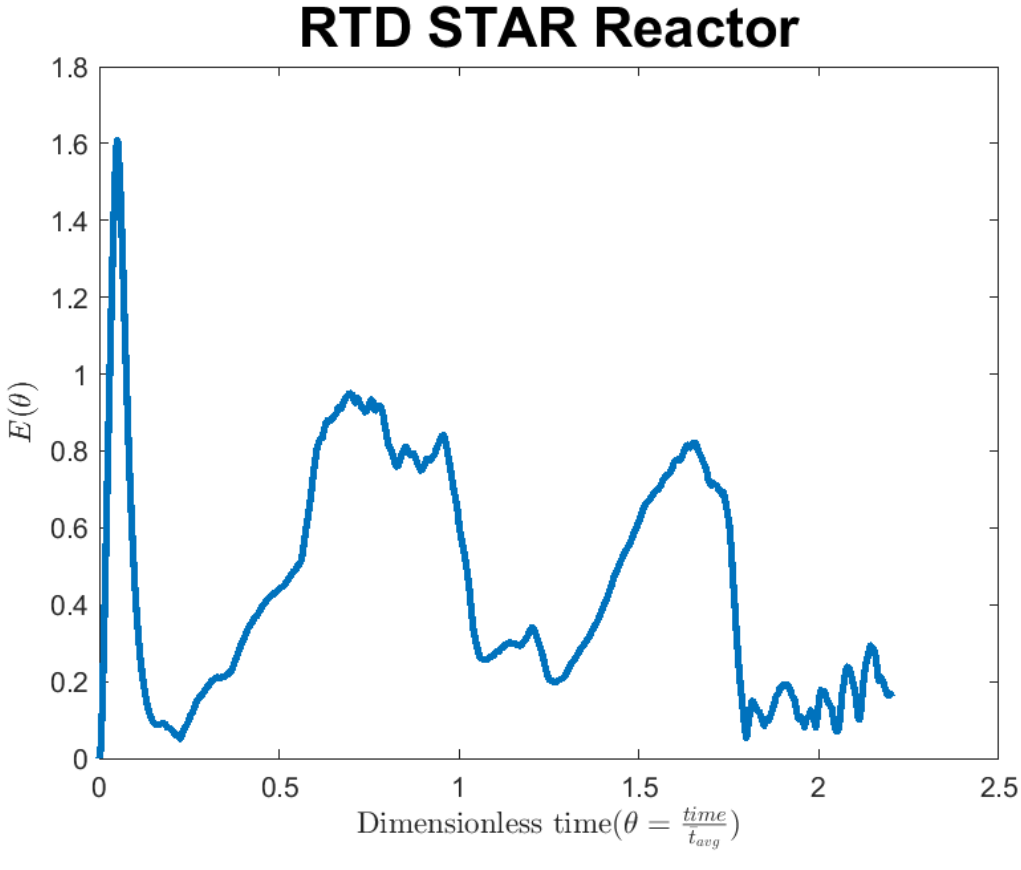

FIGURE 4.4: STAR REACTOR RESIDENCE TIME DISTRIBUTION FUNCTION

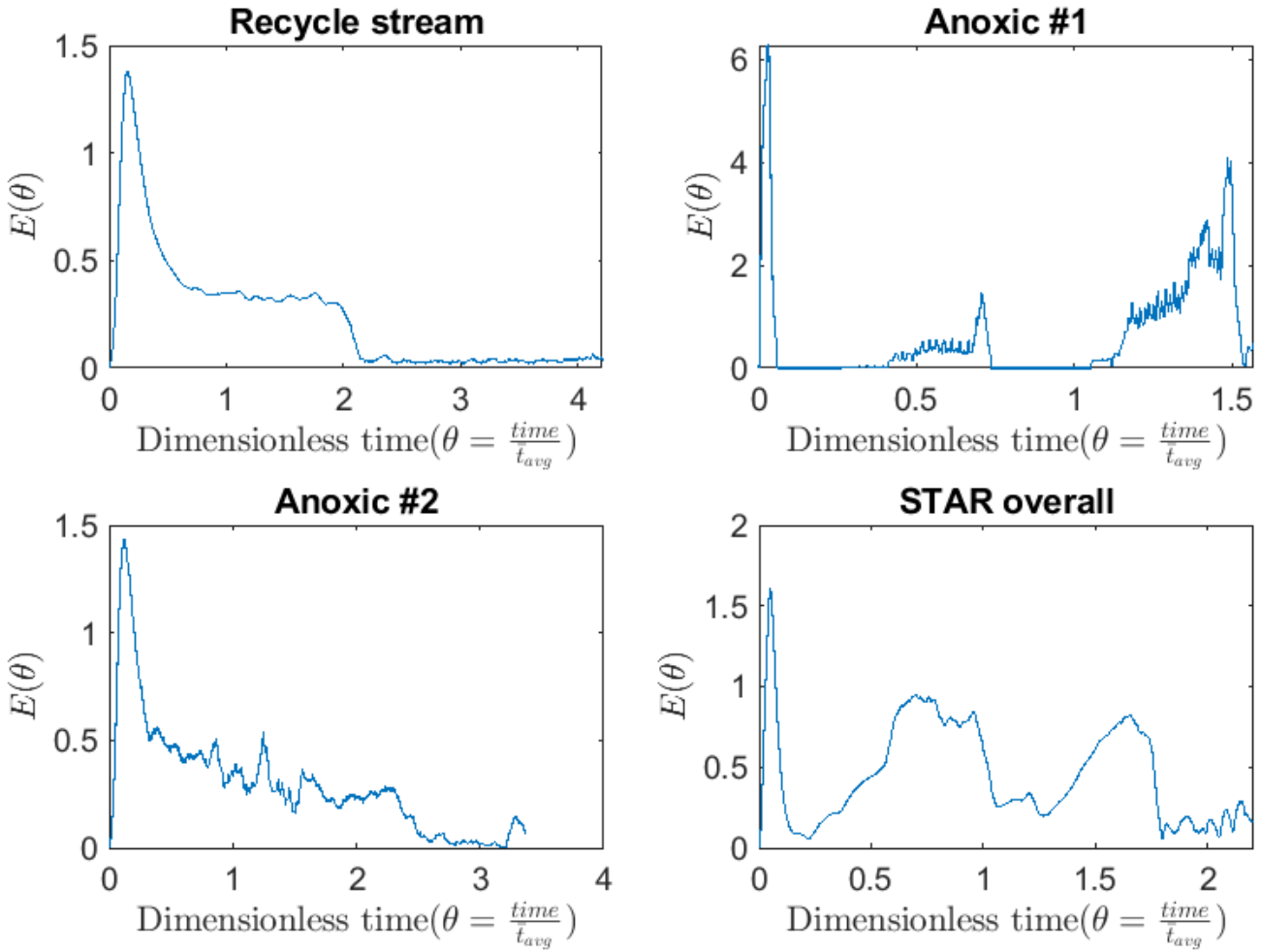

FIGURE 4.5: TRANSFORMED DIMENSIONLESS RESIDENCE TIME DISTRIBUTIONS

4.2 Model Testing

Figure 4.6 demonstrates how the ideal models fit the RTD for this trial while Figure 4.7 and Figure 4.8 test different real reactor models. In every plot, the experimental data is represented in blue. The values of the error for each model are also displayed in the legend for the respective plots. The behaviour of RTD is closer to that of the ideal CSTR than it is of the ideal PFR. The difference in error between the two ideal conditions is on a factor of 3.

There are three reactor models in Figure 4.7 and two models in Figure 4.8. The real reactors are better fits for the RTD than the previous ideal reactor models.

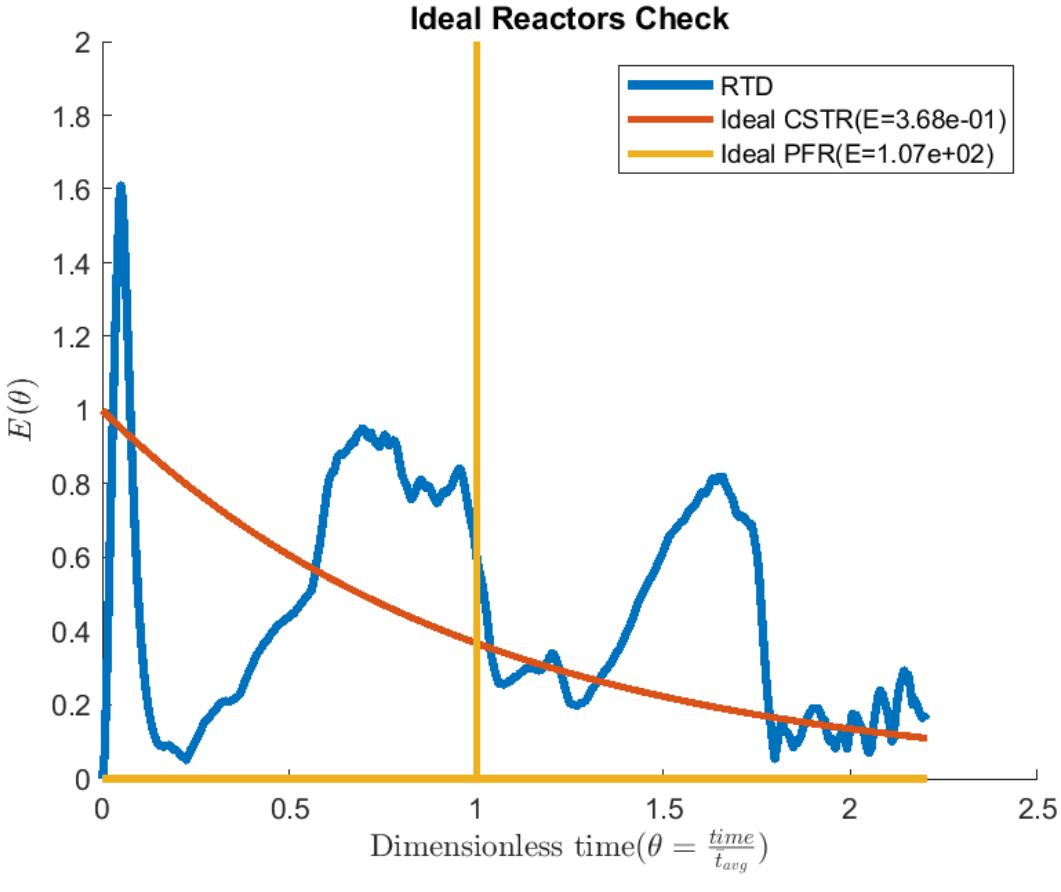

FIGURE 4.6: IDEAL MODELS TEST

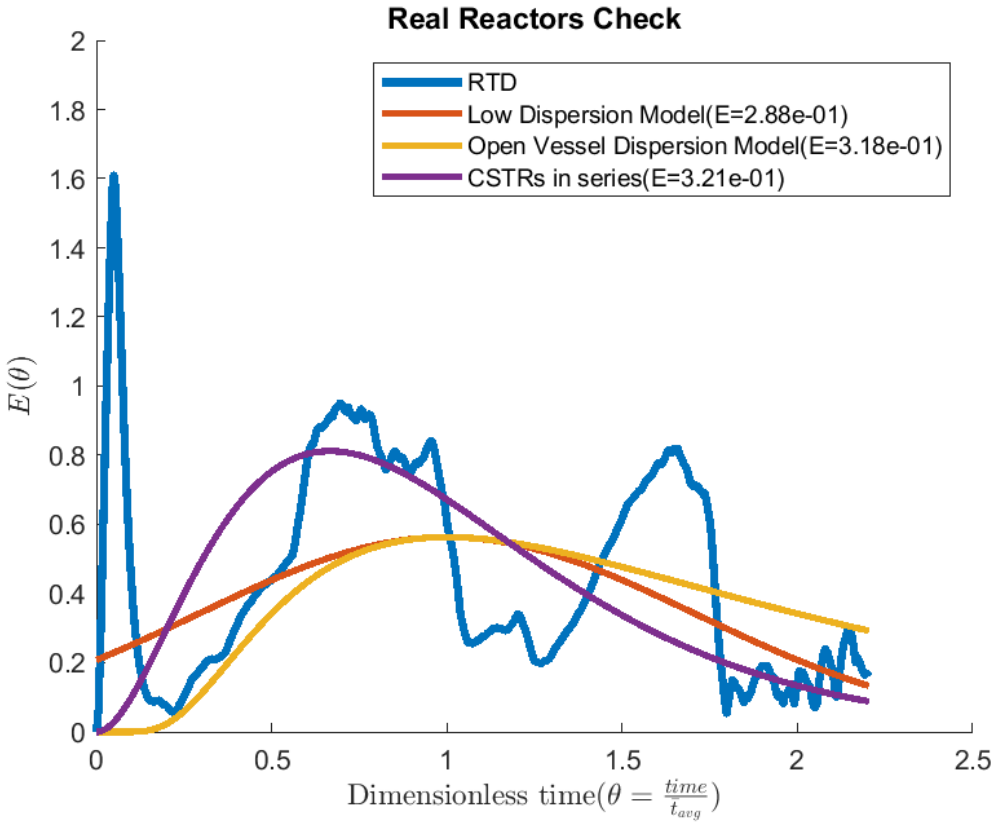

FIGURE 4.7: REAL REACTOR MODELS TEST

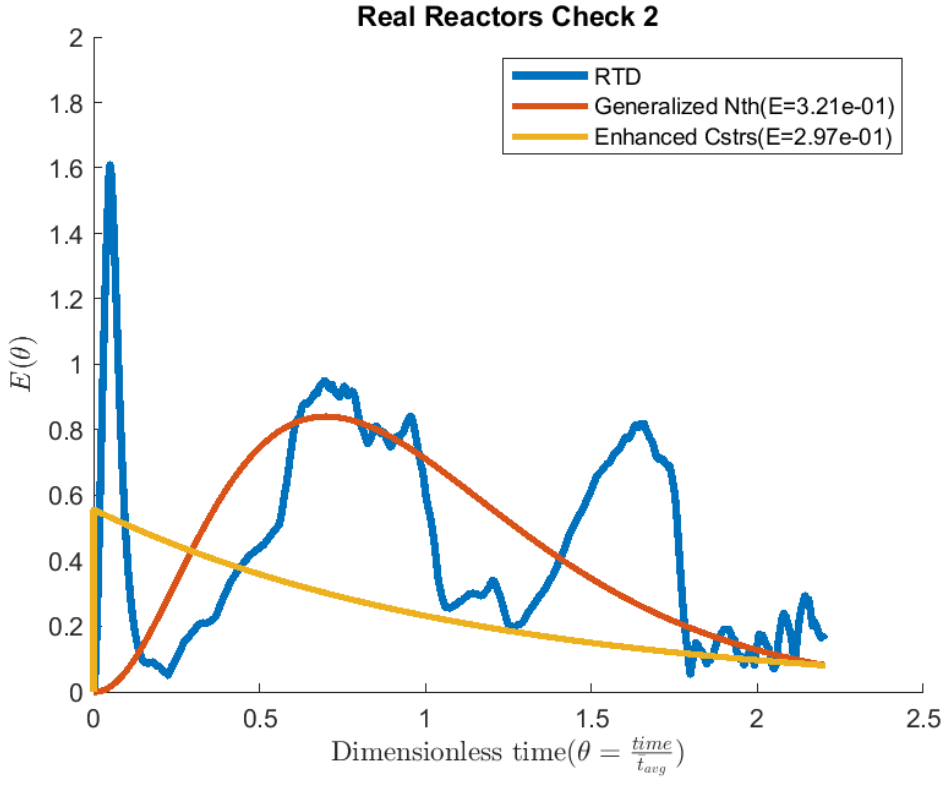

FIGURE 4.8: REAL REACTOR MODELS TEST CONT.

Table 11 shows the average error measured for each of the models against three different experiment trials while Table 12 summarizes their parameters of best fit. The enhanced CSTR in series model shows the best fit for the data, but it is on the same scale as the ideal CSTR.

	CSTRR	PFR	Low D	DispOpen	CSTRS	Nth CSTR	E-CSTRS
Trial 1	0.27	92.47	0.18	0.25	0.25	0.25	0.20
Trial 2	0.27	75.05	0.30	0.37	0.27	0.27	0.26
Trial 3	0.37	107.43	0.29	0.32	0.32	0.32	0.30
Average (fit)	0.30	91.65	0.26	0.31	0.28	0.28	0.25

TABLE 11: MODEL TEST SUMMARY

	Low D	Open D	#CSTRS	#nthCSTRS	#ECSTRS	n min	M min
Trial 1	0.25	0.25	2	1.52	3	0.64	1
Trial 2	0.42	0.67	1	1	1	0.55	0.36
Trial 3	0.25	0.25	3	3.34	1	0.64	0.73
Average	0.31	0.39	2	1.95	2	0.61	0.7

TABLE 12: MODEL OPTIMAL PARAMETERS

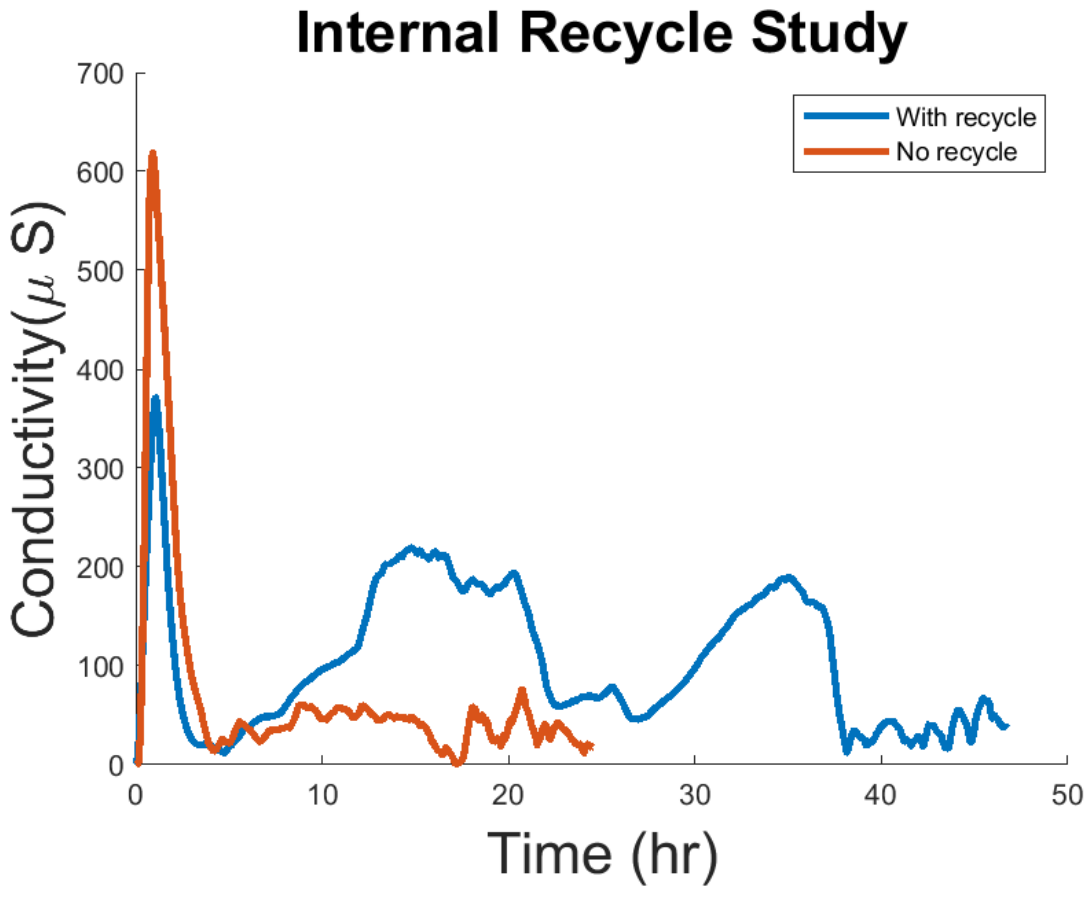

FIGURE 4.9: INTERNAL RECYCLE STUDY

4.3 Internal Recycle Experiment

Figure 4.9 shows the comparison of the RTD with and without the internal recycle turned on. The initial peak for both trials are located at the same time, but the probability is much lower when there is a recycle. The RTD with respect to real time was compared rather than the dimensionless time because the two plots have two different mean residence times. The second and third peaks are not present in the trial without the recycle signifying that the recycle stream is responsible for the additional peaks as expected.

4.4 Characteristic Parameters

4.4.1 Dead Space and By-passing

The sample mean time for the system without a recycle was found to be 7.02 hrs. This value is compared to the mean residence time for the reactor of 6.5 hrs. As the sample mean time is larger than the mean residence time, this signifies by-passing in the system. The by-pass rate was found as 7.5% of the feed into the first stage of the reactor.

4.4.2 Hold-back and Segregation

For the definition of Hold-back (H) and Segregation quantity (S), please refer to section 2.3.4 Hold-back and Segregation. The plot for the Distribution Function (F (t)) was found by taking the numerical integration of the probability density function (E (t)). The Hold-back value of H was then obtained from the area under the curve from $\theta = 0$ to $\theta = 1$. The area is illustrated in Figure 4.10 in blue, but the value H was found to be 0.2365.

The value for segregation (S) was found from plotting the F (t) with the F (t) for the ideal CSTR. The intersecting points were found with a Matlab script. Since the plots do not meet at set points, a certain tolerance (< 0.00001) was used to find their intersection. From the plot (Figure 4.11), it may appear that the reactor exhibits a dead space with the CSTR precedes the reactor. This is incorrect as there is a small region where the reactor precedes the CSTR, which is difficult to observe due to the scaling of the figure. The zoomed-in Figure 4.12 clearly demonstrates this point. This is evidence that there is no dead space. The value of segregation (S) was found to be -0.16. As this is a very low value, it signifies that the

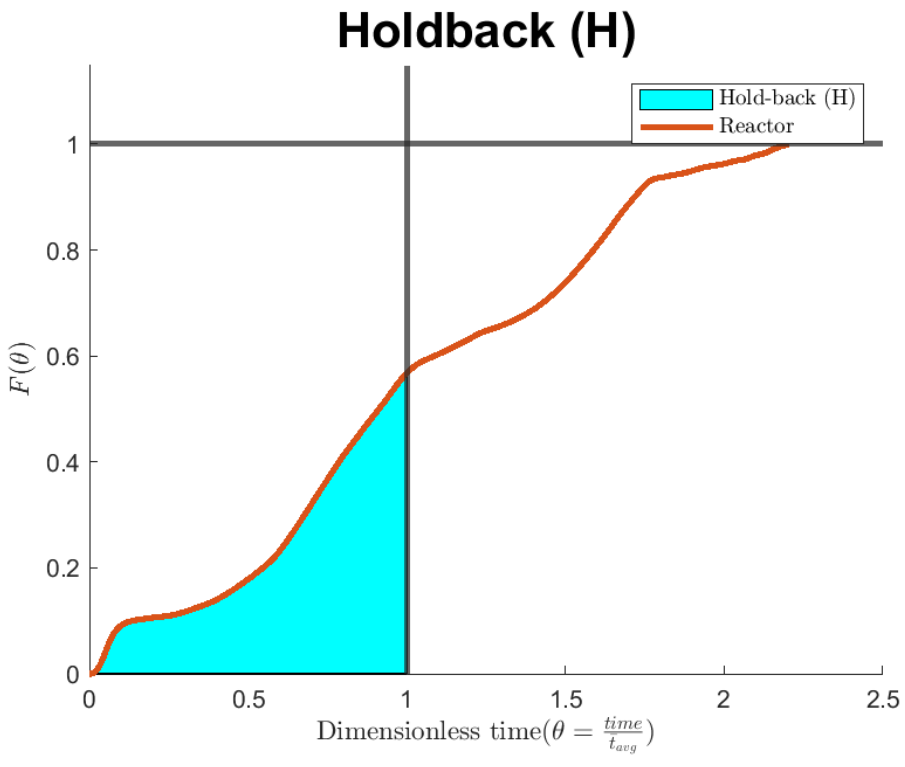

FIGURE 4.10: HOLD-BACK FOR THE VERTICAL BIOREACTOR

reactor behaves very similar to the ideal CSTR. This demonstrates that the cylindrical geometry of the STAR reactor satisfies the conditions for a high level of mixing.

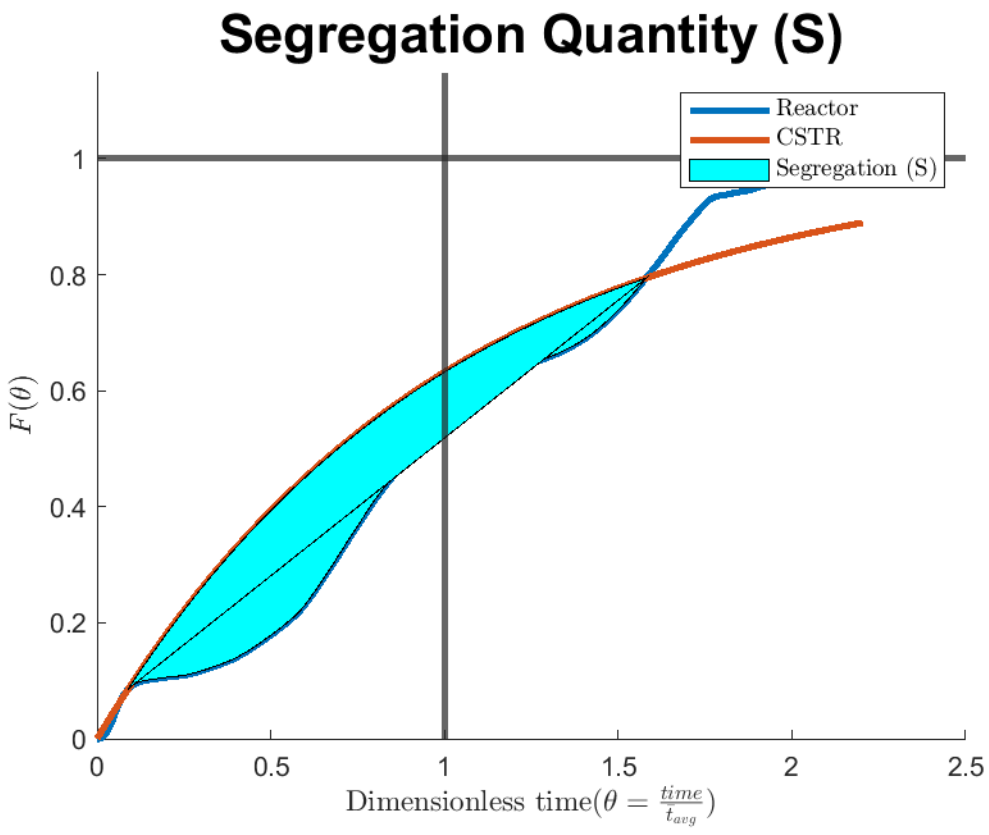

FIGURE 4.11: SEGREGATION (S) FOR THE VERTICAL BIOREACTOR

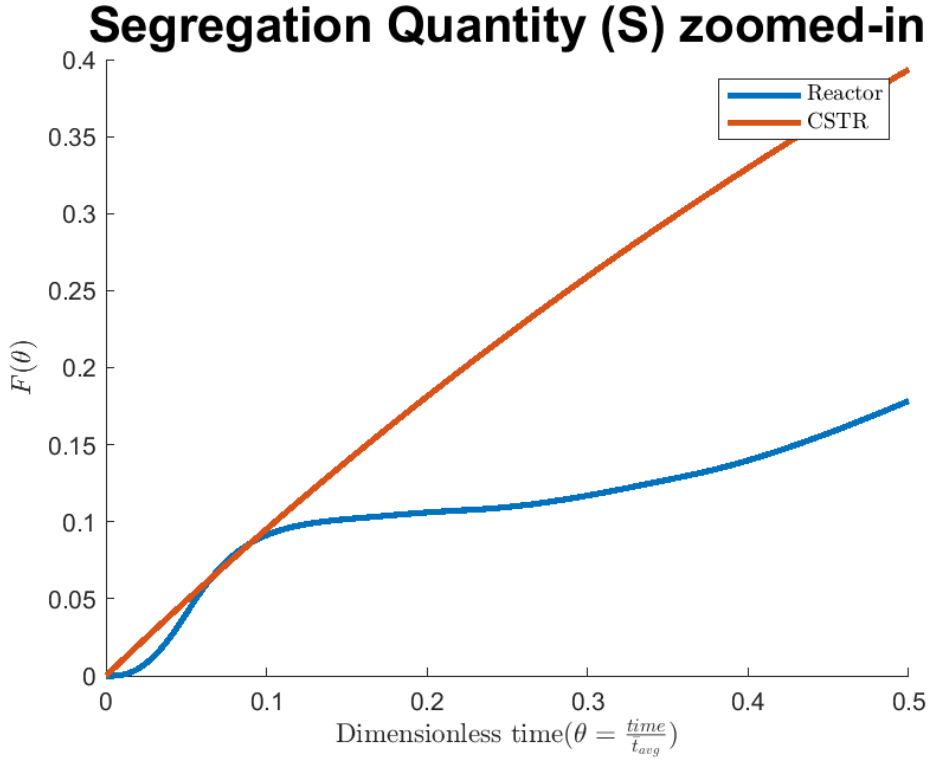

FIGURE 4.12: ZOOMED-IN SEGREGATION (S)

Chapter 5 : Discussion

The results of the tracer experiment show that the mixing profile of the vertical bioreactor can be obtained. A plot of the Residence Time Distribution (RTD) was obtained and repetition had shown to be consistent (Figure 4.3). Through analysis of the constructed RTD, different mixing models were evaluated including: the ideal CSTR, the ideal PFR, the low dispersion, the open dispersion, the CSTR in series, the Nth generalized CSTR in series and the enhanced CSTR in series. Table 11 shows that all of the CSTR in series model variants (including generalized Nth and the enhanced), the open and low dispersion models as well as the ideal CSTR accurately fit the mixing profile. It important to note that the dispersion coefficients (0.31 for low and 0.39 for open) are much greater than 0.01 and thus represent a large deviation from Plug Flow[56].

This evidence suggests a high level of mixing in a vertical bioreactor such as the low for Segregation (-0.16) and the similar level of Hold-back when compared to the CSTR (0.2365 when compare to an ideal value of 0.3679). The ideal CSTR was a very good fit while the ideal PFR was very poor. This is important for two reasons:

- It supports the claim of a high level of mixing due to the reactor geometry [9]
- High levels of mixing are desirable to secure flow uniformity and avoid stagnancies in wastewater treatment bioreactors

Secondary findings show - based on the internal recycle testing - that the reactor exhibits a by-passing of 7.5% of the feed stream.

All evidence collected suggest a high level of mixing within the vertical bioreactor. It supports the claim of a high level of mixing due to the tubular geometry. Conventional bioreactors in wastewater engineering exhibit poor mixing profiles and poor conversions (due their reaction kinetics). The field of Biological Nutrient Removal (BNR) research is ever expanding and more research into vertical bioreactors is promising.

Some limitations of this research include the assumption that the reactor with clean water will act the same as wastewater. This is a generally accepted assumption, as the density of activated sludge does not vary much for water. There is also a time constraint to consider as the reactor originally took 230 days for the biomass to get to a steady state [9]. In order to insure that each sensor was adequately submerged, fluid levels were “held-back". These actions will in fact affect the flow dynamics of the system to some degree. These measures were however necessary to obtain consistent readings.

Future research would be the application of the wastewater reaction kinetics (such as the ASM2D mentioned in the literature review) across the developed model. These models still require chemical and microbial kinetic parameters, which can be found in literature, but due to the complicated nature of a mixed population of microbes would be best found experimentally. This experiment can be performed by seeding the reactor with microbes and developing the population. Samples from each section would be taken and their reaction kinetics found in a batch reactor.

There could be some advantage in modeling the vertical bioreactor with a Computational Fluid Dynamics (CFD). CFDs can identify the physical locations of dead space and by-pass within the reactor. There was found to be 7.5% by-passing in the reactor which could be better identified with a CFD. A potential source of by-passing was observed in the anoxic zone 2 (Figure 5.1) which was not addressed due to the current public health crisis and hence time restraints. Addressing this concern, then determining the new amount of by-passing would be an easier solution.

Additionally, the vertical bioreactor has been tested experimentally and shown to be well represented by a CSTR. There is potential value of using a more complicated model to represent the mixing profile, such as the Axial Dispersion model or the Generalized N-CSTR in series model. As expected, the Dispersion coefficient ($\frac{D}{uL}$ in this study) is very high (hence the approximation to a CSTR) and represents a large deviation relative to the ideal PFR. The reactor also exhibits by-passing of 7.5%.

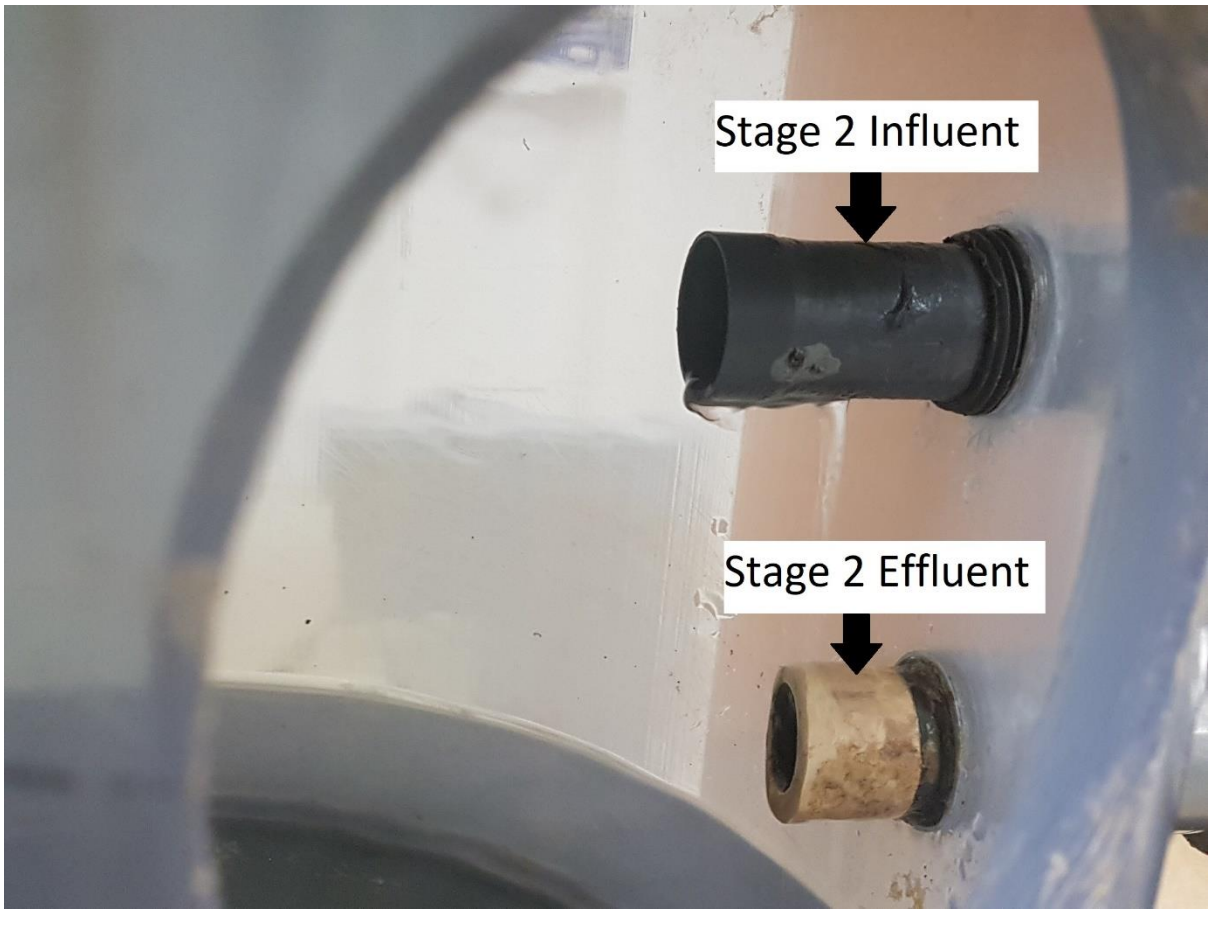

FIGURE 5.1: POTENTIAL SOURCE OF BY-PASSING IN STAGE 2 OF STAR REACTOR

Chapter 6 : Conclusions

The mixing profile for a vertical bioreactor was found by performing tracer experiments. The collected data was then converted into the dimensionless Residence Time Distribution (RTD). The behaviour of the flow was interpreted from these results with the effect of the internal recycle evident. There was no evidence of dead space, but 7.5% by-passing was found.

The mixing profile was then compared to both ideal and real reactor models. It was found that the generalized Nth CSTR in series model and the ideal CSTR fit the mixing profile observed in the vertical bioreactor. The CSTR in series could fit the overall vertical bioreactor, particularly with the generalized Nth modification, but it is unlikely to represent each individual stage well. The first and second stages (10L) are much smaller than the third stage (45L) with a much smaller resulting sampling mean time ($\bar{t}$). The average value the overall reactor was 17.6 hrs and 11hrs for the second stages across three trials. The CSTR in series model depends on reactors with the same volume and residence time, which does not represent the vertical bioreactor well. The parameters for Hold-back (H) and Segregation (S) were found to be 0.2365 and -0.16 (unit less) respectively. In both cases, this suggests a high level of mixing, similar to the ideal CSTR behaviour.

6.1 Future Work

Future work would entail the following:

- The union of the Residence Time Distribution (RTD) data with a microbial reaction kinetics model, such as the ASM2D
- Optimization of residence time by controlling internal recycle rate
- Construction of a computerized fluid dynamic model to be verified by RTD data
- Expansion of unit capacity (demonstration scale)

Appendix

Appendix 1: Gamma Function

The Gamma function was used to expand the use of a factorial from all natural number ($\mathbb{N}$) to all real numbers ($\mathbb{R}$) in the Nth generalized CSTR in series model by Martin. The Gamma function has been defined by Euler as the following:

$$\Gamma(n) = \int_0^\infty x^{n-1} \cdot e^{-n} dx$$

where the following conditions are also satisfied:

$$\Gamma(0) = \Gamma(1) = 1$$
$$\mathrm{n} \cdot \Gamma(n) = \Gamma(n+1) \forall n \in \mathbb{R}$$
$$\Gamma(n) = (n-1)! \forall n \in \mathbb{N}$$

Appendix 2: Integrating Factor

For the ordinary differential equation such as this:

$$\frac{dy}{dx} + p(x)y(x) = q(x)$$

find the function $v\ (x)$ such that this is true:

$$v(x) = \int p(x)dx$$

$$\frac{dv(x)}{dx} = p(x)$$

the integrating factor is then $e^{v(x)}$ giving the expression and substituting the initial differential equation:

$$\frac{d}{dx}\left[e^{v(x)}y(x)\right] = e^{v(x)}\left[\frac{dy(x)}{dx} + p\ (x)y(x)\right] = e^{v(x)}q(x)$$

then integrating both sides:

$$y(x) = e^{-v(x)}\int e^{v(x)}q(x)dx$$

Appendix 3: Sensor Specification

The following are exerts taking from Omega manual for the CDCE-90-1 conductivity sensor [87].

1. Wiring

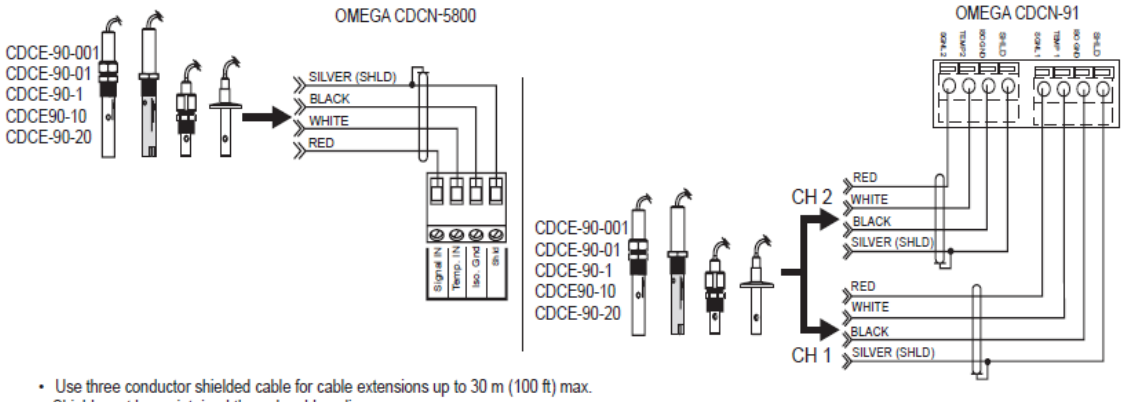

- Use three conductor shielded cable for cable extensions up to 30 m (100 ft) max.
- Shield must be maintained through cable splice

2. Recommended Position

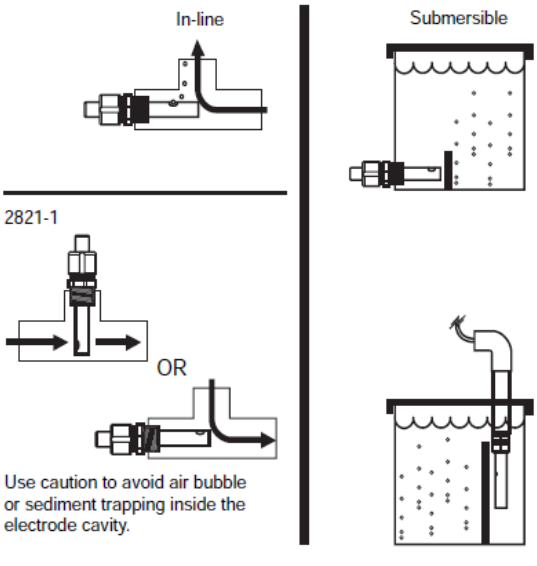

Use caution to avoid air bubble or sediment trapping inside the electrode cavity.

3. CDCE-90-001/CDCE-90-01/CDCE-90-1 In-line Installation

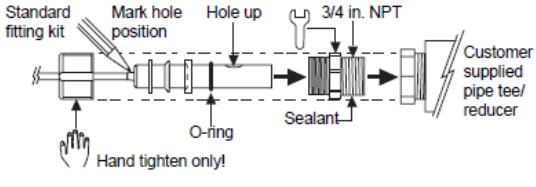

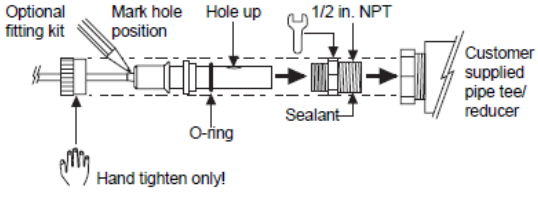

9. Specifications

Alternate wetted materials and overall lengths are available through special order. Cable length extensions to 100 ft. (30 m) are available through special order. For resistivity measurements above 10 MΩ and/or below 20°C, maximum cable length is 25 ft. (7.6 m).

CDCE-90-001, CDCE-90-01, CDCE-90-1

• CDCE-90-001 cell:	0.01
CDCE-90-001 range:	0.01 to 100 µS (10 kΩ to 100 MΩ)
• CDCE-90-01 cell:	0.10
CDCE-90-01 range:	1 to 1000 µS
• CDCE-90-1 cell:	1.0
CDCE-90-1 range:	10 to 10,000 µS
Temperature compensation:	PT1000
Wetted materials:	
O-rings:	EPR
Insulator material:	PTFE
Electrodes:	316 stainless steel
Standard fitting:	Polypropylene
Max. pressure:	6.9 bar (100 psi)
Max. temperature:	100 °C (212 °F)
Optional 3-2820.391 fitting:	316 stainless steel (1/2 in. NPT)
Max. pressure:	13.8 bar (200 psi)
Max. temperature:	120 °C (248 °F)

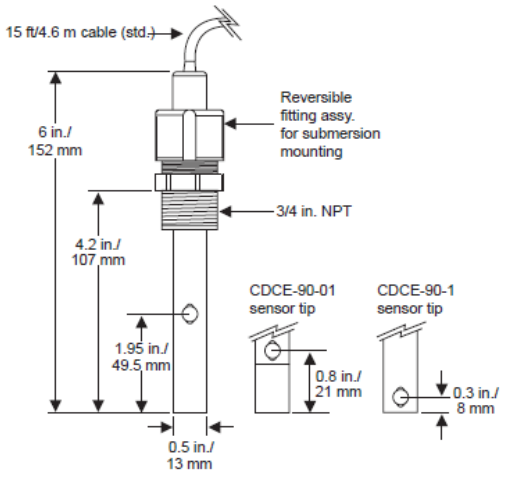

Appendix 4: Sample Data

The following table represents the different runs of the experiment as found in the github repository “Experiment” folder found at https://github.com/mark-edney/Thesis-Matlab/tree/master/Experiment.

Run name	Description
Trial 1 – 7	Experiments with the sensors themselves
Trial 8	First complete run
Trial 9-11	Trials used for modeling
Trial 11 & 13	Trials for recycle experiment

The following represents a sampling of the experiment on run 8. The sample rate was every 1000th point or every 50 mins.

Time (s)	Sensor 1 (µS/cm)	Sensor 2 (µS/cm)	Sensor 3 (µS/cm)	Sensor 4 (µS/cm)
0	351.5069	185.5928	303.5814	393.9578
3000.156	510.8313	478.3052	466.7748	841.7553
6000.28	542.757	243.9124	533.9591	544.9568
9000.391	490.9023	305.803	537.1587	457.3769
12000.53	443.5797	194.2412	397.1316	425.784
15000.67	396.6553	179.6414	489.303	418.2522
18000.71	378.9608	243.6745	428.6499	422.3181
21000.9	366.9798	287.0771	323.5771	418.5854
24000.94	352.2212	245.341	300.7252	427.9834
27001.04	349.2062	179.4035	265.8917	441.114
30001.16	338.8116	324.8465	263.2734	436.515
33001.35	344.3658	298.186	283.6654	447.8455
36001.44	349.3645	347.3017	280.3328	459.5097
39001.54	334.8443	335.479	195.9869	457.4433
42001.64	342.5409	335.7169	197.9706	476.9722
45001.76	346.9841	338.8116	200.113	471.7067
48001.96	338.732	344.7625	361.346	472.64
51002.01	346.1906	340.8744	217.7283	461.5757
54002.14	340.6364	331.1941	244.9443	477.3724
57002.3	342.7789	347.9363	338.0181	485.0372
60002.43	353.0147	335.3998	250.7364	489.5693
63002.55	344.3658	324.2909	315.5629	474.9727
66002.71	351.9036	350.3167	273.9059	465.5083
69002.74	359.1244	368.17	57.52678	493.302

Appendix 5: Sample Linear Regression Model

The following linear regression model was created to remove the conductivity of tap water from the recorded conductivity results. This regression model was only used for a specific experiment run (run 11) and required to be recalculated for each run.

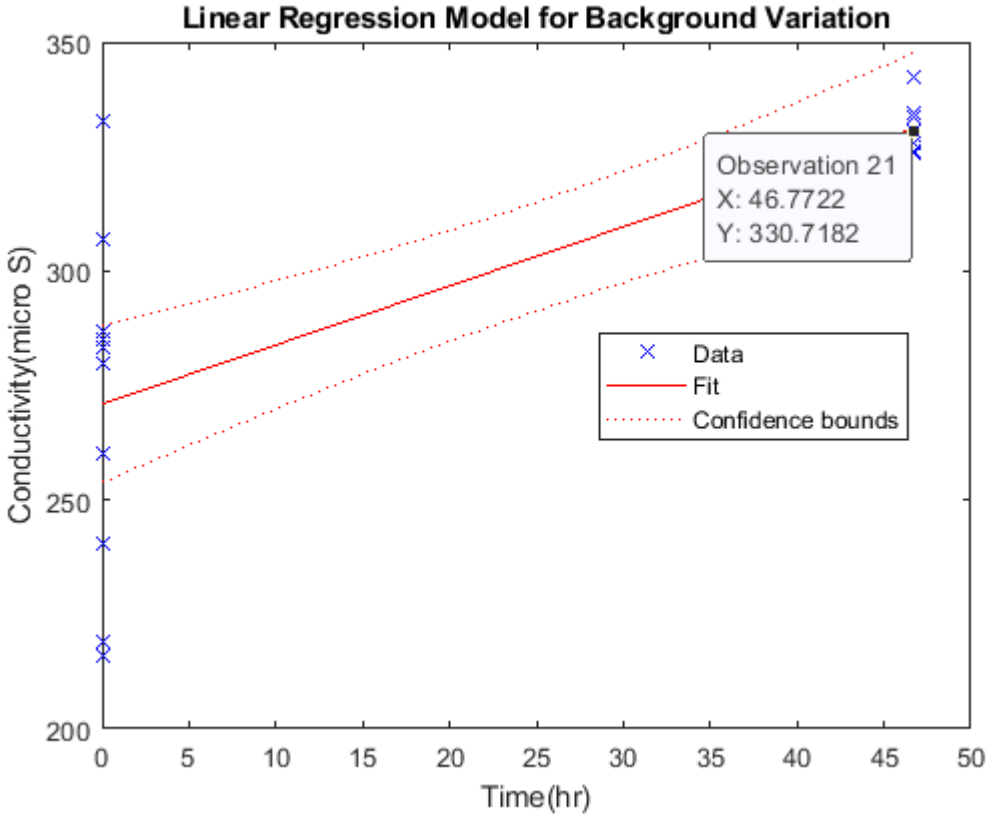

The model was created using the following results:

Time (hrs)	Conductivity (µS/cm)	Time (hrs)	Conductivity (µS/cm)
0	286.6013	46.768	334.3679
0.000849	332.7019	46.76884	326.1954
0.001667	215.8238	46.76967	334.3679
0.002525	283.3478	46.7705	342.2234
0.003359	306.9932	46.77133	333.8124
0.004165	280.0157	46.77218	330.7182
0.004999	218.9185		
0.005832	260.02		
0.006686	240.2627		
0.007503	284.8556		
46.76383	325.6399		
46.76469	329.766		
46.76551	325.5608		
46.76635	333.6541		
46.76716	327.7027		

Appendix 6: Numerical Integrations

The following numerical methods were used for integrations. The trapezoidal method was selected for its ease of use and not having a significant computational time difference.

Trapazodial:

$$\int_{a}^{b} f(x)dx \approx \sum_{k=1}^{N} \frac{f(x_{k-1}) + f(x_k)}{2} \Delta x$$

Simpson's rule:

$$\int_{a}^{b} f(x)dx \approx \frac{h}{3} \sum_{k=1}^{\frac{N}{2}} \frac{f(x_{2k-2}) + 4f(x_{2k-1}) + f(x_{2k})}{2}$$

$$h = \frac{(b-a)}{N}$$

Simpson's 3/8 rule:

$$\int_{a}^{b} f(x)dx \approx \frac{3h}{8}\left[f(x_0) + 3\sum_{i\neq 3k}^{N-1} f(x_i) + 2\sum_{j=1}^{N/3-1} f(x_{3j}) + f(x_n)\right]$$

$$h = \frac{(b-a)}{N}$$

Bibliography

[1] W. K. Dodds *et al.*, "Eutrophication of U.S. Freshwaters: Analysis of Potential Economic Damages," *Environ. Sci. Technol.*, vol. 43, no. 1, pp. 12–19, Jan. 2009, doi: 10.1021/es801217q.

[2] D. W. Schindler, "Eutrophication and Recovery in Experimental Lakes: Implications for Lake Management," *Science*, vol. 184, no. 4139, pp. 897–899, May 1974, doi: 10.1126/science.184.4139.897.

[3] J. Oleszkiewicz, "OPTIONS FOR IMPROVED NUTRIENT REMOVAL AND RECOVERY," p. 9, 2015.

[4] D. Mavinic *et al.*, "Canads's challenges and opportunities to address contaminants in wastewater," Canadian Water Network, March 2018, Mar. 2018. Accessed: Aug. 19, 2020. [Online]. Available: https://cwn-rce.ca/wp-content/uploads/2018/08/CWN-2018-Expert-Panel-Report-on-Contaminants-in-Wastewater.pdf.

[5] "AWARD OF EXCELLENCE - WATER RESOURCES Oxford Pollution Control Plant Expansion," *Canadian Consulting Engineer*. https://www.canadianconsultingengineer.com/features/award-of-excellence-water-resources-oxford-pollution-control-plant-expansion/ (accessed Aug. 23, 2020).

[6] "Smart Prosperity Institute | For a stronger, cleaner economy." https://institute.smartprosperity.ca/content/pricing-water-pollution-water-quality-trading-ontario (accessed Aug. 24, 2020).

[7] Y. Le Moullec, C. Gentric, O. Potier, and J. P. Leclerc, "CFD simulation of the hydrodynamics and reactions in an activated sludge channel reactor of wastewater treatment," *Chemical Engineering Science*, vol. 65, no. 1, pp. 492–498, Jan. 2010, doi: 10.1016/j.ces.2009.03.021.

[8] M. Alvarez Cuenca and M. Reza, "The multi-stage vertical bioreactor in water engineering," *The Canadian Journal of Chemical Engineering*, vol. 98, no. 1, pp. 172–185, 2020, doi: 10.1002/cjce.23621.

[9] M. Reza, "Simultaneous Removal of Ammonia and Phosphorus from Wastewater in a Continuous Flow Vertical Bioreactor," p. 203.

[10] C. Wallis-Lage, T. Johnson, B. Hemken, and B. Sabherwal, "New Technologies Force Change from Traditional Design-Bid-Build Strategy," *proc water environ fed*, vol. 2006, no. 13, pp. 251–262, Jan. 2006, doi: 10.2175/193864706783710893.

[11] A. Barwal and R. Chaudhary, "To study the performance of biocarriers in moving bed biofilm reactor (MBBR) technology and kinetics of biofilm for retrofitting the existing aerobic treatment systems: a review," *Rev Environ Sci Biotechnol*, vol. 13, no. 3, pp. 285–299, Sep. 2014, doi: 10.1007/s11157-014-9333-7.

[12] B. Young, B. Banihashemi, D. Forrest, K. Kennedy, A. Stintzi, and R. Delatolla, "Meso and micro-scale response of post carbon removal nitrifying MBBR biofilm across carrier type and loading," *Water Research*, vol. 91, pp. 235–243, Mar. 2016, doi: 10.1016/j.watres.2016.01.006.

[13] L. Deng *et al.*, "New functional biocarriers for enhancing the performance of a hybrid moving bed biofilm reactor–membrane bioreactor system," *Bioresource Technology*, vol. 208, pp. 87–93, May 2016, doi: 10.1016/j.biortech.2016.02.057.

[14] E. Arnold, B. Böhm, and P. A. Wilderer, "Application of activated sludge and biofilm sequencing batch reactor technology to treat reject water from sludge dewatering

systems: a comparison," *Water Science and Technology; London*, vol. 41, no. 1, pp. 115–122, Jan. 2000.
[15] K. Li, F. Fang, J. Guo, Y. Chen, J. Yang, and H. Wei, "Performance of one-stage autotrophic nitrogen removal in a biofilm reactor with low C/N ratio," *Environmental Technology*, vol. 36, no. 14, pp. 1819–1827, Jul. 2015, doi: 10.1080/09593330.2015.1013569.
[16] J. Yin, P. Zhang, F. Li, G. Li, and B. Hai, "Simultaneous biological nitrogen and phosphorus removal with a sequencing batch reactor–biofilm system," *International Biodeterioration & Biodegradation*, vol. 103, pp. 221–226, Sep. 2015, doi: 10.1016/j.ibiod.2015.02.019.
[17] H. Xiao, P. Yang, H. Peng, Y. Zhang, S. Deng, and X. Zhang, "Nitrogen removal from livestock and poultry breeding wastewaters using a novel sequencing batch biofilm reactor," *Water Science and Technology*, vol. 62, no. 11, pp. 2599–2606, Dec. 2010, doi: 10.2166/wst.2010.534.
[18] M. Chaali, M. Naghdi, S. K. Brar, and A. Avalos-Ramirez, "A review on the advances in nitrifying biofilm reactors and their removal rates in wastewater treatment," *Journal of Chemical Technology & Biotechnology*, vol. 93, no. 11, pp. 3113–3124, 2018, doi: 10.1002/jctb.5692.
[19] B. Günder and K. Krauth, "Replacement of Secondary Clarification by Membrane Separation-Results with Tubular, Plate and Hollow Fibre Modules," *Water Science and Technology; London*, vol. 40, no. 4–5, pp. 311–320, Aug. 1999.
[20] Ch. Brepols *et al.*, "Upgrading and retrofitting of municipal wastewater treatment plants by means of membrane bioreactor (MBR) technology," *Desalination*, vol. 231, no. 1, pp. 20–26, Oct. 2008, doi: 10.1016/j.desal.2007.11.035.
[21] M. Kraume and A. Drews, "Membrane Bioreactors in Waste Water Treatment – Status and Trends," *Chemical Engineering & Technology*, vol. 33, no. 8, pp. 1251–1259, 2010, doi: 10.1002/ceat.201000104.
[22] H. Monclús, J. Sipma, G. Ferrero, I. Rodriguez-Roda, and J. Comas, "Biological nutrient removal in an MBR treating municipal wastewater with special focus on biological phosphorus removal," *Bioresource Technology*, vol. 101, no. 11, pp. 3984–3991, Jun. 2010, doi: 10.1016/j.biortech.2010.01.038.
[23] F. Sun, X. Wang, and X. Li, "An innovative membrane bioreactor (MBR) system for simultaneous nitrogen and phosphorus removal," *Process Biochemistry*, vol. 48, no. 11, pp. 1749–1756, Nov. 2013, doi: 10.1016/j.procbio.2013.08.009.
[24] M. A. H. Johir *et al.*, "Removal of phosphorus by a high rate membrane adsorption hybrid system," *Bioresource Technology*, vol. 201, pp. 365–369, Feb. 2016, doi: 10.1016/j.biortech.2015.11.045.
[25] U. Bracklow, L. Manigas, A. Drews, M. Vocks, M. Barjenbruch, and M. Kraume, "Impact of different recirculation schemes on nitrogen removal and overall performance of a laboratory scale MBR," *Water Science and Technology; London*, vol. 56, no. 6, pp. 115–124, Sep. 2007, doi: http://dx.doi.org.ezproxy.lib.ryerson.ca/10.2166/wst.2007.641.
[26] R. Wang, F. Xiao, Y. Wang, and Z. Lewandowski, "Determining the optimal transmembrane gas pressure for nitrification in membrane-aerated biofilm reactors based on oxygen profile analysis," *Appl Microbiol Biotechnol*, vol. 100, no. 17, pp. 7699–7711, Sep. 2016, doi: 10.1007/s00253-016-7553-1.
[27] K. Hibiya, A. Terada, S. Tsuneda, and A. Hirata, "Simultaneous nitrification and denitrification by controlling vertical and horizontal microenvironment in a membrane-

aerated biofilm reactor," *Journal of Biotechnology*, vol. 100, no. 1, pp. 23–32, Jan. 2003, doi: 10.1016/S0168-1656(02)00227-4.
[28] M. Aybar, G. Pizarro, J. P. Boltz, L. Downing, and R. Nerenberg, "Energy-efficient wastewater treatment via the air-based, hybrid membrane biofilm reactor (hybrid MfBR)," *Water Science and Technology; London*, vol. 69, no. 8, pp. 1735–1741, Apr. 2014, doi: http://dx.doi.org.ezproxy.lib.ryerson.ca/10.2166/wst.2014.086.
[29] S. Judd and C. Judd, *The MBR Book: Principles and Applications of Membrane Bioreactors for Water and Wastewater Treatment*. Jordan Hill, UNITED KINGDOM: Elsevier Science & Technology, 2006.
[30] P. Le-Clech, V. Chen, and T. A. G. Fane, "Fouling in membrane bioreactors used in wastewater treatment," *Journal of Membrane Science*, vol. 284, no. 1–2, pp. 17–53, Nov. 2006, doi: 10.1016/j.memsci.2006.08.019.
[31] A. Drews, "Membrane fouling in membrane bioreactors—Characterisation, contradictions, cause and cures," *Journal of Membrane Science*, vol. 363, no. 1–2, pp. 1–28, Nov. 2010, doi: 10.1016/j.memsci.2010.06.046.
[32] F. Meng, S.-R. Chae, A. Drews, M. Kraume, H.-S. Shin, and F. Yang, "Recent advances in membrane bioreactors (MBRs): Membrane fouling and membrane material," *Water Research*, vol. 43, no. 6, pp. 1489–1512, Apr. 2009, doi: 10.1016/j.watres.2008.12.044.
[33] M. Martínez, "Nitrogen and phosphorus removal from urban wastewater by the microalga Scenedesmus obliquus," *Bioresource Technology*, vol. 73, no. 3, pp. 263–272, Jul. 2000, doi: 10.1016/S0960-8524(99)00121-2.
[34] J. Shi, B. Podola, and M. Melkonian, "Removal of nitrogen and phosphorus from wastewater using microalgae immobilized on twin layers: an experimental study," *J Appl Phycol*, vol. 19, no. 5, pp. 417–423, Aug. 2007, doi: 10.1007/s10811-006-9148-1.
[35] J. A. Borchardt and H. S. Azad, "Biological Extraction of Nutrients," p. 17, 2020.
[36] A. Ruiz-Martinez, N. Martin Garcia, I. Romero, A. Seco, and J. Ferrer, "Microalgae cultivation in wastewater: Nutrient removal from anaerobic membrane bioreactor effluent," *Bioresource Technology*, vol. 126, pp. 247–253, Dec. 2012, doi: 10.1016/j.biortech.2012.09.022.
[37] N. Abdel-Raouf, A. A. Al-Homaidan, and I. B. M. Ibraheem, "Microalgae and wastewater treatment," *Saudi Journal of Biological Sciences*, vol. 19, no. 3, pp. 257–275, Jul. 2012, doi: 10.1016/j.sjbs.2012.04.005.
[38] J. T. Bunce, E. Ndam, I. D. Ofiteru, A. Moore, and D. W. Graham, "A Review of Phosphorus Removal Technologies and Their Applicability to Small-Scale Domestic Wastewater Treatment Systems," *Front. Environ. Sci.*, vol. 6, p. 8, Feb. 2018, doi: 10.3389/fenvs.2018.00008.
[39] D. S. Parker and And Others, *Process Design Manual for Nitrogen Control*. 1975.
[40] W. E. Federation, *Biological Nutrient Removal (BNR) Operation in Wastewater Treatment Plants : WEF Manual of Practice No. 30: WEF Manual of Practice*. McGraw-Hill Education, 2005.
[41] Y.-H. Ahn, "Sustainable nitrogen elimination biotechnologies: A review," *Process Biochemistry*, vol. 41, no. 8, pp. 1709–1721, Aug. 2006, doi: 10.1016/j.procbio.2006.03.033.
[42] M. Strous, J. J. Heijnen, J. G. Kuenen, and M. S. M. Jetten, "The sequencing batch reactor as a powerful tool for the study of slowly growing anaerobic ammonium-oxidizing microorganisms," *Appl Microbiol Biotechnol*, vol. 50, no. 5, pp. 589–596, Nov. 1998, doi: 10.1007/s002530051340.

[43] G. Tchobanoglous, F. L. Burton, H. D. Stensel, and Metcalf & Eddy, Eds., *Wastewater engineering: treatment and reuse*, 4th ed. Dubuque, IA ; Toronto: McGraw-Hill, 2002.
[44] M. Henze, Ed., *Biological wastewater treatment: principles, modelling and design*. London: IWA Pub, 2008.
[45] G. W. Fuhs and M. Chen, "Microbiological basis of phosphate removal in the activated sludge process for the treatment of wastewater," *Microb Ecol*, vol. 2, no. 2, pp. 119–138, Jun. 1975, doi: 10.1007/BF02010434.
[46] H. T. T. Nguyen, V. Q. Le, A. A. Hansen, J. L. Nielsen, and P. H. Nielsen, "High diversity and abundance of putative polyphosphate-accumulating Tetrasphaera-related bacteria in activated sludge systems: Tetrasphaera-related bacteria in activated sludge systems," *FEMS Microbiology Ecology*, vol. 76, no. 2, pp. 256–267, May 2011, doi: 10.1111/j.1574-6941.2011.01049.x.
[47] R. Kristiansen *et al.*, "A metabolic model for members of the genus Tetrasphaera involved in enhanced biological phosphorus removal," *ISME J*, vol. 7, no. 3, pp. 543–554, Mar. 2013, doi: 10.1038/ismej.2012.136.
[48] M. Henze *et al.*, "Activated Sludge Model No.2d, ASM2D," *Water Science and Technology; London*, vol. 39, no. 1, pp. 165–182, Jan. 1999.
[49] W. C. Hiatt and C. P. L. Grady, "An Updated Process Model for Carbon Oxidation, Nitrification, and Denitrification," *Water Environment Research*, vol. 80, no. 11, pp. 2145–2156, Nov. 2008, doi: 10.2175/106143008X304776.
[50] C. P. Leslie Grady, W. Gujer, M. Henze, G. v. R. Marais, and M. Tomonori, "A Model for Single-Sludge Wastewater Treatment Systems," *Water Science and Technology*, vol. 18, no. 6, pp. 47–61, Jun. 1986, doi: 10.2166/wst.1986.0060.
[51] P. V. Danckwerts, "Continuous flow systems: Distribution of residence times," *Chemical Engineering Science*, vol. 2, no. 1, pp. 1–13, Feb. 1953, doi: 10.1016/0009-2509(53)80001-1.
[52] Th. N. Zwietering, "The degree of mixing in continuous flow systems," *Chemical Engineering Science*, vol. 11, no. 1, pp. 1–15, Aug. 1959, doi: 10.1016/0009-2509(59)80068-3.
[53] T. Salmi, J.-P. Mikkola, and P. Warna, *Chemical reaction engineering and reactor technology*. Boca Raton: CRC Press, 2011.
[54] R. W. Missen, C. A. Mims, and B. A. Saville, *Introduction to chemical reaction engineering and kinetics*. New York: J. Wiley, 1999.
[55] S. Goswami, H. J. Pant, D. Poswal, J. S. Samantray, and S. R. Asolekar, "Investigation of flow dynamics of wastewater in a pilot-scale constructed wetland using radiotracer technique," *Applied Radiation and Isotopes*, vol. 147, pp. 70–75, May 2019, doi: 10.1016/j.apradiso.2019.01.013.
[56] O. Levenspiel, *Chemical reaction engineering*, 3rd ed. New York: Wiley, 1999.
[57] H. S. Fogler, *Elements of chemical reaction engineering*, 4th ed. Upper Saddle River, NJ: Prentice Hall PTR, 2006.
[58] M. Gresch, D. Braun, and W. Gujer, "The role of the flow pattern in wastewater aeration tanks," *Water Science and Technology; London*, vol. 61, no. 2, pp. 407–414, Jan. 2010, doi: http://dx.doi.org.ezproxy.lib.ryerson.ca/10.2166/wst.2010.803.
[59] L. D. Schmidt, *The engineering of chemical reactions*, 2nd ed. New York: Oxford University Press, 2005.
[60] C. G. Hill and T. W. Root, *Introduction to Chemical Engineering Kinetics and Reactor Design*. Wiley, 2014.

[61] O. Levenspiel, *The chemical reactor omnibook*. Corvallis, Or: OSU Book Stores, Inc, 1979.
[62] A. Martin-Dominguez, V. G. Tzatchkov, I. R. Martin-Dominguez, and D. F. Lawler, "An enhanced tanks-in-series model for interpretation of tracer tests," *Journal of Water Supply : Research and Technology - AQUA; Oxford*, vol. 54, no. 7, pp. 435–448, Nov. 2005.
[63] P. Toson, P. Doshi, and D. Jajcevic, "Explicit Residence Time Distribution of a Generalised Cascade of Continuous Stirred Tank Reactors for a Description of Short Recirculation Time (Bypassing)," *Processes*, vol. 7, no. 9, p. 615, Sep. 2019, doi: 10.3390/pr7090615.
[64] A. D. Martin, "Interpretation of residence time distribution data," *Chemical Engineering Science*, vol. 55, no. 23, pp. 5907–5917, Dec. 2000, doi: 10.1016/S0009-2509(00)00108-1.
[65] M. Liu, "Age distribution and the degree of mixing in continuous flow stirred tank reactors," *Chemical Engineering Science*, vol. 69, no. 1, pp. 382–393, 2012, doi: 10.1016/j.ces.2011.10.062.
[66] M. Liu and J. N. Tilton, "Spatial distributions of mean age and higher moments in steady continuous flows," *AIChE Journal*, vol. 56, no. 10, pp. 2561–2572, Oct. 2010, doi: 10.1002/aic.12151.
[67] J. Aubin, D. F. Fletcher, and C. Xuereb, "Modeling turbulent flow in stirred tanks with CFD: the influence of the modeling approach, turbulence model and numerical scheme," *Experimental Thermal and Fluid Science*, vol. 28, no. 5, pp. 431–445, Apr. 2004, doi: 10.1016/j.expthermflusci.2003.04.001.
[68] D. Braun and W. Gujer, "Reactive tracers reveal hydraulic and control instabilities in full-scale activated sludge plant," *Water Science and Technology; London*, vol. 57, no. 7, pp. 1001–1007, Apr. 2008, doi: http://dx.doi.org.ezproxy.lib.ryerson.ca/10.2166/wst.2008.210.
[69] D. Olivet, J. Valls, M. À. Gordillo, À. Freixó, and A. Sánchez, "Application of residence time distribution technique to the study of the hydrodynamic behaviour of a full-scale wastewater treatment plant plug-flow bioreactor: Residence time distribution of a wastewater treatment plant plug-flow bioreactor," *Journal of Chemical Technology & Biotechnology*, vol. 80, no. 4, pp. 425–432, Apr. 2005, doi: 10.1002/jctb.1201.
[70] C. F. Williams and S. D. Nelson, "Comparison of Rhodamine-WT and bromide as a tracer for elucidating internal wetland flow dynamics," *Ecological Engineering*, vol. 37, no. 10, pp. 1492–1498, Oct. 2011, doi: 10.1016/j.ecoleng.2011.05.003.
[71] M. C. Collivignarelli, G. Bertanza, A. Abbà, and S. Damiani, "Troubleshooting in a full-scale wastewater treatment plant: what can be learnt from tracer tests," *Int. J. Environ. Sci. Technol.*, vol. 16, no. 7, pp. 3455–3466, Jul. 2019, doi: 10.1007/s13762-018-2032-0.
[72] M. Terashima, M. Iwasaki, H. Yasui, R. Goel, K. Suto, and C. Inoue, "Tracer experiment and RTD analysis of DAF separator with bar-type baffles," *Water Science and Technology; London*, vol. 67, no. 5, pp. 942–947, Feb. 2013, doi: http://dx.doi.org.ezproxy.lib.ryerson.ca/10.2166/wst.2013.584.
[73] I. Embry *et al.*, "Derivation of a Multiparameter Gamma Model for Analyzing the Residence-Time Distribution Function for Nonideal Flow Systems as an Alternative to the Advection-Dispersion Equation," *ISRN Chemical Engineering*, vol. 2013, pp. 1–8, 2013, doi: 10.1155/2013/539209.
[74] R. Fazli-Abukheyli and P. Darvishi, "Combination of axial dispersion and velocity profile in parallel tanks-in-series compartment model for prediction of residence time

distribution in a wide range of non-ideal laminar flow regimes," *Chemical Engineering Science*, vol. 195, pp. 531–540, Feb. 2019, doi: 10.1016/j.ces.2018.09.052.
[75] M. Knap and P. Balbierz, "Modification of Rhodamine WT tracer tests procedure in activated sludge reactors," *E3S Web of Conferences*, vol. 22, p. 00083, 2017, doi: 10.1051/e3sconf/20172200083.
[76] M. Ahnert, V. Kuehn, and P. Krebs, "Temperature as an alternative tracer for the determination of the mixing characteristics in wastewater treatment plants," *Water Research*, vol. 44, no. 6, pp. 1765–1776, Mar. 2010, doi: 10.1016/j.watres.2009.11.047.
[77] M. Gresch, D. Braun, and W. Gujer, "Using reactive tracers to detect flow field anomalies in water treatment reactors," *Water Research*, vol. 45, no. 5, pp. 1984–1994, 2011, doi: 10.1016/j.watres.2010.11.017.
[78] A. J. Stewart and L. A. Kszos, "Caution on using lithium (Li^+) as a conservative tracer in hydrological studies," *Limnology and Oceanography*, vol. 41, no. 1, pp. 190–191, Jan. 1996, doi: 10.4319/lo.1996.41.1.0190.
[79] "NaCl - Sodium Chloride | Sigma-Aldrich," *Sigma-Aldrich*. https://www.sigmaaldrich.com/programs/research-essentials-products.html?TablePage=102880799 (accessed Aug. 18, 2020).
[80] "Lab Grade Lithium Chloride, 100g for sale. Buy from The Science Company." https://www.sciencecompany.com/Lithium-Chloride-100g-P6357.aspx (accessed Aug. 18, 2020).
[81] "Bright Dyes Rhodamine WT Dye." https://www.fondriest.com/bright-dyes-rhodamine-wt-dye.htm (accessed Aug. 18, 2020).
[82] P. M. Dias and K. Sukasam, "Radiotracer Application in Wastewater Treatment Plants." https://www-pub.iaea.org/MTCD/Publications/PDF/TCS_49_web.pdf (accessed Aug. 18, 2020).
[83] "Price of Technetium-99 Cut Sharply," *Chem. Eng. News Archive*, vol. 39, no. 9, pp. 52–59, Feb. 1961, doi: 10.1021/cen-v039n009.p052.
[84] C. S. Widodo, H. Sela, and D. R. Santosa, "The effect of NaCl concentration on the ionic NaCl solutions electrical impedance value using electrochemical impedance spectroscopy methods," East Java, Indonesia, 2018, p. 050003, doi: 10.1063/1.5062753.
[85] M. Reza and M. Alvarez Cuenca, "Nitrification and denitrifying phosphorus removal in an upright continuous flow reactor," *Water Science and Technology*, vol. 73, no. 9, pp. 2093–2100, May 2016, doi: 10.2166/wst.2016.057.
[86] P. Kuhnert, "Foods, 3. Food Additives," in *Ullmann's Encyclopedia of Industrial Chemistry*, American Cancer Society, 2016, pp. 1–52.
[87] Omega, "Omega User's Guide CDCE-90-X Series," p. 8.